Aus dem Center for Regenerative Therapies Dresden
Direktor: Herr Prof. Dr. Michael Brand

Expansion of neural stem cells as a treatment for ischemic stroke

Dissertationsschrift
zur Erlangung des akademischen Grades

Doctor of Philosophy (Ph.D.)

vorgelegt

der Medizinischen Fakultät Carl Gustav Carus
der Technischen Universität Dresden

von

Simon Hertlein (M.Sc.)
aus Würzburg
Dresden 2020

1. Gutachter:

2. Gutachter:

Tag der mündlichen Prüfung:

gez.: _____
Vorsitzender der Promotionskommission

Anmerkung:
Die Eintragung der Gutachter und Tag der mündlichen Prüfung (Verteidigung) erfolgt nach Festlegung von Seiten der Medizinischen Fakultät Carl Gustav Carus der TU Dresden. Sie wird durch die Promovenden nach der Verteidigung zwecks Übergabe der fünf Pflichtexemplare an die Zweigbibliothek Medizin in gedruckter Form oder handschriftlich vorgenommen.

TABLE OF CONTENTS

Table of figures

List of tables

Abbreviations

%	per cent
˚C	degrees Celsius
~	approximately
4D	*Cdk4*/*Ccnd1*
6-OHDA	6-hydroxydopamine
AD	Alzheimer's Disease
ALS	Amyotrophic Lateral Sclerosis
ANOVA	analysis of variance
APOEε4	apolipoprotein E ε4
APP	amyloid precursor protein
araC	cytarabine
Ascl1	achaete-scute homolog 1
AV(s)	adenovirus(es)
Aβ	amyloid beta
Bcl-2	B-cell lymphoma 2
BDNF	brain-derived neurotrophic factor
BMP	bone morphogenetic protein
BrdU	5-bromo-2'-deoxyuridine
C9orf72	chromosome 9 open reading frame 72
cAMP	cyclic adenosine monophosphate
Cas9	CRISPR-associated 9
CCAo	common carotid artery occlusion
Ccnd1	cyclinD1
Cdk4	cyclin-dependent kinase 4
cm	centimetre(s)
CMV	cytomegalovirus
CNS	central nervous system
CNTF	ciliary neurotrophic factor
CPS	cryoprotectant solution
CRISPR	clustered regularly interspaced short palindromic repeats
CSF	cerebrospinal fluid
Ctip2	chicken ovalbumin upstream promoter transcription factor-interacting protein 2
DA	dopamine
DARP-32	dopamine- and cAMP-regulated neuronal phosphoprotein 32
DCX	doublecortin

DNA	deoxyribonucleic acid
DNase	deoxyribonuclease
dps	day(s) post stroke
E. coli	Escherichia coli
e.g.	exempli gratia, for example
EAE	experimental autoimmune encephalomyelitis
EdU	5-ethynyl-2´-deoxyuridine
EGF	epidermal growth factor
ERK5	extracellular-signal-regulated kinase 5
ESC(s)	embryonic stem cell(s)
ET-1	endothelin-1
etc.	et cetera, and other things
FGF-2	fibroblast growth factor-2
g	gram(s) or gravitational force equivalent
G-CSF	granulocyte-colony stimulating factor
G_1	gap 1 phase
GABA	γ-aminobutyric acid
GC	genome copies
GFAP	glial fibrillary acidic protein
GFP	green fluorescent protein
GLAST	glutamate aspartate transporter
h	hour(s)
HD	Huntington's Disease
HIV	human immunodeficiency virus
HSC(s)	hematopoietic stem cell(s)
i.e.	id est, that is
i.p.	intraperitoneal(ly)
Iba1	ionized calcium-binding adapter molecule 1
IGF-I	insulin-like growth factor-I
IgG	immunoglobulin G
iPSC(s)	induced pluripotent stem cell(s)
ITR	inverted terminal repeats
kb	kilobase(s)
l	litre(s)
L-NAME	N_ω-nitro-L-arginine methyl ester
LRRK2	leucine-rich repeat kinase 2
M	molar

m	metre(s)
MAP	microtubule-associated protein
MCAo	middle cerebral artery occlusion
min	minute(s)
ml	millilitre(s)
mm	millimetre(s)
mM	millimolar
MPTP	1-methyl-4-phenyl-1,2,3,6-tetrahydropyridine
MS	Multiple Sclerosis
MSC(s)	mesenchymal stem cell(s)
NCAM	neural cell adhesion molecule
NeuN	neuronal nuclei Fox-3
NeuroD1	neurogenic differentiation 1
Neurog2	neurogenin-2
ng	nanogram(s)
NGF	nerve growth factor
NGP1-01	8-benzylamino-8,11-oxapentacyclo[5.4.0.02,6.03,10.05,9]undecane)
nl	nanolitre(s)
NLS	nuclear localisation signal
nm	nanometre(s)
NOR	novel object recognition
NOS	nitric oxide synthase
NSC(s)	neural stem cell(s)
OB(s)	olfactory bulb(s)
pA	polyA
PD	Parkinson’s Disease
PEI	polyethylenimine
PINK1	phosphatase and tensin homolog-induced kinase 1
PSEN1/2	presenilin-1/2
(q)PCR	(quantitative) polymerase chain reaction
(r)AAV(s)	(recombinant) adeno-associated virus(es)
RFP	red fluorescent protein
RMS	rostral migratory stream
RNA	ribonucleic acid
RNAi	RNA interference
rpm	revolutions per minute
RT	room temperature

rtTA	reverse tetracycline transactivator
s	second(s)
S100β	S100 calcium binding protein β
SD	standard deviation
SDS-PAGE	sodium dodecyl sulfate polyacrylamide gel electrophoresis
SEM	standard error of the mean
SGZ	subgranular zone
shRNA	short hairpin RNA
siRNA	small interfering RNA
SOD1	superoxide dismutase 1
Sox2	sex determining region Y box 2
SVZ	subventricular zone
TDP-43	transactive response DNA-binding protein 43
TGF-α/-β1	transforming growth factor α/-β1
Tm	melting temperature
TMEV	Theiler's murine encephalomyelitis virus
U	unit(s)
UV	ultraviolet
v	volume
V	volts
VEGF	vascular endothelial growth factor
vs	versus
VSV-G	virus glycoprotein G
w	weight
Wnt	wingless type
wps	week(s) post stroke
YFP	yellow fluorescent protein
µg	microgram(s)
µl	microlitre(s)
µM	micromolar

1. INTRODUCTION

1.1 Adult neurogenesis in the mammalian brain

Adult neurogenesis in mammals is defined as the life-long addition of new neurons to the brain (Altman and Das, 1965). These newborn neurons originate from neural stem cells (NSC) that reside in two specific areas of the mammalian brain: the subgranular zone (SGZ) within the hippocampus (Toda and Gage, 2018) and the subventricular zone (SVZ) lining the ventricular walls (Figure 1)(Lim and Alvarez-Buylla, 2016). Since the identification of NSCs in the adult mammalian brain (Reynolds and Weiss, 1992), a plethora of studies have focused on their origin, properties, differentiation potential and ultimately the biological function of the newborn neurons that integrate into the existing circuitry and can add an additional layer of plasticity to the brain on demand (reviewed in (Gage and Temple, 2013; Bond et al., 2015)).

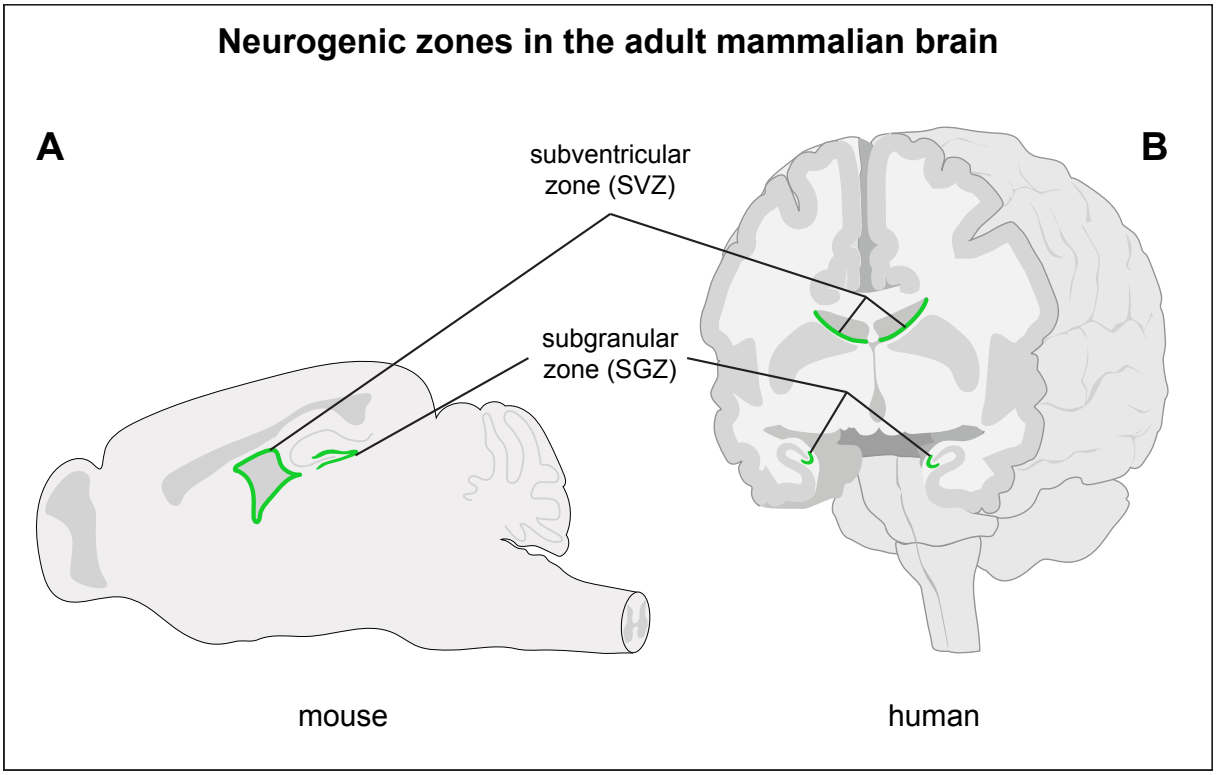

Figure 1: Neurogenic zones in the adult mammalian brain
Drawing of a sagittal section through an adult mouse brain (A) and a coronal section through an adult human brain (B) with the two neurogenic zones (subventricular zone and subgranular zone) highlighted in green. Inspired by and modified from (Magnusson and Frisen, 2016).

Adult neurogenesis in mice

In the well-studied model organism mouse, the presence of NSCs and adult neurogenesis is undebated (Figure 1A). However, it is known that the numbers of NSCs decline with ageing and two studies published in 2011 came to different conclusions as to whether the stem cell pool is exhausted at some point in life or not (Bonaguidi et al., 2011; Encinas et al., 2011).

While Bonaguidi et al. observed both symmetric and asymmetric divisions and long-time self-renewal of NSCs in the SGZ, Encinas et al. did not see symmetric divisions at all in NSCs in the SGZ. Furthermore, they observed an exhaustion of the stem cell pool because once NSCs were exiting quiescence, there was no coming back and they would eventually turn into astrocytes after several rounds of asymmetric neurogenic divisions. Both studies used Nestin$^+$ cells to identify NSCs *in vivo*, but Bonaguidi et al. used a Cre-lineage tracing approach for clonal analysis, whereas Encinas et al. investigated mainly Nestin-GFP transgenic animals on a NSC population level.

Another lineage-tracing study in the SGZ demonstrated the heterogeneity of the NSC pool by using either Nestin- or GLAST-driver lines that showed differences in terms of self-renewal capacity and responsiveness to neurogenic stimuli (DeCarolis et al., 2013). Interestingly, the Nestin-population showed a plateau and did not respond to neurogenic stimuli, whereas the GLAST-population continuously increased over time and also increased its neurogenic output upon stimulation. The heterogeneity of NSCs was further corroborated by *in vivo* longitudinal imaging of lineage-traced Ascl1$^+$ NSCs (Pilz et al., 2018). This population underwent several rounds of symmetric divisions before changing to asymmetric neurogenic divisions and eventually being consumed. The authors did not observe a shuttling between quiescent and activated NSCs but acknowledged that another population of NSCs might be able to do so.

In the SVZ, it has been found that the age-related decline in neurogenesis happens downstream of the NSC population and that the proportion of actively dividing NSCs even increases (Shook et al., 2012). SVZ NSCs mainly undergo symmetric divisions (either for expansion or differentiation) based on lineage-tracing experiments which leads to the maintenance of neurogenesis over life (Obernier et al., 2018). Notably, recent single cell transcriptomics of the SVZ showed a decrease of NSCs with ageing but a concomitant compensating increase in quiescent NSCs that had similar proliferation and differentiation capacities as “young” NSCs once activated (Kalamakis et al., 2019).

Adult neurogenesis in humans

In humans (Figure 1B), the first evidence for adult neurogenesis was provided by a study by Eriksson and colleagues where they injected the thymidine analogue BrdU into cancer patients for diagnostic purposes. BrdU is incorporated into the DNA of proliferating cells and post-mortem, they found BrdU$^+$ cells in the hippocampus of those patients (Eriksson et al., 1998). The existence of adult NSCs was indicated after the isolation and *in vitro* propagation of human neural precursor cells of post-mortem tissue that had similar properties as the already known fetal NSCs (Palmer et al., 2001). Not only the hippocampus, but also the SVZ in humans was shown to harbour neurogenic potential via the same BrdU approach as before (Curtis et al., 2007). Successive studies focusing on known markers for immature neurons such as

doublecortin (DCX) implicating neurogenesis corroborated the previous findings (Liu et al., 2008; Knoth et al., 2010). Another interesting approach was the analysis of nuclear bomb test-derived ^{14}C incorporation and based on that the calculation of the age of a cell. First, this technique showed that there were close to no new neurons in the olfactory bulb (where newborn neurons derived from the SVZ end up in other mammals typically (Bergmann et al., 2012)) but later on could provide further confirmation of adult neurogenesis both in the hippocampus (Spalding et al., 2013) and in the SVZ (Ernst et al., 2014). Remarkably, the latter study also identified that newborn neurons from the SVZ ended up in the striatum in contrast to other mammalian species.

However, all of the different techniques that had been used to identify NSCs or adult neurogenesis have their caveats. The BrdU studies used tissue from cancer patients and consequently, the detected proliferating cells in the brain could possibly originate either from metastatic tumour cells or from non-proliferative DNA damage-induced BrdU incorporation. Relying solely on markers that are known to prove neurogenesis in animal models is also not considered convincing since it is possible that other cell types such as glia express low levels of DCX. Furthermore, an increased incorporation of ^{14}C could also originate from DNA methylation or DNA repair.

Further research was also investigating whether adult neurogenesis in humans changes with ageing. One of the ^{14}C studies claimed that there was only a small decline in the hippocampus (Spalding et al., 2013) whereas subsequent marker-based data suggested either a rapid or at least a pronounced decline with ageing (Dennis et al., 2016; Mathews et al., 2017). This debate has spiked even more recently with two studies published in 2018 about adult hippocampal neurogenesis, both based on marker stainings of post-mortem brains but coming to different conclusions (Boldrini et al., 2018; Sorrells et al., 2018).

While Boldrini et al. claimed that the number of progenitors and newborn neurons does not change over life, Sorrells et al. found that neurogenesis in humans drops sharply after one year of life and that newborn neurons were below the detectable threshold in adulthood, corroborated also by similar findings in monkeys. In a follow-up commentary about those two publications, Kempermann et al. highlighted important differences in the post-mortem tissue processing of those two studies which can drastically influence the result (Bao and Swaab, 2018; Kempermann et al., 2018). Another interesting perspective came from Laura Andreae's commentary (Andreae, 2018), raising the point that the human brains analysed in the Boldrini study ranged from 14 to 79 years which is a time span where neurogenesis did not change anymore according to Sorrells et al. Thus, the reported numbers of adult-born neurons in those two studies might be actually more similar than the two groups claimed. Andreae concludes with the question "how rare is rare" and whether a few thousand newborn neurons in the entire hippocampus could actually make a difference.

More recent marker-based studies have yet again reported the detection of thousands of newborn neurons also in old human brains after optimising the protocol for post-mortem processing of the brains (Moreno-Jimenez et al., 2019; Tobin et al., 2019), leaving the field still wide open for future discoveries and debates. Although all of the used techniques have their caveats as outlined before, all the data combined rather supports at least a low level of adult neurogenesis in humans both in the striatum and in the hippocampus. The latter could explain the high cognitive functions of humans that the hippocampus contributes to and the former is raising hopes for providing a resource of neuronal regeneration (see also chapter 1.3).

1.1.1 The NSC lineage

Due to the restricted abilities to investigate NSCs in humans *in vivo*, the majority of characterisations of the NSC lineage has been conducted in the mouse. NSCs, like other stem cells, can shuttle back and forth between a quiescent and an active cycling state thereby undergoing different types of cell divisions. They can either divide symmetrically to create two new NSCs (expansion) or two differentiating progenitors (consumption), or they can alternatively divide asymmetrically to generate one NSC and one differentiating progenitor (self-renewal, reviewed in (Bond et al., 2015)), although there are several studies indicating that NSCs almost exclusively undergo symmetric divisions and asymmetric divisions are observed very rarely in both niches (Bonaguidi et al., 2011; Encinas et al., 2011; Calzolari et al., 2015; Obernier et al., 2018; Pilz et al., 2018).

In both SGZ and SVZ, NSCs can be histologically identified by their marker expressions of Sox2, GFAP and Nestin and they can differentiate either into GFAP- and S100β-expressing astrocytes or towards neural progenitors (Figure 2). These $Ascl1^+$ and $Neurog2^+$ progenitors have a limited self-renewal capacity and give rise to DCX-expressing neuroblasts. Subsequently, the neuroblasts differentiate to newborn neurons that eventually mature into $NeuN^+$ adult neurons which further specify into neuronal subtypes (Codega et al., 2014; Goncalves et al., 2016; Toda and Gage, 2018).

Neuroblasts in the SGZ remain within the dentate gyrus and locally differentiate into neurons, whereas in the SVZ, the neuroblasts migrate along the rostral migratory stream (RMS) to the olfactory bulbs (OBs) where they differentiate into neurons. All these decisions are not only driven by cell-intrinsic factors but also by extrinsic signals, mainly conveyed by the NSC niche which is comprised of the surrounding cells (Ottone et al., 2014; Licht and Keshet, 2015).

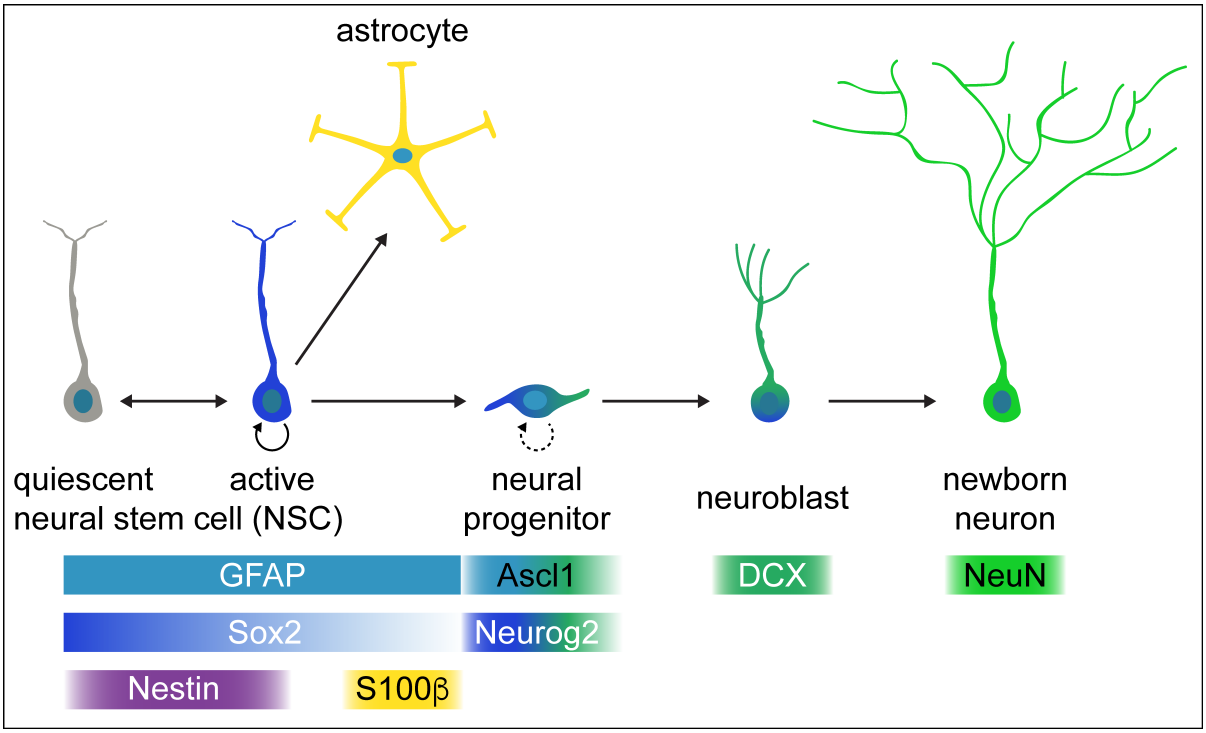

Figure 2: Neural stem cells and their progeny

Scheme of NSCs in their quiescent (grey) or active (blue) state and their progeny after differentiation: astrocytes (yellow), neural progenitors (blue-green) with limited self-renewal capacity, neuroblasts (blue-green) and newborn neurons (green). Below: important marker expression of each cell type is shown.

1.1.2 The NSC niche

The subventricular zone

The SVZ is a 3-4 cell layers thick zone separated from the ventricular cerebrospinal fluid (CSF) by the ependymal cells (Figure 3A). Both ependymal cells and NSCs are in contact with the CSF with their cilia while NSCs also have a long basal process contacting blood vessels (Mirzadeh et al., 2008). Many growth factors such as FGF-2, EGF and BDNF and signalling pathways like Hedgehog, BMP, Wnt and Notch have been shown to play a pivotal role in regulation and maintenance of the niche (Lim and Alvarez-Buylla, 2016). Neural progenitors and neuroblasts are surrounding the NSCs while neuroblasts migrate via the RMS towards the OB and differentiate into γ-aminobutyric acid (GABA)ergic interneurons (Gheusi et al., 2000; Ponti et al., 2013). Interestingly, there are also reports that the SVZ NSCs can differentiate towards the astro- and oligodendroglial lineage but this happens very rarely under physiological conditions (Menn et al., 2006).

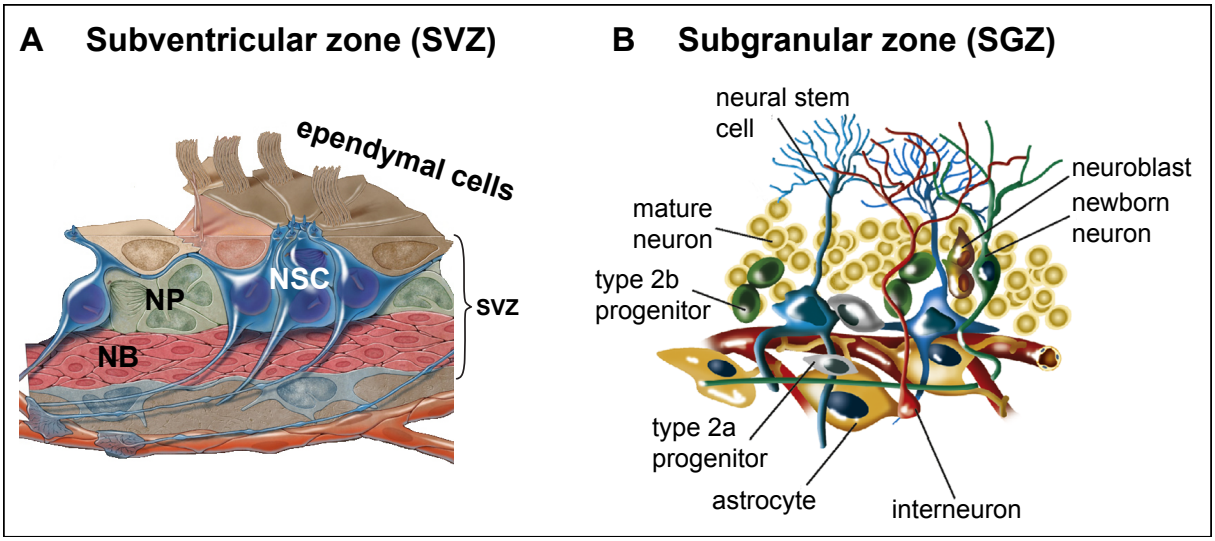

Figure 3: The neural stem cell niche in the SVZ

(A) Drawing of the NSC niche in the SVZ. Ependymal cells (brown) are surrounding NSCs (blue) and neural progenitors (NP, green). NSCs are in contact with the ventricular surface and blood vessels. Underneath are neuroblasts (red). Adapted from (Mirzadeh et al., 2008). (B) Drawing of the NSC niche in the SGZ. NSCs (blue) are in contact with blood vessels (red) and surrounded by their progeny (progenitors in grey and green, neuroblasts in brown, newborn neurons in green, adult neurons and astrocytes in yellow, interneurons in red). Modified from (Lin and Iacovitti, 2015).

The subgranular zone

The SGZ is located within the dentate gyrus of the hippocampus (Figure 3B). The NSCs are in close contact with blood vessels underneath the granule cell layer and have a radial glia-like morphology. Like in the SVZ, many growth factors and signalling pathways have been shown to influence the behaviour of the NSCs such as BDNF, FGF-2, VEGF, Notch, Hedgehog, BMP and Wnt signalling (Goncalves et al., 2016). After several rounds of proliferation and differentiation, the resulting neuroblasts only migrate very short distances into the granule cell layer where they differentiate into newborn neurons. After 6-8 weeks of maturation which is crucial for the survival and integration of the newborn neurons, they eventually become fully functional and indistinguishable from the other granule neurons (Toni and Schinder, 2015).

1.1.3 The role of neurogenesis in the adult brain

Newborn neurons from the SVZ

Since the progeny of SVZ NSCs contribute to neurons in the OB, many approaches including manipulation of neurogenesis or survival of the newborn neurons have been used to investigate the role of SVZ neurogenesis in olfaction of mice.

Knock-out of neural cell adhesion molecule (NCAM) in mice showed deficits in migration of neuroblasts leading to a 40 % size reduction of the OB and impairments in odour discrimination

but not odour detection thresholds or short-term memory (Gheusi et al., 2000). Ablation of neurogenesis by NSC-specific overexpression of diphtheria toxin fragment A, however, did not influence odour-associated memory formation nor odour long-term memory although the authors mentioned that more difficult tasks might be neurogenesis-dependent (Imayoshi et al., 2008). Injection of the antimitotic agent cytarabine (araC) into the ventricle for a month stopped the addition of newborn neurons to the OB during this period and short-term olfactory memory was impaired but no difference in spontaneous odour discrimination or long-term odour-associative memory tasks were observed (Breton-Provencher et al., 2009). Specific irradiation of the SVZ decreased neurogenesis for several months without affecting odour discrimination and short-term odour memory, but causing impairments on long-term memory (Lazarini et al., 2009).

Interestingly, when instead enhancing neurogenesis by preventing programmed cell death via local application of caspase inhibitor in the OB, the number of newborn neurons increased but olfactory reaction time was worse without changing olfactory learning or memory (Mouret et al., 2009). Similarly, knock-out of the pro-apoptotic gene Bax did not change SVZ proliferation or OB size but caused some neuroblasts to be stuck in the SVZ and to locally differentiate to neurons. Moreover, no behavioural changes were observed in that study (Kim et al., 2007). In contrast, increased differentiation and survival of newborn neurons by MAP kinase ERK5 activation in SVZ NSCs improved short-term memory (Wang et al., 2015a). BDNF has also been shown to increase both proliferation and neurogenesis in the SVZ although no behavioural tests have been conducted (Zigova et al., 1998; Henry et al., 2007). Similarly, microRNA-210 overexpression in the SVZ increased proliferation again lacking behavioural analysis (Zeng et al., 2014). Notably, when specifically activating adult-born neurons in the OB using optogenetics, mice improved in difficult odour discrimination (Alonso et al., 2012).

Despite the evidence that SVZ neurogenesis is playing a role in olfaction, these studies could still not reveal to what extent an increase in NSCs can influence the behavioural performance.

Newborn neurons from the SGZ

The hippocampus is important for learning and memory and the role of adult-born neurons is thought to be dependent on their age spanning from two to four and six weeks until they are considered completely integrated into the circuitry, fully mature and undistinguishable from other neurons (Ge et al., 2007; Toni et al., 2007). Different methods have been used to investigate the contribution of adult neurogenesis to the function of the hippocampus, amongst them several that manipulated neurogenesis itself at different levels.

For example, dividing NSCs were specifically killed using the herpes simplex virus thymidine kinase leading to reduced neurogenesis by as much as 98 % accompanied by behavioural deficits in spatial and/or contextual memory (Garcia et al., 2004; Saxe et al., 2006; Deng et al.,

2009). When DCX^+ cells were targeted, expectedly the number of newborn neurons was reduced resulting in a worse outcome in behaviour after stroke (Jin et al., 2010). Other strategies like NSC-specific overexpression of toxins such as the pro apoptotic protein Bax or diphtheria toxin fragment A both yielded spatial and/or contextual memory impairments (Dupret et al., 2008; Imayoshi et al., 2008).

On the other hand, efforts have been made to increase the existing levels of neurogenesis, one of the first being animals living in an enriched environment (Kempermann et al., 1997) leading to more proliferation and cell numbers accompanied by better performance in water maze learning. Furthermore, physical exercise (mice in a running wheel) has been shown to be sufficient to induce increased proliferation and neurogenesis in the SGZ (van Praag et al., 1999). Additionally, dietary restriction increased the number of proliferating cells due to a reduction of cell death of newborn neurons (Lee et al., 2000). These more holistic approaches affecting many aspects of the animal led to the discovery of more targeted ways of increasing neurogenesis such as growth factors.

Systemic administration of IGF-I promoted proliferation and neurogenesis in the SGZ (Aberg et al., 2000) whereas injection of NGF directly into the brain promoted survival of newborn neurons (Frielingsdorf et al., 2007) and increased proliferation in the SGZ and the animals' performance in recognition memory (Birch and Kelly, 2013). Similar effects were observed with BDNF (Pinnock and Herbert, 2008), CNTF (Chohan et al., 2011) and the adipose-derived hormone leptin (Garza et al., 2008). Besides injection of growth factors, also their overexpression has led to increased neurogenesis. When overexpressing VEGF in the entire brain, its total size was increased as were the proliferation rates in both SGZ and SVZ and animals showed reduced fear and aggression (Udo et al., 2008).

Furthermore, transgenic overexpression of the anti-apoptotic protein Bcl-2 in the dentate gyrus increased the number of DCX^+ cells older than 7 days without affecting early progenitors or proliferation (Kuhn et al., 2005). Conversely, knock-out of phosphodiesterase-4D increased proliferation in the SGZ via the cyclic adenosine monophosphate (cAMP) pathway improving reference memory of mice (Li et al., 2011).

All these examples of different manipulations have revealed a complex network of factors influencing neurogenesis in the SGZ, some of them even leading to behavioural changes. This underlines the importance of adult neurogenesis and also its responsiveness to external stimuli (e.g. physical exercise) for the hippocampal role in learning and memory – yet, more mechanistic studies are needed to further investigate its function.

1.1.4 Specific NSC pool expansion by *Cdk4*/*Ccnd1* overexpression

Since all the previously mentioned studies were not able to elucidate the explicit contribution of neurogenesis to brain function due to the lack of targeted approaches, our lab had established a method to specifically expand the NSC pool. Lange et al. first demonstrated that overexpression of *Cdk4*/*Ccnd1* (4D) in NSCs in the developing mouse cortex shortens their G_1 thus leading to an increased proliferation (Lange et al., 2009). When using this technique in a transgenic mouse model instead of local electroporation as before, a 4D-triggered NSC expansion right before the peak of embryonic neurogenesis led to adult mice with bigger brains (Nonaka-Kinoshita et al., 2013). Moreover, this effect was not restricted to embryonic development as 4D overexpression in the adult mouse brain using a lentiviral system was triggering increased proliferation in the hippocampal SGZ (Artegiani et al., 2011) and also in the SVZ using a transgenic mouse (Figure 4 A&B) (Bragado Alonso et al., 2019). In both cases, this increased stem cell pool gave rise to more newborn neurons after switching off 4D overexpression (Figure 4C) and for OB neurons, it was demonstrated that this increased number of neurons enabled mice to differentiate better between very similar odours (Bragado Alonso et al., 2019). This was the first direct manipulation of SVZ NSCs that described an improvement of the olfactory performance when facing a very difficult task. Hence, 4D overexpression does not only provide a useful approach to study the role of neurogenesis but could also enable exploiting the endogenous plasticity potential of the brain in the context of diseases.

Many studies have reported a response of the SVZ neurogenic niche to different brain damages (reviewed by (Nemirovich-Danchenko and Khodanovich, 2019)). SVZ neural progenitors have been shown to migrate towards the site of injury in addition to their normal migratory path along the RMS. This fact has been raising the question whether or not an increased level of neurogenesis might be beneficial for recovery from those adverse events and will be discussed in a separate section (see chapter 1.3).

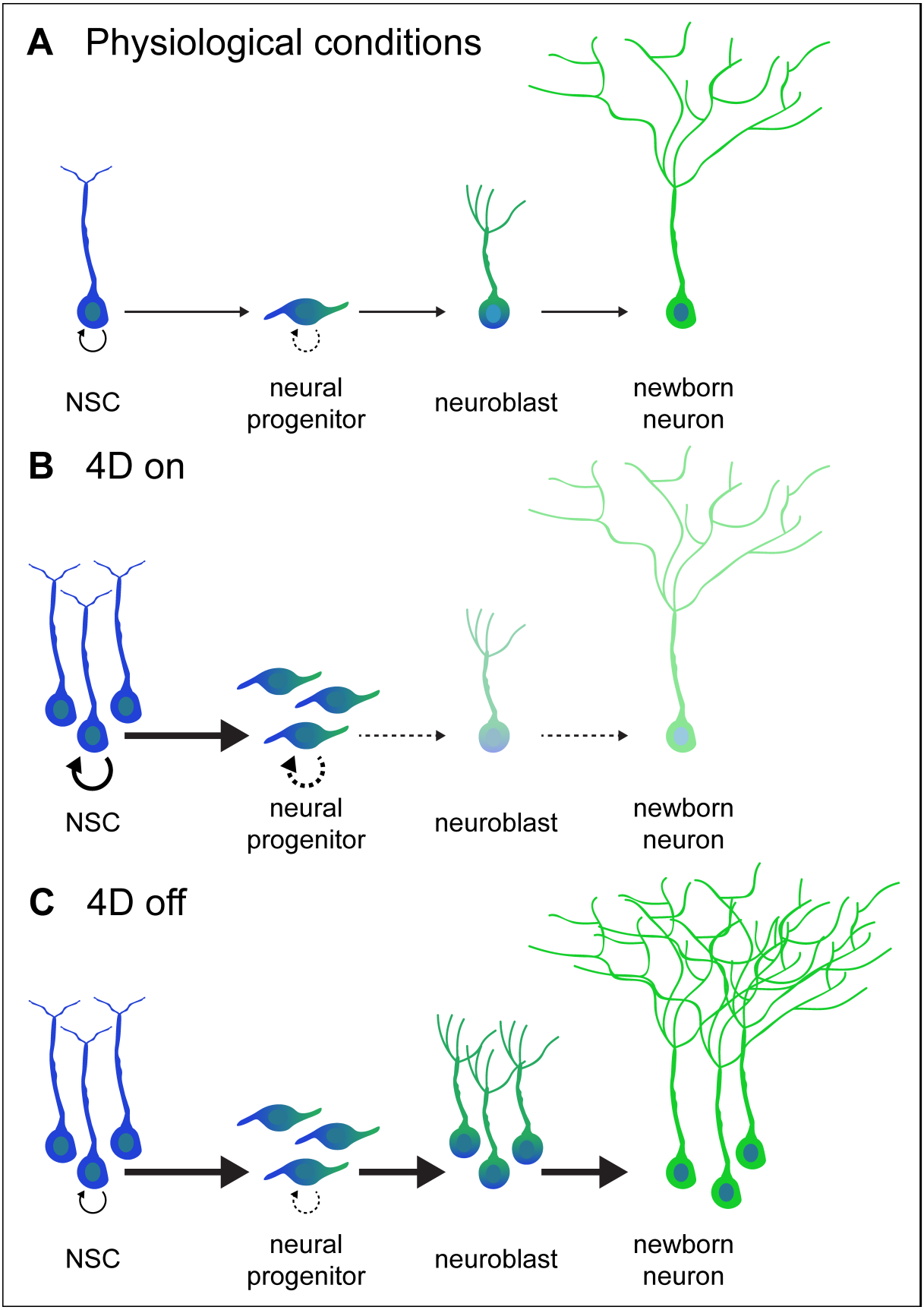

Figure 4: Effect of 4D overexpression on NSCs and their progeny

Scheme of NSCs (blue), neural progenitors (blue-green), neuroblasts (blue-green) and newborn neurons (green) under physiological conditions (A), during 4D overexpression in NSCSs (B) and after 4D overexpression (C).

1.2 Mouse models of neurodegenerative diseases

Neurodegenerative diseases are characterized by the loss of neurons and are mostly sporadic with an increasing risk with age, although there are monogenetic early-onset forms in some instances. With an increasingly ageing population, it is more and more important to find effective treatments which have been elusive in many cases until now (Logroscino and Tortelli, 2015). Thus, preclinical research in animal models is highly needed and mice depict a useful model organism because of the advanced available genetic tools. In the following, the most common neurodegenerative diseases, the respective potential relevance of the two neurogenic niches and their mouse models will be presented.

1.2.1 Alzheimer's Disease

Alzheimer's Disease (AD) is characterised by an early cognitive decline including memory deficits and impairments in executive functions. Histologically, AD is defined by three hallmarks: Aβ plaques (characteristic for AD only), tau tangles (also in other neurodegenerative diseases) and hippocampal and cortical neurodegeneration. It has been found that mutations in APP, PSEN1 and PSEN2 are main drivers for early-onset AD, whereas APOEε4 is a risk factor for late-onset (Carmona et al., 2018).

Since AD affects also the hippocampus, investigating a potentially beneficial contribution of SGZ neurogenesis to AD in different mouse models is of high interest. These models are either focused on Aβ plaques, tau tangles or both and thus reproduce more or less histological and behavioural aspects of neurodegeneration and cognitive impairments. The vast majority consists of genetically modified models (knock-in or transgenic with human mutations of affected proteins), but other models like seeding of Aβ by injection also exist. Yet, AD is a very complex neurodegenerative disease to model because of the heterogeneity of the disease itself and of available models (Jankowsky and Zheng, 2017).

1.2.2 Parkinson's Disease

Parkinson's Disease patients typically show motor symptoms like resting tremor and rigidity. It is caused by a progressive loss of dopamine (DA) neurons in the substantia nigra pars compacta due to misfolded α-synuclein in Lewy bodies and neurites (Savitt et al., 2006). Despite the majority of cases being sporadic, genetic mutations in several genes have been linked to the disease such as in α-synuclein or LRRK2, parkin and PINK1 (Klein and Westenberger, 2012).

Due to the close proximity of the striatal DA neurons to the SVZ, the therapeutic potential of SVZ NSCs in PD models is of high interest. The most commonly used animal models are drug induced by either 1-methyl-4-phenyl-1,2,3,6-tetrahydropyridine (MPTP) or 6-hydroxydopamine

(6-OHDA) both specifically killing dopaminergic neurons in the striatum when administrated systemically leading to variable motor deficits (Vingill et al., 2018). Alternatively, genetic models with mutations in PD affected genes have been used such as DA neuron-specific overexpression of mutant α-synuclein (Lin et al., 2012) or LRRK2 (Xiong et al., 2018), or knockout of parkin (Shin et al., 2011) and knockdown of PINK1 (Lee et al., 2017).
However, the drug induced models have so far failed to identify potential therapeutical approaches (Athauda and Foltynie, 2016) and genetic models only highlight a certain aspect of the disease that only affect a minority of patients.

1.2.3 Huntington's Disease

The autosomal-dominant Huntington's Disease (HD) is characterised by development of chorea and psychiatric and cognitive disabilities that typically lead to death of the patients within 10-20 years after onset (Glorioso et al., 2015). A poly-glutamine extension in the huntingtin protein is causing the disease resulting in misfolding and cytoplasmic aggregations that induce the death of medium spiny neurons in the striatum and degeneration of the cortex and hippocampus (Cisbani and Cicchetti, 2012).

Similar to AD and PD, HD affects areas either containing a neurogenic niche (hippocampus) or in close proximity to it (striatum to SVZ) thus raising the question whether increased neurogenesis could be beneficial for this disease. A variety of genetic mouse models have been created introducing the poly-glutamine repeats, ranging from transgenic N-terminal huntingtin fragments to full length and knock-in models (Farshim and Bates, 2018). Importantly, humans usually have less repeats with a more severe phenotype compared to the mouse models, also because the aim of the models is usually to speed up the disease process.

1.2.4 Amyotrophic Lateral Sclerosis

In amyotrophic lateral sclerosis (ALS), upper and lower motor neurons are lost, ultimately leading to respiratory failure and death typically within 1-5 years (Andersen and Al-Chalabi, 2011). Histologically, TDP-43 inclusions have been identified as pathological hallmark (Neumann et al., 2006). ALS is sporadic most of the times, but mutations in SOD1 and other genes (Taylor et al., 2016) among them the *C9orf72* gene (DeJesus-Hernandez et al., 2011; Renton et al., 2011) have been linked to the disease.

ALS does not affect specific brain areas but the migratory potential of SVZ-derived neuroblasts could still be beneficial. There are three main genetic mouse models being used. Overexpression of SOD1 mutations (Philips and Rothstein, 2015) recapitulate many aspects of the human disease, both on the cellular and behavioural level although there is no TDP-43 pathology. On the other hand, TDP-43 overexpression models show varying symptoms based

on how the overexpression is achieved and what form of TDP-43 is used (Swarup et al., 2011). More recently developed *C9orf72*-based models have also been reported to present neurodegeneration and cognitive impairments (Liu et al., 2016).

1.2.5 Multiple Sclerosis

Multiple sclerosis (MS) is different compared to the previously introduced neurodegenerative diseases because of the involvement of the immune system. For unknown reasons, the patient's immune cells in this disease target the own oligodendrocytes causing demyelination and axonal damage in the brain leading to motor and cognitive dysfunctions (Peruga et al., 2011).

It has been shown that SVZ NSCs can also contribute to the oligodendroglial lineage highlighting the potential versatility of endogenous NSCs (Menn et al., 2006). There are three established mouse models described in the literature: the experimental autoimmune encephalomyelitis (EAE), Theiler's murine encephalomyelitis virus (TMEV) infection-induced demyelination and toxin-induced demyelination.

EAE is most commonly used and is achieved by injection of a myelin peptide, the immune-system activating Freund's adjuvant and pertussis toxin to disrupt the blood brain barrier. These injections prime the immune cells against oligodendrocytes, recapitulating all important features of MS: inflammation, demyelination, axonal loss and gliosis plus behavioural deficits both as paralysis of body parts and motor coordinative impairments (Miller and Karpus, 2007; van den Berg et al., 2016).

TMEV infection causes chronic progressive inflammatory demyelinating disease in mice and depending on the TMEV type used, the severity and onset of symptoms are variable, but in either case, the obtained phenotype includes paralysis, locomotor impairments and also increased sensitivity to thermal pain as observed in MS patients (Lynch et al., 2008; Procaccini et al., 2015).

Finally, for the toxin-induced demyelination, cuprizone is most commonly used which specifically kills oligodendrocytes and leads to demyelination. Remyelination occurs when stopping the cuprizone treatment and subtle behavioural symptoms can be detected using a complex running wheel (Liebetanz and Merkler, 2006) although this model does not involve the immune system.

1.2.6 Stroke

Stroke can be divided into two categories, the ischemic and the haemorrhagic stroke. While ischemic stroke is more common in humans (80 % of the cases) and is characterized by a cut-off in blood supply for a brain area, haemorrhagic stroke occurs less frequently (20 %) and is

caused by the rupture of blood vessels (Bamford et al., 1991). The SVZ NSC niche has been reported to be responsive upon stroke and migration of neuroblasts to the injury site might be beneficial (Marques et al., 2019; Nemirovich-Danchenko and Khodanovich, 2019). There are three conceptually different models of ischemic stroke in rodents, the artery occlusion, light-inducible and chemically inducible stroke.

1.2.6.1 Artery occlusion

One of the oldest and still most commonly used model of ischemic stroke is occlusion of arteries (Koizumi et al., 1986). This can be achieved by different methods like injecting preformed blood clots or by inserting a surgical filament (Beech et al., 2001; Gerriets et al., 2004). In both cases, the middle cerebral artery is targeted for the occlusion (MCAo) which can be complemented with occlusion of the common carotid artery (CCAo). In case of the surgical filament insertion, this occlusion can be made permanent or transient, allowing reperfusion to occur. This stroke model has the advantage of closely resembling the pathophysiology of stroke in humans and does not require craniotomy but the mortality rate is high because the reported ischemic damage can affect up to half of a hemisphere. Moreover, the size and location of the stroke are highly variable and show a variety of impairments in different behavioural tests for motor coordination (rotarod, chimney test, pole test) or sensorimotor function (corner test, adhesive removal test, staircase test) and memory function (passive avoidance and water maze) (Hunter et al., 2000; Bouet et al., 2007; Wen et al., 2017).

1.2.6.2 Light-inducible stroke model

Another stroke model is light-inducible and called photothrombotic stroke. In this model, the photosensitive dye Rose Bengal is injected intraperitoneally (i.p.) to the mouse and distributed in the blood system of the entire body within a few minutes. This dye itself does not induce any damage, but upon activation by a cold-light source, it causes the formation of oxygen radicals that damage the endothelial wall of blood vessels, leading to the activation of thrombocytes and of the thrombotic cascade ultimately forming a blood clot (Watson et al., 1985). This technique is usually used to induce cortical ischemia because it is minimally invasive. The skin has to be cut, but the cold light can be shined directly on top of the skull. For a targeted stroke in deeper brain areas, an optic fibre can be used (Kuroiwa et al., 2009). In this case, the procedure is not as minimally invasive anymore since a small hole has to be drilled into the skull and the optic fibre (~1 mm diameter) has to be inserted into the brain. Several studies have reported sensorimotor impairments in both rats and mice after cortical photothrombotic stroke (Diederich et al., 2012; Li et al., 2014; Okabe et al., 2017; Alamri et al., 2018).

1.2.6.3 Chemically inducible stroke model

A third model of stroke is taking advantage of the small peptide hormone Endothelin-1 (ET-1). It is naturally produced by vascular endothelial cells and used by the body to control vasoconstriction of blood vessels (Davenport et al., 2016). For the stroke model, ET-1 is combined with the NOS inhibitor L-NAME preventing NOS-induced vasodilatation (Horie et al., 2008). Both those chemicals can be stereotaxically injected into any desired brain area to cause local vasoconstriction and thereby resulting in relatively small but targeted ischemic damage. ET-1 has been used to mainly target cortical areas and has shown both in mice and rats impairments in sensorimotor, locomotor and anxiety tests (Windle et al., 2006; Tennant and Jones, 2009; Roome et al., 2014; Happ et al., 2018).

Taken together, all three stroke models cause ischemic stroke in various brain areas in mechanistically different ways but the aim is always to mimic the natural cause of stroke i.e. a blood clot cutting off nutrition for certain brain areas.
While MCAo/CCAo are least invasive in regard to the brain itself and cause the biggest damage, they have the major disadvantage of high variability and unspecificity to certain brain regions.
The photothrombotic stroke on the other hand is the least invasive model when targeting cortical areas, can be relatively precise when using focused cold-light and causes minor local damage. If deeper layer structures shall be targeted the use of an optic fibre increases variability of the stroke and is not minimally invasive anymore.
ET-1 stroke is less invasive for deeper structures as compared to the photothrombotic stroke because only a very thin glass capillary is inserted into the brain to inject the chemicals instead of a relatively thick optic fibre. Since the capillary is also less flexible than the optic fibre, the precision and thus the reproducibility should be higher for ET-1. Moreover, the small ischemic damage usually caused by ET-1 can be scaled easier since the volume of injected ET-1 is much more precisely controllable as compared to the cold-light of the optic fibre (and also its exact orientation within the tissue).

1.3 Neuronal replacement approaches for neurodegenerative diseases

Ongoing efforts have been made to identify new treatments of the aforementioned neurodegenerative diseases. Besides pharmacological therapies to ameliorate the symptoms and to ease the burden of each of those diseases, the increasing knowledge about stem cells has opened the door to many therapeutic approaches, among them cell transplantations or the use of endogenous cells as a regenerative source by *in vivo* reprogramming or manipulation of the NSCs in the neurogenic niches.

1.3.1 Cell transplantations

Initially, cells from fetal midbrains as a mixed source of neurons and NSCs were used and provided positive results for both HD (Bachoud-Levi et al., 2000) and PD (Mendez et al., 2005; Mendez et al., 2008) patients. Surprisingly, not only motor coordination was improved but cells were shown to survive as long as 14 years after transplantation. However, in a double-blinded study, the behavioural improvements observed in the previous open-label PD trials could not be seen (Olanow et al., 2003). Furthermore, fetal cells do not depict a good resource of cells for regenerative therapies due the limited access to fetal material and ethical concerns.

Remarkably, the isolation and discovery of embryonic stem cells (ESCs) (Thomson et al., 1998) and induced pluripotent stem cells (iPSCs) (Takahashi and Yamanaka, 2006; Takahashi et al., 2007) have expanded the toolbox of stem cell research enormously. Differentiation *in vitro* of iPSCs/ESCs to DA neurons, for example, and their subsequent transplantation into PD mice has been achieved successfully (Kim et al., 2002; Kriks et al., 2011). Moreover, this technique cannot only be used for neuronal replacement, but could also enable correction of mutations prior to differentiation of patient iPSCs into the neuronal subtypes needed. This has been successfully done for HD (An et al., 2012). Furthermore, instead of differentiating the iPSCs to neurons, protocols have also been developed to stop the differentiation process at the NSC stage (Thier et al., 2012). These cells have the advantage that they are expandable in culture but are already committed to the neural lineage and they were shown to also be transplantable. Alternatively, fibroblasts can also be directly converted to NSCs (Lujan et al., 2012).

Transplantations of NSCs have improved cognition and memory in many AD mouse models according to a meta-analysis (Wang et al., 2015b) and were also shown to be effective for HD (Armstrong et al., 2000) and for MS (Pluchino et al., 2005). Of note, in the MS model, the NSCs were homing to demyelinated areas, differentiated locally and there was also evidence for anti-inflammatory effects of the NSCs themselves. For ALS, transplantation of NSCs is rather unlikely to make an impact because replacing motor neurons that functionally integrate into the existing network is considered difficult. Instead, astrocyte transplantation could be helpful since they are important for axonal growth, delivery of neurotrophic factors and neuroprotection (Clement et al., 2003).

For stem cell transplantations in stroke, the biggest hurdle is the hostile ischemic environment (Figure 5). Thus, NSCs have been preconditioned under hypoxic conditions (Theus et al., 2008) or pre-treated with small molecules (Sakata et al., 2012b) or cytokines (Sakata et al., 2012a). Moreover, supporting the transplanted cells with a hydrogel as supporting scaffold has also proven to be beneficial (Zhong et al., 2010). Finally, NSCs overexpressing growth factors have also shown to additionally boost endogenous neurogenesis and promote survival (Bernstock et al., 2017).

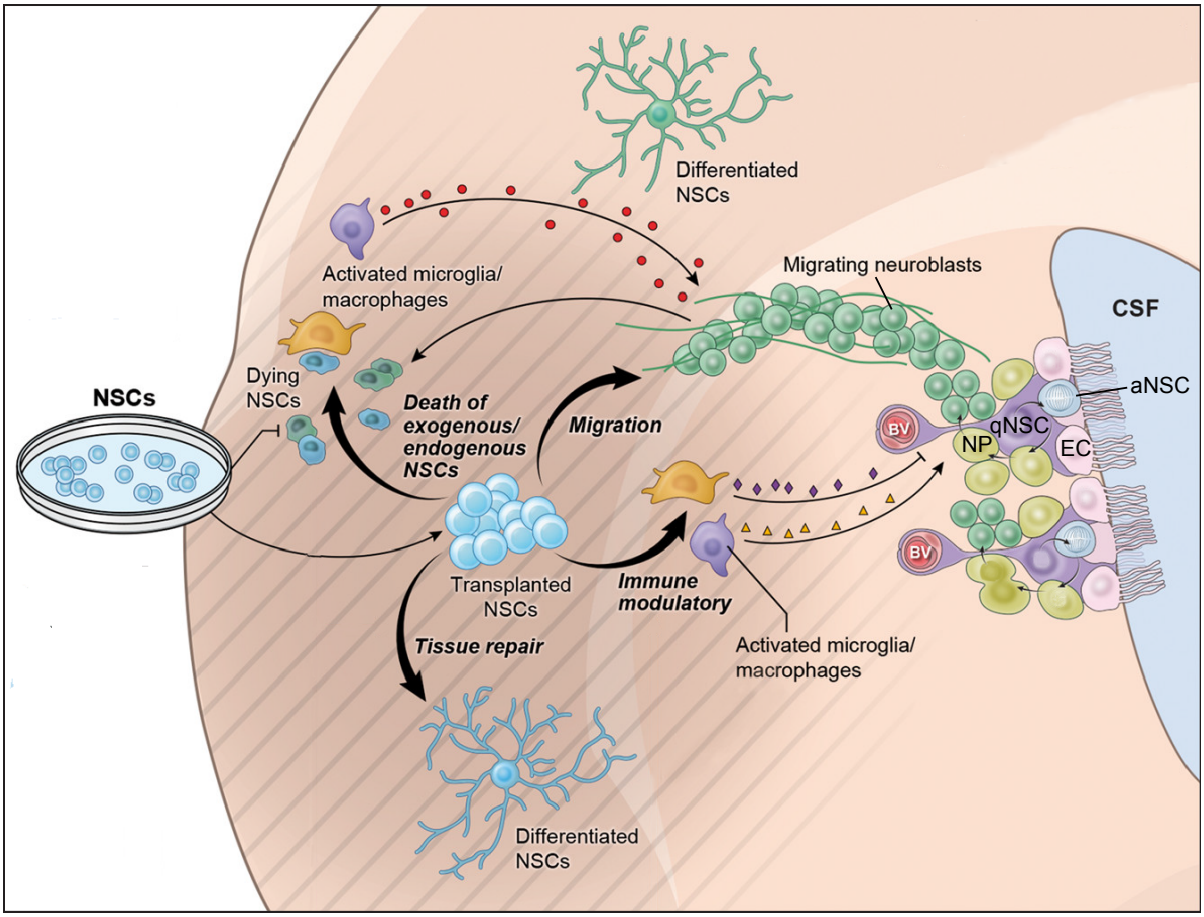

Figure 5: NSC transplantation and endogenous NSC response after ischemic stroke
Drawing of ischemic mouse brain and different fates of either transplanted or endogenous NSCs. Modified from (Bernstock et al., 2017)

Besides NSCs, mesenchymal stem cells (MSCs) have also been used for ALS, HD, PD and AD (Wang et al., 2015b; Lo Furno et al., 2018) although most studies did not show long-lasting engraftment of transplanted MSCs, irrespective of the administration route and both undifferentiated or as neurons. Thus, it has been concluded that the main therapeutic observed effect seems to rely on paracrine activity rather than neural differentiation (Paul and Anisimov, 2013). Similar results were also obtained in MSC transplantations for stroke where they were shown to migrate to the injury site and mainly exert their positive function via secretion of trophic factors and neuroprotection (Ishizaka et al., 2013; Toyoshima et al., 2015). Besides the research in animal models, there are also ongoing clinical trials for MSCs as a treatment for stroke (Toyoshima et al., 2017).

Of note, hematopoietic stem cells (HSCs) have also been used for MS. Patients' HSCs were isolated followed by irradiation therapy and subsequent autologous reconstitution of the immune system. The idea was to reset the immune system that had been triggered against the own oligodendrocytes and this method has been shown effective especially for aggressive forms (Atkins and Freedman, 2013).

Taken together, transplantations of different stem cell types in neurodegenerative disease models have shown promising results. Nevertheless, they have clear disadvantages considering the costs of (patient-specific) production of a suitable number of cells in a sterile controlled environment and especially in the case of patient-engineered approaches, they are also very time consuming. Yet, if instead endogenous cell populations could be used for regenerative approaches, many of these caveats would be diminished.

1.3.2 Endogenous cell sources

The two major proliferative cell populations in the adult brain are NSCs and glia (Bordiuk et al., 2014). In case of neurodegenerative diseases, glia are known to increase their proliferation and ever since the discovery of reprogramming and direct conversion, they have been considered as a potential source for *in vivo* reprogramming (Li and Chen, 2016). For example, iPSC reprogramming factors were overexpressed in reactive glia after traumatic brain injury and it was shown that the glia were indeed first reprogrammed to iPSCs and then differentiated to NSCs and subsequently to neurons and glia (Gao et al., 2016). Furthermore, in an AD mouse model, reactive glia were reprogrammed to neurons *in vivo* by NeuroD1 (Guo et al., 2014) and different transcription factor combinations have been proven effective for directly converting proliferating cells both in the cortex and in the striatum after ischemia (Grande et al., 2013; Yamashita et al., 2019). Yet, *in vivo* reprogramming still has to provide evidence for improvements on the behavioural level in neurodegenerative disease models. Moreover, the limited efficiency to target and reprogram a sufficient number of cells has been a major disadvantage so far accompanied by the concern that the concomitant decrease of the targeted glia population might be detrimental. In other words, the endogenous response of glia to an injury or inflammation might be necessary and beneficial for the recovery but would be diminished if a majority of this population was forced to convert into neurons. Without the supporting network surrounding them, these newly generated neurons would be likely to die instead of integrating into the existing circuitry.

The other endogenous cell source for regeneration are NSCs. Regarding the discussed neurodegenerative diseases, this approach is particularly interesting for PD and stroke because they are both locally restricted neuronal losses in contrast to systemic neuronal degradation in AD, HD, ALS and MS.

In PD mouse models, there is no convincing evidence for newborn neurons in the substantia nigra or striatum (Tande et al., 2006; Borta and Hoglinger, 2007). Nevertheless, efforts have been made to increase adult neurogenesis for treating PD (van den Berge et al., 2013): some growth factors such as BDNF (Mohapel et al., 2005), TGF-α (Cooper and Isacson, 2004) and FGF-2 (Peng et al., 2008) managed to increase neurogenesis, but there was no evidence of differentiation into DA neurons. Peptide hormone Exendin-4 was able to increase SVZ

neurogenesis, improved motor behaviour in a PD model and increased the number of DA neurons, but the results did not clearly dissect whether this was due to a rescue of DA neurons or increased neurogenesis (Bertilsson et al., 2008).

For stroke, different approaches have been used to enhance neurogenesis, among them growth factors. Overexpression of BDNF in the SVZ promoted migration towards the ischemic area and improved locomotor function (Yu et al., 2013). Furthermore, drugs that reportedly increase BDNF expression such as atorvastatin and citalopram have shown similar results not only in rodent stroke models (Chen et al., 2005; Espinera et al., 2013) but also in clinical trials (Zhang et al., 2017). Moreover, a BDNF peptide-loop mimetic managed to reduce stroke volume and improved the neurological score, further corroborating BDNF as a suitable means to treat stroke via manipulating endogenous NSCs and neuroblasts (Gudasheva et al., 2016).

Not only BDNF, but also other growth factors such as TGF-β1 and G-CSF have been used for stroke treatment, although G-CSF did not improve the stroke outcome in a meta-analysis of clinical trials (Ma et al., 2008; England et al., 2016).

Besides growth factors, there have been also a number of small molecules and drugs like bumetanide, NGP1-01 and citicoline successfully being used to increase neurogenesis, reduce stroke volume and/or improve sensorimotor function not only in animal models but also in humans (Hao et al., 2008; Alvarez-Sabin and Roman, 2013; Xu et al., 2017).

However, all these techniques relied either on ectopic expression of growth factors that might have other systemic effects and local or even global administration of reagents that most likely did not only exert their function on neurogenesis. A direct manipulation of increasing NSC proliferation without the accompanying potential side effects of other treatments is still missing in a stroke therapeutic approach.

The aforementioned 4D overexpression developed in our lab to specifically increase NSC proliferation in the SVZ or SGZ is representing such a suitable candidate. Recently, Berdugo Vega et al. found that 4D overexpression in SGZ NSCs in the context of ageing both increased neurogenesis and improved performance in hippocampus-dependent tasks (Berdugo-Vega et al., 2020). This is a first indication that the 4D-mediated overexpression in NSCs cannot only be beneficial under physiological conditions but could potentially also be used to replace lost neurons due to diseases or injuries.

Regarding the disease model to test this hypothesis, stroke can be considered as most reasonable candidate because it is an inducible model thus allowing the experimenter to decide when the injury occurs and to some extend also where and how big depending on the model. Moreover, stroke is a single instant injury that might be more suitable for an initial treatment test as opposed to other models like AD, PD, HD, ALS or MS. These diseases systemically affect either big brain structures, the whole brain or even the entire central

nervous system (CNS) and are often characterized by accumulative effects over the life-span of the animal or patient. Thus, increasing neurogenesis in one or even both neurogenic niches with 4D is much more likely to demonstrate significant improvements after a locally confined damage like in stroke.

Yet, the current methods of overexpressing 4D are not suitable for clinical applications since they rely on both transgenic animals and integrating lentiviruses accompanied by the risk of insertional mutagenesis. Thus, choosing a different viral strategy for this gene therapy approach is preferable.

1.4 Gene therapy approaches in the CNS

Ever since the discovery of virus-mediated gene transfer (Rogers and Pfuderer, 1968), the term 'gene therapy' has been formed representing the idea of therapeutical use of viruses to either replace defective genes or to introduce new genes to treat or cure diseases. Of note, also non-viral methods were developed and since they followed the same idea of introducing genetic material into cells, the name gene therapy is still used in this context.

1.4.1 Non-viral gene therapy

Non-viral gene therapy can be categorised in two ways, by the kind of genetic material that is being transferred and by the vector material that is being used. Not only DNA, either in form of plasmids or oligonucleotides but also RNAs (mostly small interefering (siRNA) or short hairpin (shRNA)) have been delivered to cells *in vivo* using different categories of so-called "vectors" ranging from cationic liposomes and lipid nanoparticles to cationic polymers (Pahle and Walther, 2016; Shim et al., 2018).

Remarkably, the first non-viral gene therapy attempts were very simple and consisted of intramuscular injection of pure plasmid DNA (Manthorpe et al., 1993) that was shown to be more effective than viruses (Davis et al., 1993; Draghia-Akli et al., 1997; Horton et al., 1999). Hydrodynamic tail vein injection in mice was also demonstrated for plasmid DNA delivery mainly to the liver (Liu et al., 1999) that has also been used more recently for genome editing with the CRISPR/Cas9 system (Yin et al., 2014).

For gene delivery to skin cells, cationic liposome complexes were injected into tumour tissue of melanoma patients and proved gene expression (Nabel et al., 1993). In another study, injection of only plasmid DNA obtained similar results (Heinzerling et al., 2005).

More recently, RNAi was conducted in liver cells by injection of lipid nanoparticle-packaged siRNAs (Nair et al., 2014; Butler et al., 2016). Furthermore, oral administration of calcium pectinate-coated cationic polymer microbeads in rats achieved gene delivery to colon cells highlighting the complex degree of chemical engineering that can be accomplished (Bhatt et

al., 2015). Of note, systemic administration of oligonucleotides to target liver cells is in clinical trial phases I/II (Sehgal et al., 2013).

Non-viral gene therapy has the advantage of lower potential immunogenicity and no integration into the host genome. However, transduction efficiencies are typically low and long-term sustained gene expression is not always achievable. Thus, depending on the goals, non-viral gene therapy may or may not be an alternative to virus-based methods.

Moreover, targeting cells of the CNS is more challenging and has only been achieved by injection of a cationic polymer-complexed plasmid into the brain of newborn mouse pups (Boussif et al., 1995).

1.4.2 Virus-based gene therapy

The first gene therapy on humans was conducted in 1990 and famously cured two patients with severe combined immuno-deficiency (Blaese et al., 1995). The general concept of all viral gene therapy approaches is creating so-called recombinant viruses. These have the same (or even engineered/modified) transduction capacities as their wildtype counterparts but are made replication-deficient, typically by removing viral genome parts that are not necessary for gene expression or single-time transduction. Yet, the early use of viruses still harboured a lot of risks for replication-competent viruses and has been improved drastically since then.

Below, the most common types of viruses used for gene therapy will be discussed, both with their advantages and disadvantages.

1.4.2.1 Retroviruses

Retroviruses are single-stranded RNA-based viruses and human immunodeficiency virus (HIV) is probably the most famous member of this family. Retroviral particles are 100 nm in diameter and are comprised of both an inner protein capsid structure and an outer lipid-based envelope originating from the plasma membrane of their host cell. Upon transduction of a new host cell, those viruses reverse transcribe their single-stranded RNA genome into double-stranded DNA and ultimately integrate into the host genome (Kotterman et al., 2015a).

The two mainly used genera for gene therapy approaches among retroviruses are the γ-retrovirus and the lentivirus. One important difference between those two is the type of cells they can transduce. While γ-retroviruses can only transduce dividing cells for integrating their genome into the host DNA, lentiviruses are able to achieve this task in a cell division independent manner (Naldini et al., 1996).

This is an important difference when considering what kind of cells shall be transduced for gene therapy. γ-Retroviruses have the advantage of being specific to dividing cells whereas lentiviruses can show a much broader tropism. This can also be manipulated depending on

what kind of envelope is being used during production of these viruses. Typically, the envelope of vesicular stomatitis virus glycoprotein G (VSV-G) is used in this process called pseudotyping (i.e. packaging a virus in a different envelope as compared to its naturally occurring counterpart), but other pseudotypes can turn out to be useful in particular cases (Joglekar and Sandoval, 2017).

Their packaging capacity is around 8-10 kb based on the viral genome size which is enough for the majority of single gene expression cassettes or even multiple smaller genes.

The safety of retroviruses in gene therapy has improved over the past decades since their initial use, leading to different generations of recombinant retroviruses. The major improvements consisted of reducing the amount of original viral genome to the bare minimum needed for gene transfer and separating the in *trans* supplied viral genes for viral production into different plasmids in order to avoid assembly of replication-competent viral particles. Thus, the only major drawback of these viruses nowadays is their random integration into the host genome accompanied by the risk of disruption of an important gene or dysregulation of its expression (Naldini, 2015). Remarkably, there is ongoing research about non-integrating lentiviral vectors although there is still a lot to optimise before potential clinical usage (Shaw and Cornetta, 2014; Shaw et al., 2017).

1.4.2.2 Adeno- and Adeno-associated viruses

The family of adenoviruses (AVs) are double-stranded DNA viruses and with 90-100 nm very similar in size to retroviruses. In contrast to retroviruses, AVs do not have an envelope but only a protein capsid and do not integrate into the host genome after entering the cell. Since their genome can be imported through the nuclear pores into the nucleus, they do not rely on cell division and thus can transduce both dividing and non-dividing cells. Yet, when used in gene therapies, one major drawback is their high immunological response compared to retroviruses (Wilson, 2009). On the other hand, AVs have a considerably bigger genome size of ~36 kb. Depending on the production strategy for gene therapy approaches, their packaging capacity ranges from ~36 kb (helper virus-dependent) to only 8 kb (helper virus-independent) (Choudhury et al., 2017).

Adeno-associated viruses (AAVs) are small (25 nm diameter) single-stranded DNA viruses that have first been identified as contaminants of AV preparations (Atchison et al., 1965). However, they are not related to AVs since AAVs belong to the family of parvoviruses. AAVs have a protein capsid without a surrounding envelope and several receptors on the capsids have been identified. These so-called different serotypes of AAVs were isolated either from humans or other mammals and all show specific tropisms. Once entered into a dividing or non-dividing host cell, AAVs can persist as episomal DNA in the nucleus or integrate into the host genome mainly in a viral protein-dependent manner (Salganik et al., 2015).

Based on their small packaging capability of ~4.8 kb, they have limited use for gene therapy approaches. If the gene expression cassette of interest is within that range, AAVs have several advantages over retro- and adenoviruses: (I) very low immunogenicity, (II) no integration into the host genome for recombinant AAVs (rAAVs) and (III) a big variety of available serotypes. This set of serotypes is even further extended because researchers have developed different techniques in order to mutate the capsid proteins thus leading to engineered serotypes that are able to transduce the cell type of choice (Kotterman and Schaffer, 2014; Grimm and Zolotukhin, 2015).

In conclusion, rAAVs are one of the best choices for clinical gene therapy studies because of their aforementioned advantages as long as the packaging capacity is not a limiting factor. Due to their non-integrative nature, rAAVs should be used with caution for targeting dividing cell types such as stem and progenitor cells as they could get diluted out over cell divisions. Depending on the aim of the gene therapy, this might impede long-term gene expression.

1.5 Aim of the thesis

The aim of the thesis was to test 4D overexpression in mouse NSCs *in vivo* for its possible use in treatment of stroke for future clinical applications.

To this end, I intended to develop a 4D overexpression system in mice that allowed its potential transfer to humans in one of the two mammalian neurogenic niches (SVZ or SGZ). Due to their low immunogenicity and non-integrative nature, rAAVs were chosen as the ideal approach. However, the big variety of available serotypes and their limited packaging capacity required thorough screening and careful construct design in order to achieve NSC transduction *in vivo*. Subsequently, the identified serotype candidate had to reproduce the basic hallmarks of the 4D effect on NSCs (i.e. increase in proliferation of NSCs and progenitors and increased number of newborn neurons) while dealing with potential hurdles of dilution of the virus over cell divisions.

Two different models of stroke – the photothrombotic and ET-1 stroke – were assessed on the histological level while testing the mice in different behavioural tasks. The more suitable model in terms of reproducibility and robustness of its effect would then be chosen for ultimately testing rAAV-mediated 4D overexpression in NSCs as a potential treatment for stroke in mice with possible applications to humans in the future.

2. MATERIALS AND METHODS

2.1 Materials

2.1.1 Bacteria, cell and mouse strains

Table 1: Bacteria, cell and mouse strains

Bacteria, cell or mouse strain	Supplier
One Shot™ TOP10 Chemically Competent E. coli	Thermo Fisher Scientific
AAV293	Stratagene
C57BL/6JRj	Janvier Labs
R26R-Confetti	Gift from Ader lab, CRTD

2.1.2 Plasmids

Table 2: Plasmids

Plasmid	Source
p6nts-GFPloxpNLS4Dloxp	Artegiani et al., 2011
pAAV, pHelper and pRC2	Gift from Mansfeld lab, BIOTEC
pRC9 and pRCrh10	Penn Vector Core, University of Pennsylvania
pRCr3.45	Gift from Schaffer lab, University of California Berkely
pMC-Cre	Gift from Anastassiadis lab, BIOTEC
$pRFP^{nls}$	Lange et al., 2009

2.1.3 Primers

All primers were purchased from Eurofins. Restriction sites are underlined.

Table 3: List of primers

Primer name	Sequence (5'-3')
AgeI CMV pr. rev	CAAGACCGGTAGCTCTGCTTATATAGACCTC
ApaI 3xStop-polyA fw	TAATGGGCCCTGATAATGAGATCCAGACATGATAAG
ApaI Cre rev	TATAGGGCCCATCGCCATCTTCCAGCAGGC
BsrGI GFP-3xStop-pA fw	CAAGTGTACAAGTGATAATGAGATCCAGACATGATAAG
BsrGI-SV40pA rev	GTAATGTACAGAACTTGTTTATTGCAGC
Cre qPCR fw	GTTTCCCGCAGAACCTGAAGATG
Cre qPCR rev	CATTGCTGTCACTTGGTCGTGG
EcoRI CMV pr. fw	CAATGAATTCCGTTACATAACTTACGGTAAATG
FseI polyA fw	CAAGGGCCGGCCGATCCAGACATGATAAG
FseI polyA rev	CTAAGGCCGGCCAACTTGTTTATTGCAGC

GFP qPCR fw	CAGAAGAACGGCATCAAGGT
GFP qPCR rev	GTGCTCAGGTAGTGGTTGTC
HindIII Cre fw	CACGAAGCTTGCCACCATGCCCAAGAAGAAGAGGAAGGTGTCC
NotI polyA rev	CAATGCGGCCGCAACTTGTTTATTGCAGC
NotI Ub. pr fw	CAATGCGGCCGCGAATTCTGGCCTCCGC
SacI polyA rev	CAAGGAGCTCAACTTGTTTATTGCAGC

2.1.4 Chemicals, buffers and culture media

Chemicals were purchased from Invitrogen, Life Technologies, Merck, Roche or Sigma-Aldrich.

Table 4: Buffers and solutions for general usage

Solution	Composition
AAV cell lysis buffer	50 mM Tris-HCl pH 8.5 150 mM NaCl 2 mM $MgCl_2$
Endothelin-1/L-NAME	5.7 µg/µl L-NAME 2 µg/µl Endothelin-1 in PBS
2xHBS buffer	280 mM NaCl 1.5 mM Na_2HPO_4 50 mM HEPES in H_2O, pH adjusted to 7.05 with NaOH
Ketamine/xylazine	0.5 ml 10 % ketamine 0.25 ml xylazine 0.75 ml 0.9 % NaCl 10 µl per g mouse body weight
PBS	137 mM NaCl 2.7 mM KCl 10 mM Na_2HPO_4 1.8 mM KH_2PO_4 in H_2O, pH adjusted to 7.4 with HCl
4 % PFA	4 % paraformaldehyde in PBS
TAE	Purchased as 50xTAE, diluted 1:50 in H_2O
1xTE pH 7.5	500 µl 1 M Tris-HCl pH 7.5 100 µl 0.5 M EDTA pH 8.0 49.4 ml H_2O

Table 5: Culture media

Medium	Composition
DMEM growth medium	DMEM (Gibco) supplemented with 10% (v/v) fetal bovine serum (FBS) 100 U/ml penicillin-streptomycin
Freezing medium	50 % (v/v) DMEM 40 % (v/v) FBS 10 % (v/v) DMSO
LB agar (BIOTEC media kitchen)	1.5 % agar in LB medium
LB medium (CRTD media kitchen)	1 % (w/v) tryptone 0.5 % (w/v) yeast extract 171 mM NaCl in H_2O, pH adjusted to 7.0
SOC medium	2 % w/v tryptone 0.5 % w/v yeast extract 8.56 mM NaCl 2.5 mM KCl 10 mM $MgCl_2$ 20 mM glucose in H_2O, pH adjusted to 7.0

Table 6: Iodixanol solutions for rAAV gradient purification

Reagent (final concentration)	**15 % solution**	**25 % solution**	**40 % solution**	**58 % solution**
60 % (v/v) iodixanol stock	12.5 ml	20.83 ml	33.8 ml	50 ml
10x D-PBS (1x)	5 ml	5 ml	5 ml	-
5 M NaCl (1 M)	10 ml	-	-	-
1 M $MgCl_2$ (1 mM)	50 µl	50 µl	50 µl	50 µl
1 M KCl (2.5 mM)	125 µl	125 µl	125 µl	125 µl
0.5 % Phenol red	75 µl	100 µl	-	25 µl
H_2O	22.25 ml	23.895 ml	11.025 ml	-
Σ	50 ml	50 ml	50 ml	50 ml

Table 7: Solutions for SDS-PAGE and silver staining

Solution	Composition
Basic developer solution	30 g/l K_2CO_3 0.00125 % (w/v) $Na_2S_2O_3$ 0.00025 % (v/v) formaldehyde (added maximum 1 h before use) in H_2O
Fixation solution	30 % (v/v) ethanol 10 % (v/v) acetic acid in H_2O
2x Laemmli buffer	4 % (w/v) SDS 20 % (v/v) glycerol 120 mM Tris-HCl pH 6.8 0.02 % (w/v) bromophenol in H_2O before use, add 10 % (v/v) 2-mercaptoethanol
NuPAGE™ MOPS SDS running buffer (20X)	Purchased from ThermoFisher Scientific, diluted 1 : 20 in H_2O
Stop solution	4 % (w/v) Tris 2 % (v/v) acetic acid in H_2O

Table 8: Solutions for immunohistochemistry

Solution	Composition
Antibody solution	10 % (v/v) donkey serum 0.3 % (v/v) triton-x 100 in PBS
Blocking solution	10 % (v/v) donkey serum 0.5 % (v/v) triton-x 100 in PBS
Cryoprotectant solution (CPS)	25 % (v/v) ethylenglycol 25 % (v/v) glycerol 10 % (v/v) 10xPBS in H_2O
1000xDAPI	0.1 % (w/v) DAPI in H_2O
Quenching solution	0.1 M glycine pH 7.4 in PBS

2.1.5 Antibodies

Table 9: Primary antibodies

Antigen	Species	Supplier	Catalog number	Dilution
BrdU	rat	Abcam	ab6326	1:250
Ctip2	rat	Abcam	ab18465	1:300
DCX	guinea pig	Merck Millipore	AB2253	1:500
GFP	goat	Rockland	600-101-215	1:500
Iba1	rabbit	Wako	019-19741	1:1000
Nestin	mouse	BD Biosciences	556309	1:100
NeuN	rabbit	Abcam	ab104225	1:1000
S100β	rabbit	Abcam	ab14688	1:1000
Sox2	goat	SantaCruz	sc-17320	1:100

Fluorophore-conjugated (DyLight or Alexa) secondary antibodies were IgG raised in donkey against goat, guinea pig, mouse, rabbit and rat and all purchased from Jackson Immunoresearch.

2.1.6 Kits and enzymes

Table 10: Kits and enzymes

Kit/enzyme	Supplier	Catalog number
Antarctic Phosphatase	NEB	M0289S
Benzonase	Merck	70746-3
Click-iT Edu Alexa Fluor 647 Imaging Kit	ThermoFisher Scientific	C10340
DNase I	NEB	M0303S
iQ™ SYBR® Green Supermix	Bio-Rad	170-8880
Proteinase K, Molecular Biology Grade	NEB	P8107S
Q5® High-Fidelity 2X Master Mix	NEB	M0492S
QIAGEN® Plasmid Maxi Kit	Qiagen	12162
QIAprep Spin Miniprep Kit	Qiagen	27104
QIAquick Gel Extraction Kit	Qiagen	28704
QIAquick PCR Purification Kit	Qiagen	28104
Restriction enzymes	NEB	
T4 DNA ligase	NEB	M0202S

2.2 Methods

2.2.1 Cloning

2.2.1.1 Polymerase chain reaction (PCR)

For amplification of DNA for cloning purposes, the following PCR mix was used:

12.5 µl	2x Q5 Master Mix
1.25 µl	10 µM primer fw
1.25 µl	10 µM primer rev
~1 ng	plasmid DNA
up to 25 µl	H_2O

PCR program:

1. Initial Denaturation

98˚C	30 s

2. Amplification (35 cycles)

98˚C	10 s
Tm	20 s (Tm: melting temperature of respective primer pair)
72˚C	30 s/kb of PCR product

3. Final extension

72˚C	120 s
4˚C	∞

The resulting PCR product was visualised using Agarose gel electrophoresis (see below) and the band of expected size was either extracted out of the gel (QIAquick Gel Extraction Kit) or the PCR mix (QIAquick PCR Purification kit) in case there was only one visible band.

2.2.1.2 Restriction hydrolysis

For restriction hydrolysis of plasmid DNA,

1 µg	plasmid DNA
2 µl	10x buffer
0.2 µl	restriction enzyme
up to 20 µl	H_20

were mixed together and incubated for 1 h at 37˚C and then heat inactivated according to the conditions of the respective enzyme. For PCR products, 500 ng of DNA was used and the incubation was extended to 2 h at 37˚C. Subsequently, the resulting ends were dephosphorylated in case of the plasmid DNA by adding

2 µl	10x AP buffer
1 µl	antarctic phosphatase (AP)

to the DNA, followed by a 30-min incubation at 37˚C. Finally, AP was heat inactivated at 80˚C for 2 min.

The different resulting fragments of plasmid DNA were separated by Agarose gel electrophoresis and the respective band was extracted out of the gel.
Restriction hydrolysed PCR products were purified using the PCR Purification Kit.

2.2.1.3 Agarose gel electrophoresis

For visualisation of DNA fragments, an agarose gel was prepared as follows:

x g Agarose (x = 0.5 g for 1 % or x = 2 g for 2 % Agarose)
50 ml 1xTAE buffer

For DNA fragments <1kb to be resolved, a 2 % agarose gel was prepared, for bigger fragments, the 1 % agarose gel was used. The solution was boiled in the microwave until the agarose was completely dissolved, briefly cooled down and then 1:10,000 SYBR Safe DNA gel stain (Invitrogen) was added. The agarose solution was poured into a chamber with a comb to form the lanes. After the gel was solidified, the comb was removed and the gel placed into an electrophoresis chamber filled with 1xTAE buffer. Samples and a 1 kb marker GeneRuler were loaded into the lanes and electrophoresis was conducted at 90 V for 60-90 min. DNA was visualised afterwards on a gel documentation system under UV light.

2.2.1.4 Ligation

Plasmid DNA and PCR fragments were ligated after restriction hydrolysis using a 3:1 ratio (PCR:plasmid) with 50 ng plasmid DNA in a total volume of 20 µl, 1 µl T4 Ligase and 2 µl 10x ligase buffer. Incubation was conducted over night at 16˚C, followed by heat inactivation the next day at 65˚C for 10 min. The ligation mix was then stored at 4˚C until transformation.

2.2.1.5 Heat-shock transformation

For heat-shock transformation of ligated plasmid DNA, 50 µl competent cells (E.coli TOP10) were thawed on ice. Two µl of DNA was added to the cells and the tube was flicked for a few times. After incubation on ice for 30 min, the heat-shock was conducted in a water bath at 42˚C for 30 s followed by immediate chilling on ice for at least 2 min. Then, 950 µl SOC medium was added and the bacteria were incubated on a shaker at 950 rpm at 37˚C for 1 h. One hundred µl of transformed bacteria were spread on a LB agar plate with antibiotics according to the plasmid and incubated over night at 37˚C.

2.2.1.6 MiniPrep

A single colony of transformed bacteria grown on an LB agar plate over night was picked and transferred to 1.9 ml LB medium and appropriate antibiotics and shaken over night at 950 rpm and 37˚C. The next day, 500 µl of the bacterial culture were stored at 4˚C and the rest was used for plasmid isolation using the Qiagen MiniPrep Kit. Plasmids were eluted from the

column using 50 µl nuclease-free H_2O and stored at -20˚C or immediately used for analysis of the cloning by restriction hydrolysis or sequencing.
In case of a positive clone and confirmed sequence, 500 µl glycerol was added to the remaining 500 µl bacterial culture and this glycerol stock was stored at -80˚C.

2.2.1.7 MaxiPrep

Bacteria from a glycerol stock were inoculated into 250 ml of LB medium with appropriate antibiotics and shaken at 220 rpm and 37˚C over night. Plasmids were isolated using the MaxiPrep Kit from Qiagen following the QuickStart protocol with the following modifications:

Step 5: Centrifugation at 10,000 g for 10 min at 4˚C, then supernatant was filtered using Qiagen Maxi Cartridges and loaded onto the column

Step 11: Centrifugation was extended to 30 min

Step 12: 200 µl nuclease-free H2O were used to dissolve the plasmid per 250 ml LB culture used

MaxiPrep-isolated plasmids were analysed on a NanoDrop machine to determine purity and concentration of the DNA and then stored at -20˚C.

2.2.1.8 Constructs and cloning strategy

In order to achieve overexpression of *Cdk4*, *Ccnd1* and GFP as a reporter protein (Ub4D, Figure 6), the G^{lox}4D expression cassette from Artegiani et al. was used as a template (Artegiani et al., 2011). The polyA (pA) sequence was introduced using the *Fse*I restriction site and $pRFP^{nls}$ as a PCR template (Lange et al., 2009). Subsequently, the resulting construct was PCR-amplified from the ubiquitin promoter to the pA sequence using primers flanked by *Not*I-restrictions sites and subcloned into a pAAV backbone containing AAV2 ITRs.
The UbGFP construct was created by inserting a pA fragment with three upstream Stop codons into the *Bsr*GI restriction site of the Ub4D construct. This resulted in a remaining partial out-of-frame *Cdk4* and a full *Ccnd1* coding sequence downstream of the pA.
For the CMV-GFP construct, the CMV promoter was PCR-amplified from the pAAV plasmid and subcloned into the *Eco*RI and *Age*I restriction sites of UbGFP.
For UbCre4D, *cre* was PCR-amplified from pMC-Cre and replaced GFP in the Ub4D construct using *Hind*III and *Apa*I restriction sites.
UbCre was obtained by PCR amplification of the 3xStop Codon-polyA sequence from UbGFP and cloning it into the *Apa*I and *Sac*I restriction sites of UbCre4D.

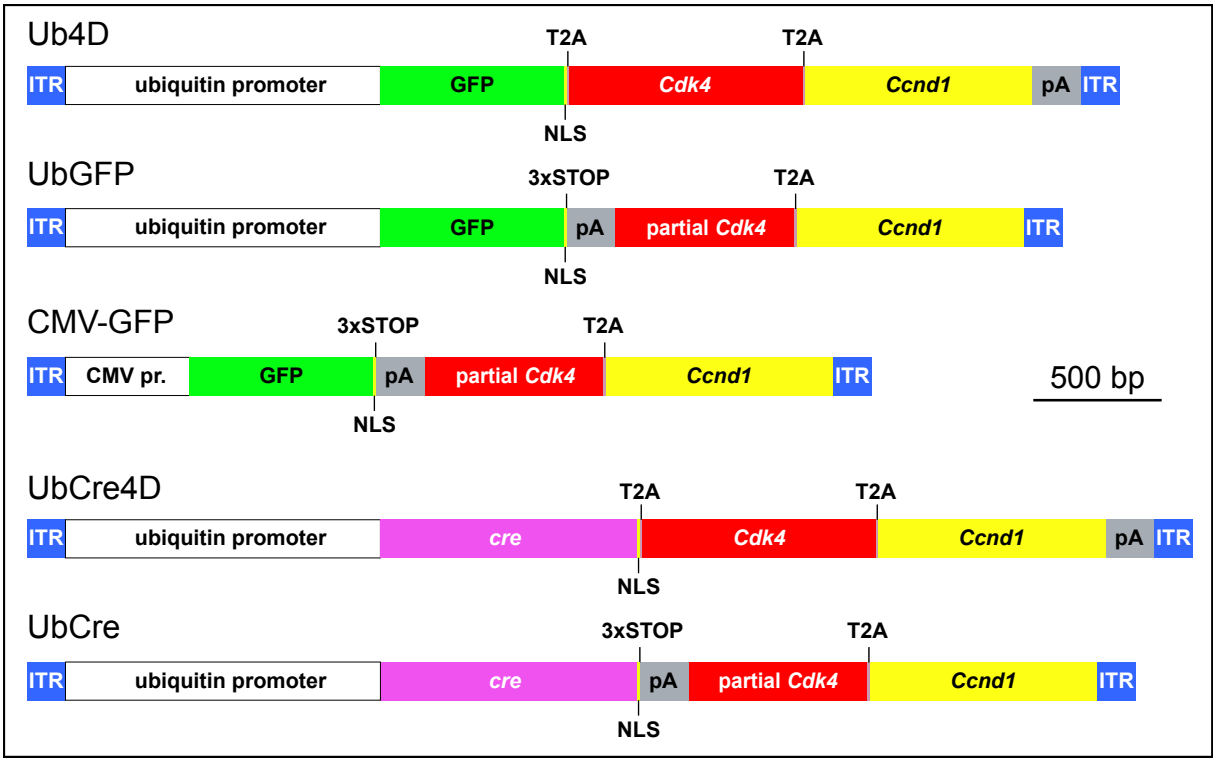

Figure 6: rAAV constructs

rAAV expression cassettes of all cloned constructs in scale are shown.

2.2.2 rAAV

2.2.2.1 Cell culture of AAV293

AAV293 cells were purchased from Stratagene (La Jolla, USA) and thawed in a 37˚C water bath. The cell suspension was mixed by pipetting up and down and then added to 10 ml DMEM growth medium and centrifuged at 200 g for 3 min at room temperature (RT). The resulting cell pellet was resuspended in new DMEM growth medium and cells were cultured at 37˚C and 5.0 % CO_2. When reaching a confluence of ~50 %, cells were washed once with PBS and then detached from the cell culture vessel by adding Trypsin/EDTA for 2 min at 37˚C. Cells were flushed off with DMEM growth medium, pellet by centrifugation at 200 g for 3 min at RT and then distributed into a new vessel at a split ratio of approx. 1:10. Alternatively, cells were frozen (~10^6 cells/vial) in freezing medium and cryo vials for long-term storage.

2.2.2.2 $CaPO_4$ transfection

Twenty-four hours prior to $CaPO_4$ transfection, AAV293 cells were detached as described above, counted with a hemocytometer and ~3x10^6 cells per 10 cm dish were seeded in 10 ml DMEM growth medium. Plasmids for transfection (pAAV, pHelper and one of the serotype plasmids pRC2, pRC9, pRCrh10 or pRCr3.45, 5 µg per plasmid per 10 cm dish) were adjusted to a concentration of 1 µg/µl with TE pH 7.5 and diluted in 1 ml 0.3 M $CaCl_2$ per 10 cm dish. Subsequently, the $CaCl_2$-DNA mixture was added dropwise to 1 ml of 2xHBS buffer, mixed

gently and then added dropwise to the 10-cm dish containing 10 ml DMEM growth medium and the AAV293 cells seeded the day before. The medium was replaced with new DMEM growth medium 7-8 hours after transfection and the cells were incubated at 37˚C and 5.0 % CO_2 for a total of 72 hours after transfection.

2.2.2.3 rAAV harvest and purification

Seventy-two hours after transfection, 125 µl 0.5 M EDTA pH 8.0 per 10-cm dish was added to the cells and they were incubated for 10 min at RT. Then, cells were flushed off the dishes, collected in tubes together with the DMEM growth medium and pelleted at 300 g for 3 min at RT. After a washing step with PBS and another centrifugation at 300 g for 3 min at RT, the cells were resuspended in 500 µl AAV lysis buffer per 10 cm dish. Cells were lysed with four freeze/thaw cycles using a dry-ice/ethanol bath and a 37˚C water bath. After each thawing step, cells were additionally vortexed for 30s. Next, cell debris was pellet at 2,500 g for 15 min at 4˚C and the supernatant (i.e. cell lysate) was treated with 100 U Benzonase per dish for 1 h at 37˚C. Followed by another centrifugation at 2,500 g for 15 min at 4˚C, the supernatant was loaded on top of an Iodixanol gradient comprised of four layers from top to bottom:

8 ml 15 % iodixanol solution
6 ml 25 % iodixanol solution
8 ml 40 % iodixanol solution
5 ml 60 % iodixanol solution

The ultracentrifuge tubes were sealed and subsequently centrifuged at 63,000 rpm for 2 h at 4˚C using a 70Ti fixed-angle rotor. The ultracentrifuge tubes were then penetrated with an 18G needle at the interphase between the 40 % and 60 % layer. Fractions of ~1 ml were collected with the needle facing bevel up. Identification of rAAV containing fractions was done by measuring the refractive index of each fraction and the ones with a refractive index between 1.4000 and 1.4199 were pooled. The pooled fractions were filled up to 15 ml with PBS and loaded onto an Amicon Ultrafilter 15 ml 100k MWCO tube and centrifuged at 4,000 g for 1 min at 4˚C. Centrifugation was repeated until the remaining liquid level in the top of the tubes was ~1 ml, then it was filled up to 15 ml with PBS again. This step was repeated another three times resulting in a total of four washing steps and a reduction of the iodixanol concentration to <0.001 %. At the end, the rAAV solution was concentrated to a final volume of ~200 µl, aliquoted and stored at -80˚C.

2.2.2.4 rAAV quantitative PCR (qPCR) titration

rAAV sample preparation for qPCR titration

For determining the titer of the rAAVs, they were first treated with DNase I to degrade any extraviral DNA using the following pipetting scheme:

2 µl	rAAV sample
1 µl	10xDNase I buffer
1 µl	DNase I (2U/µl)
6 µl	H_2O

The samples were incubated for 30 min at 37˚C. Then, DNase I was inactivated by adding 1 µl 50 mM EDTA pH 8.0 and incubation for 10 min at 75˚C. After briefly chilling the sample on ice, rAAV particles were broken open by adding the following proteinase K reagents:

6.5 µl	H_2O
2 µl	100 mM Tris/HCl, pH 8.0
0.5 µl	proteinase K (20 µg/µl)

After incubation at 55˚C for 1 h, proteinase K was heat-inactivated at 95˚C for 10 min. The sample was then stored on ice until the qPCR.

qPCR

For rAAV qPCR titration, the following mix was used

10 µl	2x iQ SYBR Mix
4.9 µl	H_2O
0.05 µl	100 µM primer fw
0.05 µl	100 µM primer rev
5 µl	sample

For detecting the packaged rAAV genome, either GFP or Cre primers were used. Each sample was run in technical triplicates using the following program:

1. Initial Denaturation
   - 95˚C 10 min
2. Amplification (40 cycles)
   - 95˚C 30 s
   - 60˚C 30 s (read fluorescence)
   - 72˚C 60 s
3. Dissociation curve
   - 95˚C 60 s
   - 55˚C 30 s
   - *continuously increasing temperature and fluorescence reading*
   - 95˚C 30 s

rAAV titer was determined using a standard curve of GFP or Cre plasmid, respectively.

2.2.2.5 SDS-PAGE and silver staining of purified rAAV

For assessing the purity of the purified rAAV particles, SDS-PAGE followed by silver staining was conducted. To this end, at least 10^9 rAAV particles were diluted with an according volume of 2x Laemmli buffer and heated at 95˚C for 5 min before loading on the gel. The SDS-PA gel was a 4-12 % Bis-Tris gel (NuPAGE™) purchased precast from ThermoFisher Scientific and the samples were run at 200V for 1 h in MOPS buffer.

Silver staining is a very sensitive method to detect very small amounts of protein in a SDS-PA gel and the protocol used was adapted from Chevallet et al., 2006.

The gel was first fixed in fixation solution for 30 min followed by over night (up to 24 h) continued fixation with new fixation solution. The next day, the gel was rinsed twice in 20 % ethanol for 10 min each and then twice in H_2O for 10 min per wash. Subsequently, the gel was sensitized for 1 min in 0.02 % (w/v) $Na_2S_2O_3$ followed by two one minute washes with water and impregnation of the gel with 12 mM $AgNO_3$ for 20 min. For revealing the silver staining, the gel was first dipped into water for 10 s and then transferred to basic developer. The most intense bands usually started appearing within a few minutes, but depending on the amount of protein and the desired degree of staining, developing was continued up to 45 min. The reaction was then stopped by transferring the gel to the stop solution for 30 min. Finally, the gel was washed twice with water for 30 min each and then stored in water until imaging.

2.2.3 Immunohistochemistry

Free floating staining was performed on 40 µm vibratome brain sections stored in CPS at -20˚C. Sections were first washed twice in PBS for 10 min each and then blocked using blocking solution for 1.5 h at RT, followed by incubation with the primary antibodies over night in antibody solution at 4˚C. After 3 washes with PBS for 5, 10 and 15 min, respectively, secondary antibody staining was performed in antibody solution in the dark for either 4 h at RT or over night at 4˚C. Donkey serum and secondary antibodies were centrifuged for 10 min at 16,000 g at 4˚C before every use. In all subsequent steps, the sections were always kept in the dark to prevent bleaching of the fluorophores. Next, the sections were washed once for 10 min with PBS followed by incubation with DAPI (1:1000 in PBS) for 10 min and finally washed another three times with PBS for 5, 10 and 15 min, respectively. Sections were mounted on glass slides, and covered with cover slips using AquaPolymount. Until imaging, the slides were stored in the dark at 4˚C.

For BrdU staining, the following steps after primary antibody (all antibodies except for BrdU antibody) incubations and the PBS washes were included. Sections were post-fixed with 4 % PFA for 30 min and then washed three times for 10 min each with PBS. DNA was exposed by incubation with 37˚C pre-warmed 2M HCl for 25 min followed by three washes for 5, 10 and 15 min, respectively with PBS. After incubation in quenching solution for 20 min, sections were

washed again three times with PBS for 5, 10 and 15 min, respectively. Another blocking with blocking solution was performed for 1 h at RT before incubation with the primary anti-BrdU antibody in antibody solution at 4˚C over night. The remaining protocol was the same as for a normal staining after the primary antibody incubation.

For EdU staining, there were also additional steps introduced after primary antibody incubation and the PBS washes. The tissue was post-fixed with 4 % PFA for 30 min followed by two 10 min wash steps in PBS + 3 % (w/v) BSA. Quenching was performed as in the BrdU protocol and after another 10-minute wash step with PBS + 3 % BSA, sections were permeabilised with 0.5 % triton-x 100 in PBS for 1 h. Next, two washes with PBS + 3 % BSA were performed and then the EdU Click-iT reaction mix was added for 30 min. This and all subsequent steps were done in the dark to prevent bleaching of the fluorophore. After one more wash step with PBS + 3 % BSA for 10 min and two washes with PBS for 10 min each, the standard protocol was continued with secondary antibody incubation (see above).

2.2.4 Animals

Animals were housed in standard cages with a 12h:12h light:dark cycle and had access to water and food ad libitum. All procedures were performed according to local regulations (TVV13/2016 and TVV39/2018).

2.2.4.1 Stereotaxic injection

For rAAV or Endothelin-1/L-NAME injection, a stereotaxic system was used (Kopf Instruments). Mice were anaesthetised in a chamber filled with oxygen and 3 % isoflurane and then mounted on the stereotaxic frame with continuous supply of the oxygen/isoflurane mixture for sustained anaesthesia. The body was placed on a heating pad to ensure maintenance of the body temperature during the surgery. The head was fixed using the ear bars and mice were injected with 100 µl painkiller (carprofen) subcutaneously. Eyes were prevented from drying out by applying protective creme and the head was shaved with a scalpel after ethanol disinfection before the skull was exposed by a small surgical incision on top of the head. After identification of bregma and adjusting the mouse's head in a flat orientation, coordinates for the respective injection location were marked and a ~1 mm hole was drilled (Table 11). A glass capillary mounted on a microinjector pump was filled with paraffin oil, PBS and then virus or ET-1 and slowly inserted into the brain until the respective depth needed. After injecting the required volume and 5 minutes waiting time, the capillary was slowly pulled out and the skin was closed using surgical single stitches. After applying antiseptic solution on top of the skin, the mouse was released from the frame and placed into its cage under red light until waking up under surveillance.

Table 11: Coordinates for stereotaxic injections

Targeted area	Coordinate direction	Coordinates (in mm from bregma)	Injected volume and speed
Dentate gyrus rAAV injection	medial-lateral	± 1.600	1000 nl, 200 nl/min
	anterior-posterior	- 1.900	
	dorsal-ventral	- 1.900 (from pia)	
Lateral ventricles rAAV injection	medial-lateral	± 0.700	4000 nl, 250 nl/min
	anterior-posterior	+ 0.400	
	dorsal-ventral	- 2.500 (from pia)	
Striatum ET-1 single injection	medial-lateral	± 1.800	500 nl, 100 nl/min
	anterior-posterior	+ 0.700	
	dorsal-ventral	- 3.000 (from pia)	
Striatum ET-1 double injection	medial-lateral	(I) ± 1.500 (II) ± 1.800	500 nl, 100 nl/min at each site
	anterior-posterior	(I) + 1.100 (II) + 0.200	
	dorsal-ventral	(I) - 2.500 (from pia) (II) - 2.800 (from pia)	

2.2.4.2 Perfusion

At the end of an experiment, mice were anaesthetised with an i.p. injection of ketamine/xylazine and perfused with 4 % PFA as follows. As soon as the mouse reached deep anaesthesia level (no toe-pinching or eye-twitching reflex), needles were poked through its fore limbs to fix it on a styrofoam board. The thorax was opened and the still beating heart was exposed and a blunt needle connected to a pump was inserted into the left ventricle. A small incision in the right atrium was made and then 0.9 % (w/v) NaCl solution pumped through the blood vessel system. After ~50 ml of saline solution, the pump was switched to 4 % PFA for fixation of the mouse. Once the body was stiff, perfusion was stopped, the mouse dissected and the brain was stored in 4 % PFA over night at 4˚C. The next day, the brain was washed twice with PBS and then stored in PBS at 4˚C until it was cut in 40 µm sections using the vibratome.

2.2.4.3 Novel object recognition (NOR) task

In the NOR task, certain aspects of learning and memory can be assessed (Lueptow, 2017). Mice were placed individually into a multi-conditioning box (TSE) with a square-shaped arena and a camera on top. On the training day, two identical objects were placed in two opposite corners and mice were positioned into one of the other corners and subsequently allowed to

explore the environment freely for 5 min. The time the animal was exploring either of the objects was recorded. The next day, one of the two objects was exchanged with a different one and mice were again exploring for 5 min and exploration time was recorded. The same procedure was repeated with another new object on the next day. The training object that was considered the old object on the second and third day was a water filled 250 ml glass bottle with a blue lid, the first new object a pink liquid filled 250 ml glass bottle with a green lid and the new object on the last day was a water filled 250 ml plastic bottle with an orange lid.

2.2.4.4 Corner test

The corner test was originally developed by (Zhang et al., 2002) to assess sensorimotor dysfunction after unilateral brain damage caused by ischemic stroke. The setup was built based on the modifications made by (Hao et al., 2008). A parallelogram-shaped box with angles of 30˚ and measures of 20x35x20 cm (length x width x height) was built in-house and mice were tested during their night cycle for more active behaviour.

A mouse was placed in the middle of the box and filmed from top under red light. Once the mouse approached one of the two narrow corners ten times with a clear result of turning either left or right, the trial was finished. The video analysis was conducted blinded regarding the treatment of the mouse and the read-out was percentage of ipsilateral turns relative to the stroke/PBS injected hemisphere.

2.2.4.5 Catwalk

The Catwalk system (Noldus) is typically used in quantitative analysis of gait and locomotion of mice and rats. It consists of a 1.2 m long glass platform with green light shining through its side. A corridor is created by two adjustable walls and there is red light on top for optimal contrast for the camera attached to the system below. The mouse is placed on one end of the corridor whereas there is a goal box on the other side containing a hole in the bottom leading to its home cage. When the mouse walks over the glass platform, the green light is deflected down which is dependent on how much weight the mouse is putting on each paw. The catwalk system automatically detects the mouse and films the run, enabling later software-supported analysis of a plethora of parameters related to gait analysis (e.g. speed, pressure of each paw, stride length, paw placement etc).

The following three days training protocol before stroke was established. The first day, mice were allowed to freely explore the catwalk for three trials with two min each introducing them to the goal box at the end of each run. The day after consisted of a total of five trials. The first two were again free exploration trials of one minute each. The last three trials, mice were not allowed to turn around anymore and if they did, the trial was aborted and mice were guided to the goal box. The goal was to have the mouse run once across the glass platform without

stopping or turning around in between since this would cause a “non-compliant” trial for the software and would require repetition. The last day of training was also used as baseline values for after stroke. On this day, mice had to complete 6 compliant trials (running in one direction only) with an average speed of at least 25 cm/s and less than 60 % speed variance. Once this was achieved, stroke could be induced the following days and mice were subsequently tested once per week with the same requirements as on day three of training.

2.2.4.6 Rotarod

The accelerating rotarod (Intelli-Bio) was used for assessing motor coordination of mice after stroke. It consisted of a cylinder with ~3 cm diameter that was separated by 20 cm diameter disks into 5-6 cm wide lanes. The cylinder had a rough surface enabling good grip for the mice. This setup was built 20 cm above a platform used to detect the fall of the animal. The cylinder was set to a starting speed of 3 rpm and once all mice of one trial were placed into their respective lane facing forward, the trial was started. This caused the rotarod to constantly accelerate over the total trial length of 300 s reaching an end speed of 30 rpm. A trial was finished once all mice either fell within these 300 s or managed to stay on the cylinder for 20 s at the maximum speed. As a readout, the time a mouse managed to stay on the cylinder was used and expressed as “latency to fall” in s.

Different training protocols were tested varying the number of trials per day (3 or 5), the number of training days (3 or 4) and increasing the acceleration after two days. In all cases, an inter-trial-interval of at least 15 min was maintained and this interval was kept constant throughout one experiment. After training, mice were separated into groups ensuring a similar average value and standard deviation of all groups before stroke. Mice that did not manage to reach at least 100 s at the last day of training or did not show improvement over the course of the four days were excluded. The surgery was usually performed 3-4 days after the last day of training followed by weekly rotarod testing starting at day 7 after surgery.

3. RESULTS

3.1 Establishment of a rAAV purification system for *in vivo* transduction of NSCs

The first goal was to establish and optimize a production and purification protocol for rAAVs (Figure 7) suitable for many serotypes in order to identify one that allowed the efficient transduction of NSCs *in vivo* (adapted from (Strobel et al., 2015)).

For production, the cell line AAV293 was used which had been derived from conventional HEK293 cells by selection for a larger cell surface, flattened morphology and a firm attachment to cell culture vessels in order to enable high titer rAAV production. The cells were transfected with three plasmids: the transgene carrying plasmid (pAAV), the serotype defining plasmid (pRC) and a 'helper' plasmid (pHelper) expressing essential AAV proteins. The $CaPO_4$ transfection was compared to the PEI transfection to determine which method resulted in a higher produced rAAV titer. Titration of viral particles by qPCR showed $CaPO_4$ as the better transfection method which was further optimised considering the following parameters: (I) pH-value of the $CaPO_4$ solution, (II) seeding density of cells and (III) plasmid concentration.

After rAAV production in the AAV293 cells (Figure 7A), the mainly intracellularly residing rAAV particles were released by lysing the cells via freeze/thaw cycles. Following DNase treatment, the cell lysate was subjected to a layered iodixanol gradient which is commonly used for separation and purification of cell organelles, vesicles and viruses. Here, it was used to isolate the packaged rAAV particles from empty virus capsids and the cell lysate. Subsequently, the iodixanol gradient was ultracentrifuged, the clear colourless 40 % iodixanol layer was collected in fractions and the refractive index of each fraction was measured. DNA-packaged rAAV particles reside in the 40 % iodixanol layer as opposed to empty capsids that accumulate in the lower end of the 25 % layer (Strobel et al., 2015). Therefore, the refractive index allowed to draw precise conclusions about which fractions contained 40 % iodixanol and which had impurities from layers above or below. Corresponding fractions were collected, pooled and concentrated. The purity of rAAV containing fractions and of the final concentrate was assessed using SDS-PAGE and subsequent silver staining, indicating that the pooled fractions indeed showed the three bands of the main AAV proteins (viral protein 1, 2 and 3, Figure 7B). As an additional quality control, the titer of the rAAV particles was routinely assessed using qPCR (Figure 7C).

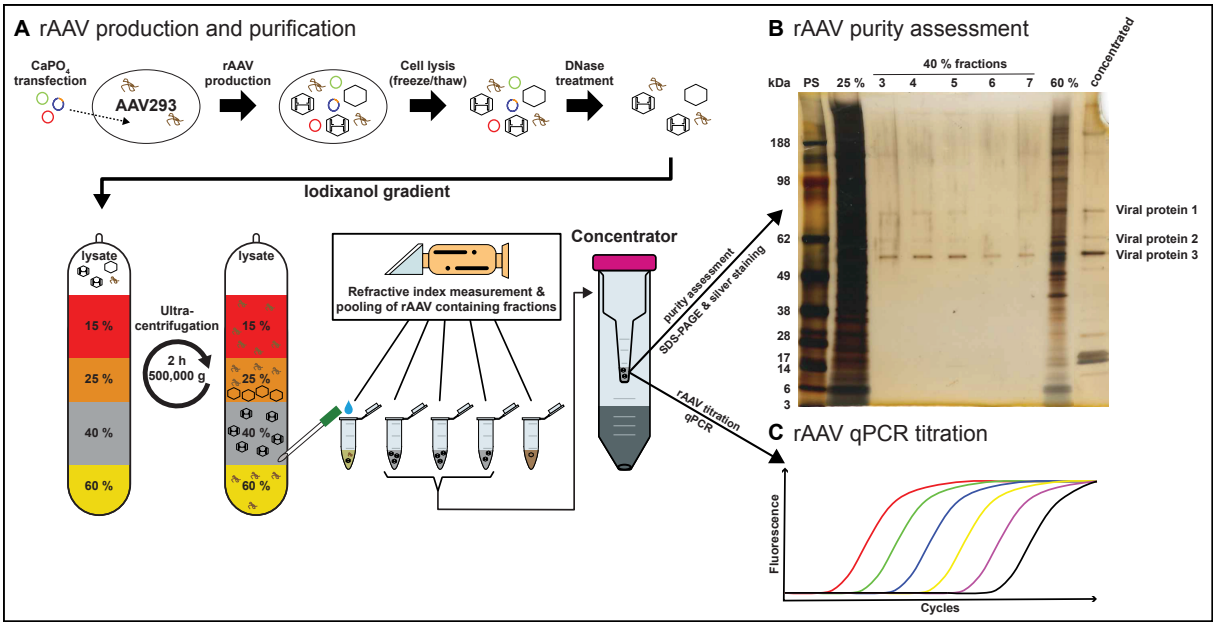

Figure 7: Production and purification of rAAVs

(A) Schematic of $CaPO_4$ transfection for rAAV production followed by purification via iodixanol ultracentrifugation. (B) Silver stained SDS-PA gel of iodixanol fractions after rAAV purification. PS: pre-stained marker. (C) Sketch of an amplification plot after rAAV qPCR titration.

Using the method described above (Figure 7), four rAAV serotypes were generated yielding titers ranging from $5x10^8$ genome copies (GC)/µl up to $1x10^{10}$GC/µl. High titer rAAVs were diluted so that all used viruses were in a comparable range.

rAAVs have variable but usually low transduction efficiencies *in vitro* regarding different cell lines depending on the serotype (Ellis et al., 2013). Therefore, a comparison of the produced serotypes after qPCR titration was directly conducted *in vivo*.

3.2 rAAV-4D increases SVZ NSC proliferation and OB neurogenesis

For the first rAAV *in vivo* tests, a UbGFP expression cassette was cloned (Figure 8A). It contained the constitutive human ubiquitin C promoter driving GFP expression that was tagged with a nuclear localisation signal (NLS) for more precise quantification of transduced cells. Up- and downstream of this expression cassette were the necessary inverted terminal repeats (ITR) of AAV2 that allowed packaging into the rAAV particles. Stereotaxic injection of rAAVs into the ventricle of adult mice (Figure 8B) resulted in GFP^+ cells only for serotype r3.45 among all the tested serotypes after one week (Figure 8D). Interestingly, although injection was done in only one hemisphere, the contralateral hemisphere also showed GFP^+ cells lining the ventricle walls indicating a wide distribution of the rAAV particles within the ventricle after injection. A first analysis demonstrated that rAAVr3.45 transduced 1.94 ± 0.59 % of all SVZ NSCs that were identified as $Nestin^+$ and $S100\beta^-$ (Figure 8E).

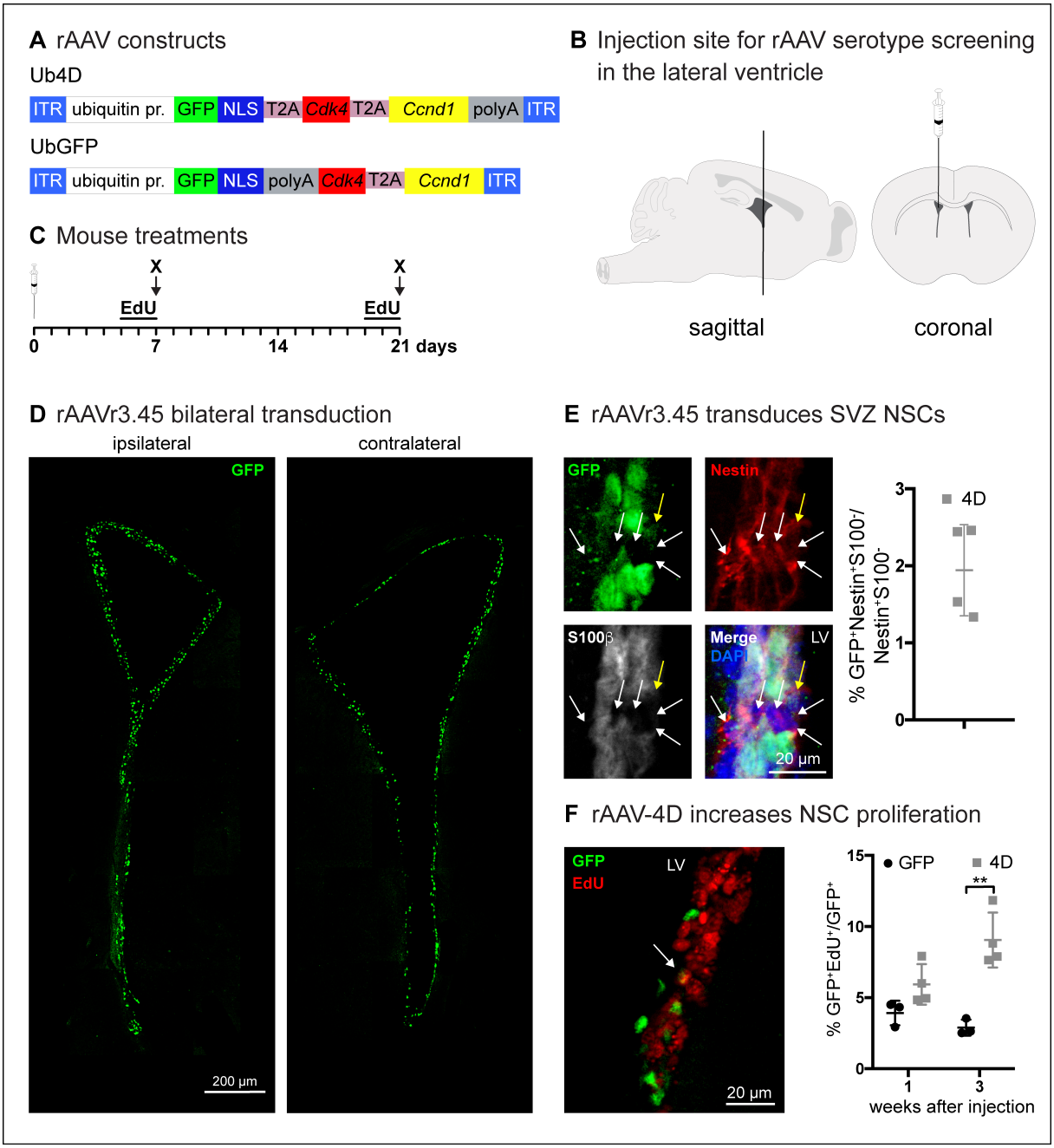

Figure 8: rAAV SVZ NSC transduction and 4D-mediated increase in NSC proliferation

*(A) Constructs used for rAAV ventricle injections. Ub4D coding for GFP and 4D overexpression whereas UbGFP only coded for GFP expression. (B) Schematic sagittal and coronal view of rAAV ventricle injection. (C) Timeline of mouse treatments in this experiment. 'X' indicates time points of sacrifices, EdU i.p. injections were given twice per day. (D) GFP$^+$ (green) cells after rAAV transduction in both ipsi- and contralateral hemisphere. (E) Non-transduced NSCs (Nestin$^+$ (red) and S100β$^-$ (white) cells) are indicated with white arrows and GFP$^+$ NSCs with a yellow arrow (LV = lateral ventricle). Quantification of transduced NSCs is shown as average ± standard deviation (SD). (F) Transduced (GFP$^+$, green) EdU$^+$ (red) cells were quantified one and three weeks after injection. Average ± SD is shown in all graphs. **p<0.01, student's t-test using Holm-Sidak correction.*

In order to assess the effect of rAAV-mediated 4D overexpression, a Ub4D construct was cloned (Figure 8A). In this construct, the coding sequences of cdk4 and cyclinD1 were inserted after the NLS-tagged GFP and all three proteins were separated by two self-cleaving T2A peptides enabling an equimolar expression while ensuring that they were separated into three proteins. This expression strategy had already been used successfully in our lab using lentiviral transduction of SGZ NSCs and was adapted for the rAAV construct (Artegiani et al., 2011; Berdugo-Vega et al., 2020). The corresponding control construct UbGFP contained the same elements as Ub4D, however, after the NLS-tag, three stop codons were introduced followed by the polyA sequence, ensuring that both transcription (polyA) and translation (stop codons) stopped before the *Cdk4*-T2A-*Ccnd1* fragment. Additionally, *Cdk4* was only partially present and the whole fragment was out-of-frame with regard to the GFP reading frame. This strategy was chosen to make the UbGFP control construct on DNA level as similar to the Ub4D construct as possible both in length and sequence without expressing 4D.

For investigating the proliferation of SVZ NSCs, mice were injected i.p. with EdU the last two days before sacrifice either one or three weeks after rAAV injection (Figure 8C). When comparing GFP vs 4D injected animals, there was a threefold increase in proliferation from 2.90 ± 0.56 % to 9.05 ± 1.93 % (p=0.0033, multiple t-test with Holm-Sidak correction) of transduced EdU^+ cells among all transduced cells after three weeks (Figure 8F). Of note, this analysis included both proliferating NSCs and progenitors since EdU is taken up by any cell in S phase within the 48 hours of EdU administration.

Furthermore, the percentage of transduced DCX^+ differentiating neuroblasts in the SVZ was similar for GFP and 4D animals both after one or three weeks (13.44 ± 3.07 % vs 11.35 ± 2.99 % after one week, 14.13 ± 5.59 vs 15.40 ± 4.84 % after three weeks, Figure 9B). Since differentiating cells migrate along the RMS towards the OB, changes in neuronal output were assessed by quantification of $BrdU^+$ newborn neurons in the OB birthdated the third week after rAAV injection (Figure 9A), where the peak in proliferation was observed (Figure 8F). Four weeks later, the number of total $BrdU^+$ cells per volume in the granule cell layer of the OB showed a remarkable increase by 44.19 % for 4D injected animals ($0.93x10^5 \pm 0.19x10^5$ cells per mm^3 vs $1.34x10^5 \pm 0.11x10^5$ cells per mm^3, p=0.0095, student's t-test with Holm-Sidak correction, Figure 9C). Since this quantification was conducted irrespective of infected cells, this result is an underestimation of the magnitude of the 4D effect on OB neurogenesis. Concluding, rAAVr3.45 transduced SVZ NSCs (Figure 8E) and rAAV-mediated 4D overexpression increased their proliferation (Figure 8F) resulting ultimately in more newborn neurons in the OB (Figure 9C).

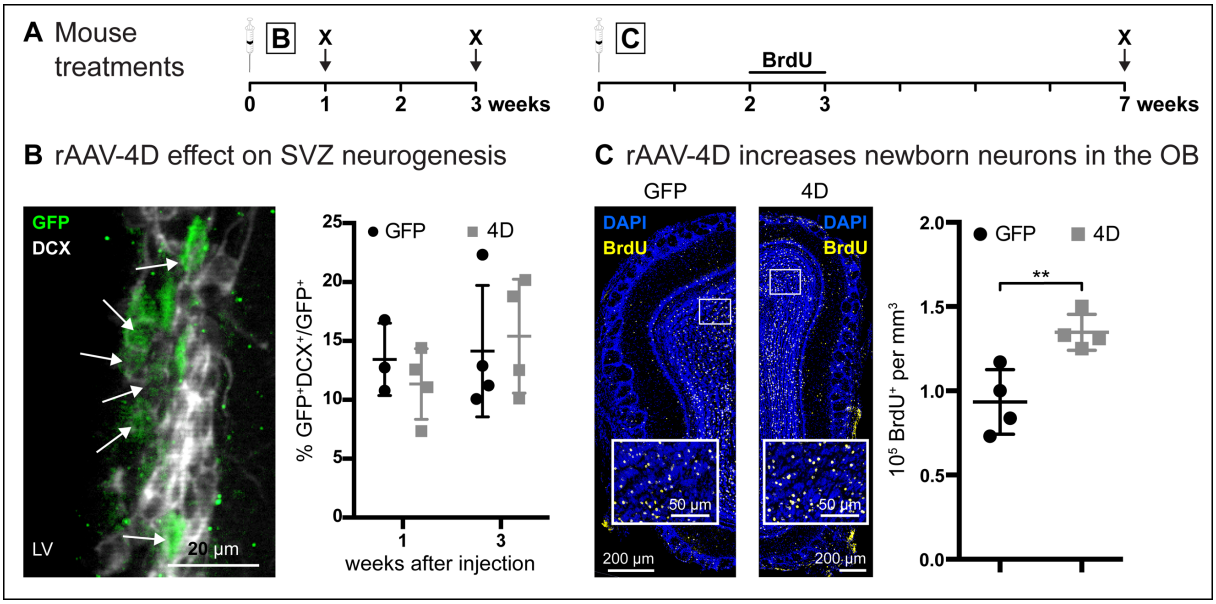

Figure 9: rAAV-4D mediated increase in olfactory bulb neurogenesis

*(A) Timeline of mouse treatments in this experiment. 'X' indicates time points of sacrifices, BrdU i.p. injections were given twice per day. (B) Transduced (GFP$^+$, green) DCX$^+$ (white) cells were quantified one and three weeks after injection. (C) BrdU$^+$ (yellow) cells in the olfactory bulb were quantified 7 weeks after injection. Average ± SD is shown in all graphs. **p<0.01, student's t-test using Holm-Sidak correction.*

Of note, there were no GFP$^+$ cells present neither in the RMS nor in the OB in any injected animal. One explanation for this unexpected result could be that rAAVs and the GFP concomitantly get diluted out over cell divisions of the differentiating cells while migrating towards the OB. To address this hypothesis, a Cre-lineage tracing approach was used (Figure 10). To this end, the well-established Confetti mouse line (Snippert et al., 2010) was used as a reporter (Figure 10B).

For this lineage tracing experiment, UbCre4D was cloned which contained the same elements as Ub4D except for Cre recombinase instead of GFP (Figure 10A). rAAVr3.45 with UbCre4D was injected into the ventricle and three weeks later, animals showed fluorescent protein expression (YFP shown as an example) not only in the SVZ (Figure 10C) but also in the RMS (Figure 10D) and OB (Figure 10E). Therefore, rAAVs and/or GFP seem to get diluted out over the differentiation of SVZ NSCs and the migration process of their progeny.

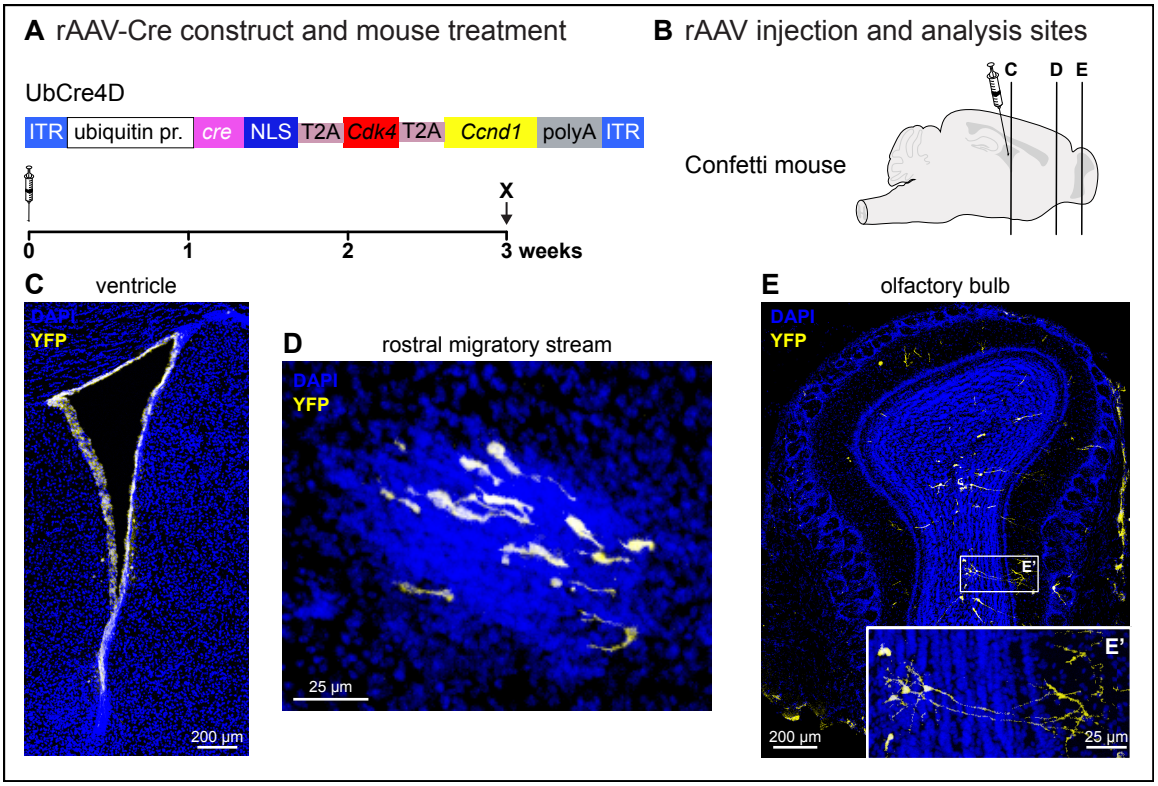

Figure 10: Cre-lineage tracing in Confetti mice after rAAV-UbCre4D ventricle injection
(A) rAAV-UbCre4D containing Cre instead of GFP. Mice were injected into the ventricle and sacrificed three weeks later ('X'). (B) Schematic sagittal view of rAAV ventricle injection. (C) YFP$^+$ cells three weeks after rAAV injection into the ventricle that have migrated via the RMS (D) towards the OB (E).

3.3 Two rAAV serotypes efficiently transduce SGZ NSCs

Besides the SVZ, the four produced rAAV serotypes were also tested for transduction of SGZ NSCs. Here, a CMV-GFP and the UbGFP control construct were used to also investigate the influence of the promoter on the apparent transduction efficiency of the rAAV serotypes (Figure 11A). CMV-GFP expressing rAAVs were stereotaxically injected into the hippocampus of adult mice (Figure 11B) and all serotypes resulted in different GFP expression patterns that were qualitatively assessed (Figure 11C). While serotypes 9 and rh10 showed a high preference for cells in the hilus, serotype 2 was more efficient in transducing cells in the granular cell layer (GCL). Of note, rAAV9 was the only serotype that yielded a much higher titer after purification ($1x10^{10}$ GC/µl as compared to $5x10^8$ GC/µl of the other serotypes), and when injecting a high titer rAAV9, there were also more GFP$^+$ cells observed in the GCL (data not shown).

Thus, serotype 9 and the previously for SVZ NSCs used serotype r3.45 were injected in a second round of testing. Here, the UbGFP construct was used instead of CMV-GFP. For both serotypes 9 and r3.45, the majority of cells in the GCL were GFP$^+$ additional to the hilus (Figure 11D). Sox2$^+$ cells were used to identify NSCs in the SGZ and the two serotypes showed a transduction rate of 14.33 ± 0.95 % (r3.45) and 12.45 ± 2.15 % (9) of NSCs when normalised to all GFP$^+$ cells (Figure 11E).

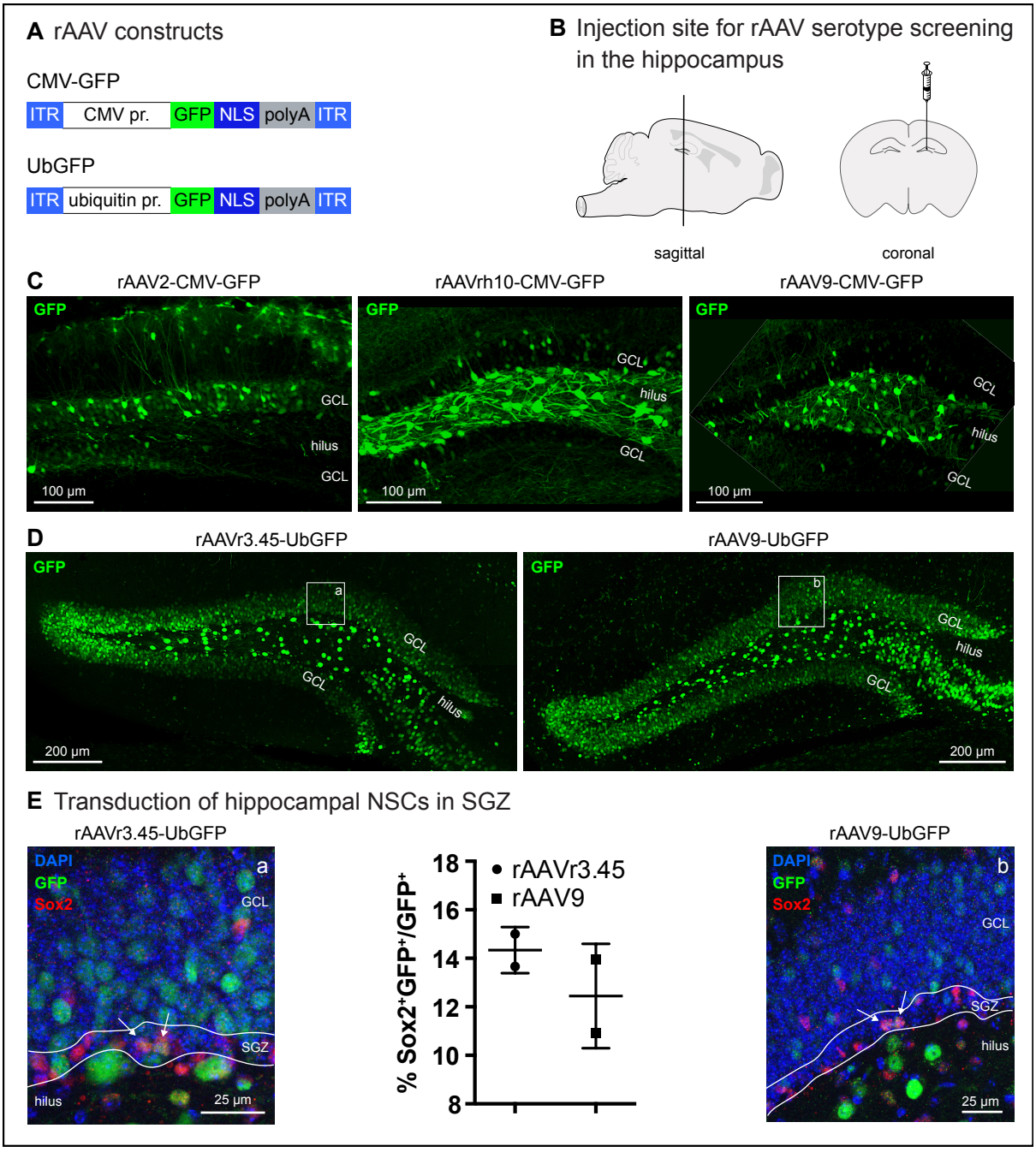

Figure 11: rAAV serotype screening for NSC transduction in the hippocampal SGZ

(A) rAAV constructs used in this experiment. (B) Schematic sagittal and coronal view of rAAV injection into the hippocampus of adult mice. (C) GFP expression (green) of rAAV-transduced cells using the CMV-GFP constructs and different serotypes one week after injection. (D) GFP expression (green) of rAAV-transduced cells using the UbGFP construct of serotypes r3.45 and 9 one week after injection. (E) Quantification of transduced NSCs ($GFP^+/Sox2^+$) normalised to all transduced cells (GFP^+). SGZ = subgranular zone, GCL = granular cell layer. Average ± SD is shown.

The identification of two suitable serotypes for SGZ NSC transduction indicated the usefulness of rAAVs for gene delivery and future experiments are needed to show that rAAV-4D expression in SGZ NSCs would lead to similar results as observed in the SVZ.

3.4 Establishment of an inducible striatum stroke model

There are various stroke models being used in rodents, all of them with their advantages and caveats. Two inducible stroke models were established and assessed both histologically as well as on a behavioural level. In the photothrombotic stroke model, the photosensitive dye Rose Bengal is injected i.p. systemically to the mouse. For a targeted stroke in a specific brain area, cold light has to be shined at that area leading to local blood clot formation and ultimately brain ischemia.

Endothelin-1 (ET-1) on the other hand is a small peptide that can cause local vasoconstriction if injected into the brain. For mice, it has been recommended to combine ET-1 with the NOS inhibitor L-NAME (preventing NOS-induced vasodilatation).

For both stroke models, the striatum was targeted for several reasons. First, the SVZ and its residing NSCs are in close proximity to the striatum which increases the likelihood of migration and potential therapeutic effects upon 4D treatment later on. Furthermore, the effects of stroke and the neurogenic response was not only supposed to be analysed histologically but also on a behavioural level. To this end, the striatum is well known to be important for motor learning and coordination for which there are several tests available for rodents (reviewed in (Balkaya et al., 2013)).

3.4.1 ET-1 stroke causes reproducible ischemic striatal damage

In order to induce local ischemia in the striatum, either an optic fibre was inserted into the striatum for the photothrombotic stroke (in collaboration with Dr. Sara Bragado Alonso in the lab) or a mixture of ET-1/L-NAME was injected stereotaxically (Figure 12A). Three days after surgery, both methods resulted in a dark stained core of ischemic damage and a penumbra of affected tissue surrounding it in a brightfield view (Figure 12B&C). Further histological characterization of the ET-1 stroke revealed massive gliosis ($GFAP^+$ cells) around the whole striatum whereas an invasion of $Iba1^+$ microglia into the striatum was eminent (Figure 12D). DCX^+ neuroblasts could be observed outside the SVZ that had migrated into the stroke-affected area. This effect was not clearly seen after photothrombotic stroke (data not shown) as opposed to ET-1. Thus, further histological analysis was focused on the ET-1 stroke only.

Three weeks after ET-1 stroke, $GFAP^+$ astrocytes had occupied areas in the striatum that were absent of $Ctip2^+$ cells and there were still DCX^+ migrating neuroblasts indicating the further ongoing endogenous stroke response in the brain (Figure 12E). Quantification of these migrating neuroblasts relative to the respective stroke volume (at 3 days post stroke (dps)

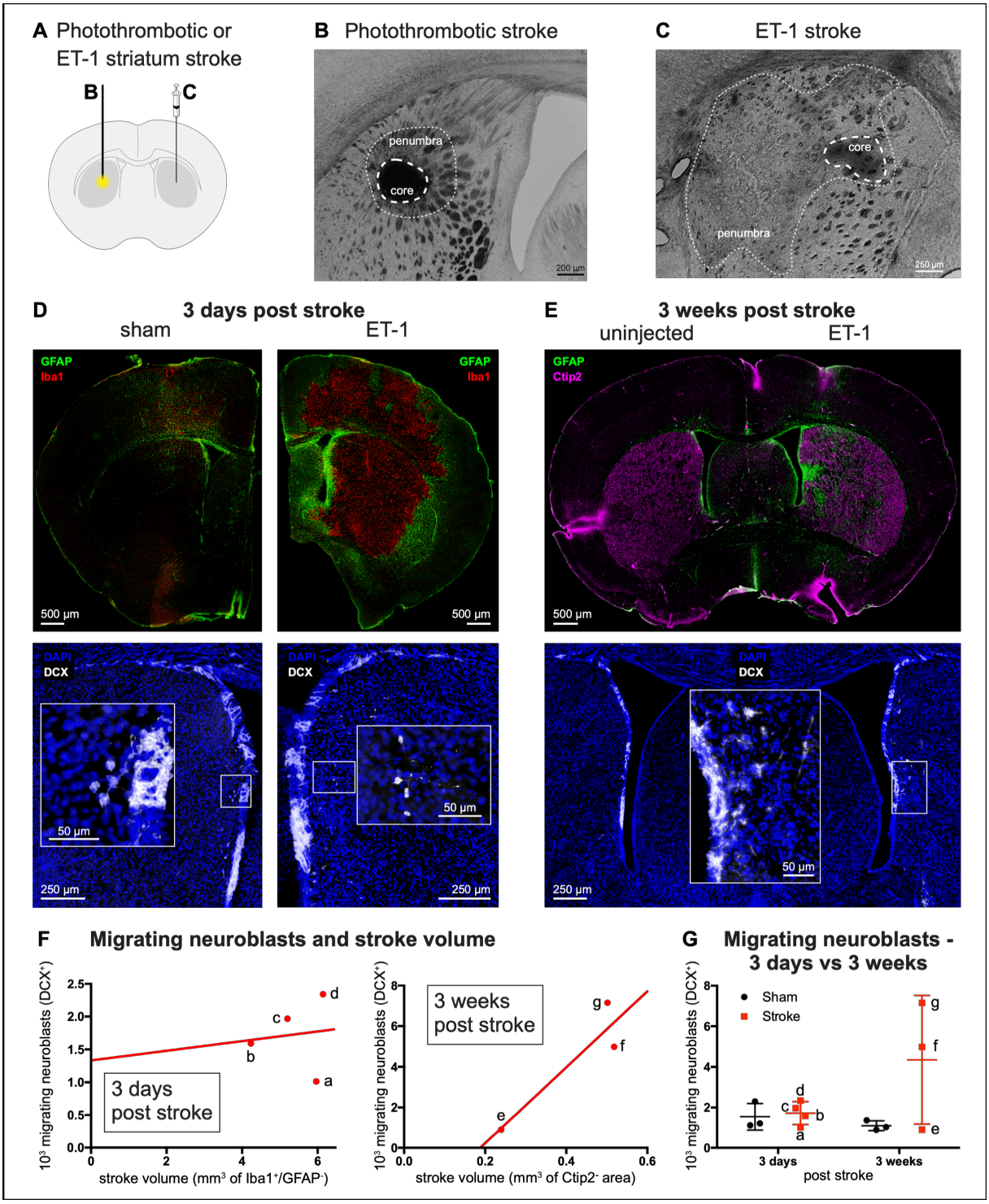

Figure 12: Histology of photothrombotic and ET-1 stroke model in the striatum

(A) Schematic coronal view of stroke site for either photothrombotic (left) or ET-1 stroke (right). Brightfield view of photothrombotic (B, courtesy of Dr. Sara Bragado Alonso) or ET-1 (C) stroke after three days. Core and penumbra of ischemic area are indicated. (D) Astrocytes (GFAP$^+$, green), microglia (Iba1$^+$, red) and neuroblasts (DCX$^+$, white) 3 dps. (E) Astrocytes (GFAP$^+$, green), striatal neurons (Ctip2$^+$, magenta) and neuroblasts (DCX$^+$, white) in the striatum 3 wps. (F) Correlation of stroke volume and migrating neuroblasts after 3 dps and 3 wps, respectively. Note the different assessment of stroke volume based on Iba1$^+$/GFAP$^-$ (3 dps) or Ctip2$^-$ (3 wps) areas. (G) Comparison of migrating neuroblasts at 3 dps and 3 wps in stroke vs sham injected animals. Letters 'a-g' indicate same animals as in (F).

identified as Iba1^{+}/GFAP^{-} area and at 3 weeks post stroke (wps) as Ctip2^{-} area) showed a positive correlation (R^2=0.15 at 3 dps and R^2=0.85 at 3 wps) between neuroblast migration and stroke volume (Figure 12F). Interestingly, there was no difference of migrating neuroblasts in sham vs stroke treated animals 3 dps (1542 ± 656 cells vs 1725 ± 567 cells, p=0.7081, student's t-test with Holm-Sidak correction) but a tendency of elevated migration was seen in stroke animals 3 wps (1096 ± 240 cells vs 4348 ± 3171 cells, p=0.1513, student's t-test with Holm-Sidak correction, Figure 12G).

3.4.2 Behavioural assessment of ET-1 and photothrombotic striatum stroke

As mentioned above, the striatum is an important brain area for motor function. Hence, damage caused by ischemic stroke in that area should lead to impairments of motor coordination and learning. To address this, animals were first trained before and then tested after either photothrombotic or ET-1 stroke on the Catwalk (in collaboration with Dr. Sara Bragado Alonso in the lab). This apparatus allows precise gait analysis by recording the mouse while walking over a glass platform. Green light shining through the sides of this platform is being deflected downwards in a pressure dependent manner where a camera is capturing the green light. Using the provided software, the Catwalk system enabled measurement and analysis of a plethora of parameters that infer different aspects of gait. However, in both stroke models, there were no reproducible differences found in any of the parameters as compared to respective sham-treated animals. Here, the "MaxContactMaxIntensity" is shown as a representative example for each individual paw after one, two and three weeks after stroke as a fold-change compared to the training before ("Baseline", Figure 13A). This parameter describes the maximum intensity of weight the animal puts on the respective paw at the area of maximum contact on each step.

There were two major issues using the Catwalk system ruling it out for future experiments: I) the high variability and low reproducibility of trends in some parameters and II) the possibility that the caused striatum damage was not big enough to show an effect in such a comparably easy task for the mice (walking on a glass platform). Since the ET-1 stroke was histologically more promising (Figure 12D-F), all further behaviour tests were only conducted with this model.

ET-1 injections were always performed unilaterally and a past study (Hao et al., 2008) has shown that unilateral striatal damage leads to a behavioural effect in the so-called corner test (Figure 13B). Here, the mouse is placed into a box with two narrow corners (30˚) and filmed from top while moving freely. During its exploratory behaviour, the animal will approach the narrow corner and when the whiskers on both sides touch the wall, it will rear back, get up on its hind legs and turn around. This turning is performed randomly by healthy animals but is supposed to be biased towards the side of striatal damage in stroke animals (i.e. ipsilateral).

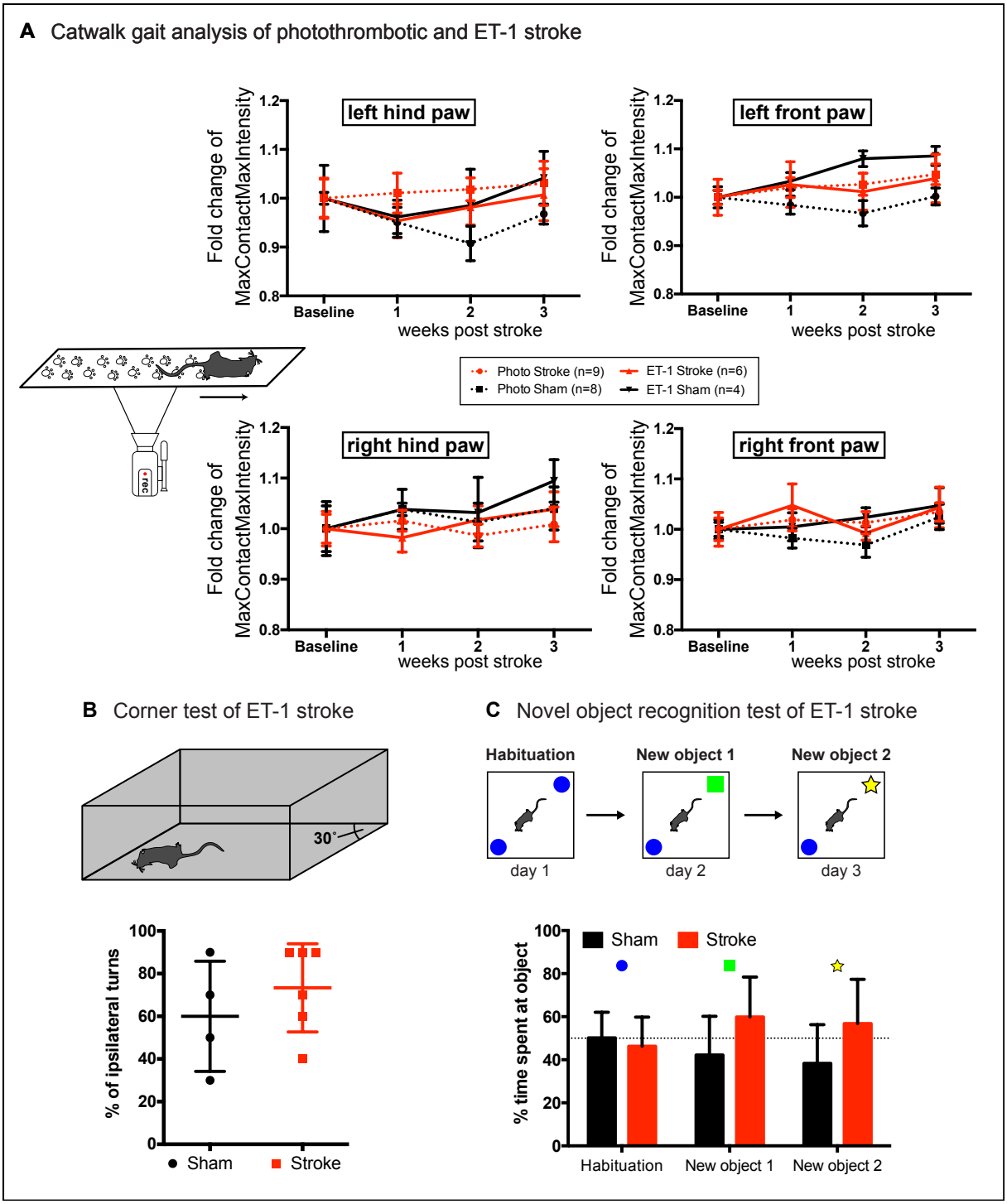

Figure 13: Behavioural assessment of photothrombotic and ET-1 striatum stroke

(A) Catwalk gait analysis after stroke. Fold change of MaxContactMaxIntensity compared to baseline for each individual paw is shown 1, 2 and 3 wps after photothrombotic (dotted lines) or ET-1 (continuous lines) in stroke (red) and sham (black) animals. Data is presented as average ± standard error of the mean (SEM). (B) Percentage of ipsilateral turns of mice was assessed in the corner test for stroke (red) or sham (black) animals 1 wps as average ± SD. (C) Percentage of time spent at object of stroke (red) and sham (black) animals in the novel object recognition task 1 wps is shown as average ± SD.

Yet, this effect could not be observed in this experiment (Figure 13B), mainly due to the high variability among animals (60.00 ± 25.82 % (sham) vs 73.33 ± 20.66 % (stroke) of ipsilateral turns, p=0.4233, unpaired t-test).

Besides motor coordination, the striatum is also involved in certain memory tasks and a commonly used test for striatum-dependent memory is the novel object recognition (NOR) task (Figure 13C). In this test, the animal is first habituated in an experimental box with two identical objects in two opposite corners and the time is measured that the animals takes exploring either of the objects. In following days, a new object replaces one of the two identical ones and the exploration time of the new vs the old object is measured. This task can be repeated as long as new objects that are different to the previous ones are available. Healthy animals are reported to spend more time at new objects due to their curious nature. Mice with impaired striatal memory function are supposed to stay at a 50:50 ratio for both objects as it is thought that they do not remember the old object. Both the habituation as well as the introduction of two new objects were conducted after ET-1 stroke (in collaboration with Dr. Sara Bragado Alonso in the lab, Figure 13C). While during habituation, both groups showed no preference to either of the two identical objects (50.18 ± 11.86 % vs 46.27 ± 13.56 %, p=0.5110, multiple t-test with Holm-Sidak correction), there was a trend of stroke animals spending slightly more time at the new object whereas sham animals spent either the same or less time at the new object (42.18 ± 18.02 % vs 59.89 ± 18.54 % for new object 1, p=0.0500, multiple t-test with Holm-Sidak correction and 38.34 ± 17.98 % vs 56.80 ± 20.55 % for new object 2, p=0.0520, multiple t-test with Holm-Sidak correction, Figure 13C). Besides the small magnitude of this difference, it was the opposite of the expected effect excluding the NOR from further experiments.

Revisiting the motor coordinative functions of the striatum, a more difficult behavioural task compared to the Catwalk was tested. The rotarod consists of a cylinder that the mouse is placed on which then starts rotating in an accelerating manner. With higher speed, this task becomes more and more difficult until the mouse ultimately cannot walk on the cylinder anymore and falls down (Figure 14A). The latency time to fall is the parameter that is measured and mice with striatal damage are supposed to fall earlier than control animals. In a first experiment, mice were tested on the rotarod 8 days after stroke for two subsequent days per week over a course of three weeks with three trials per day (Figure 14B). Both groups showed a similar learning curve although stroke animals always performed slightly worse, both during learning and after reaching the plateau phase (p=0.1534, two-way ANOVA).

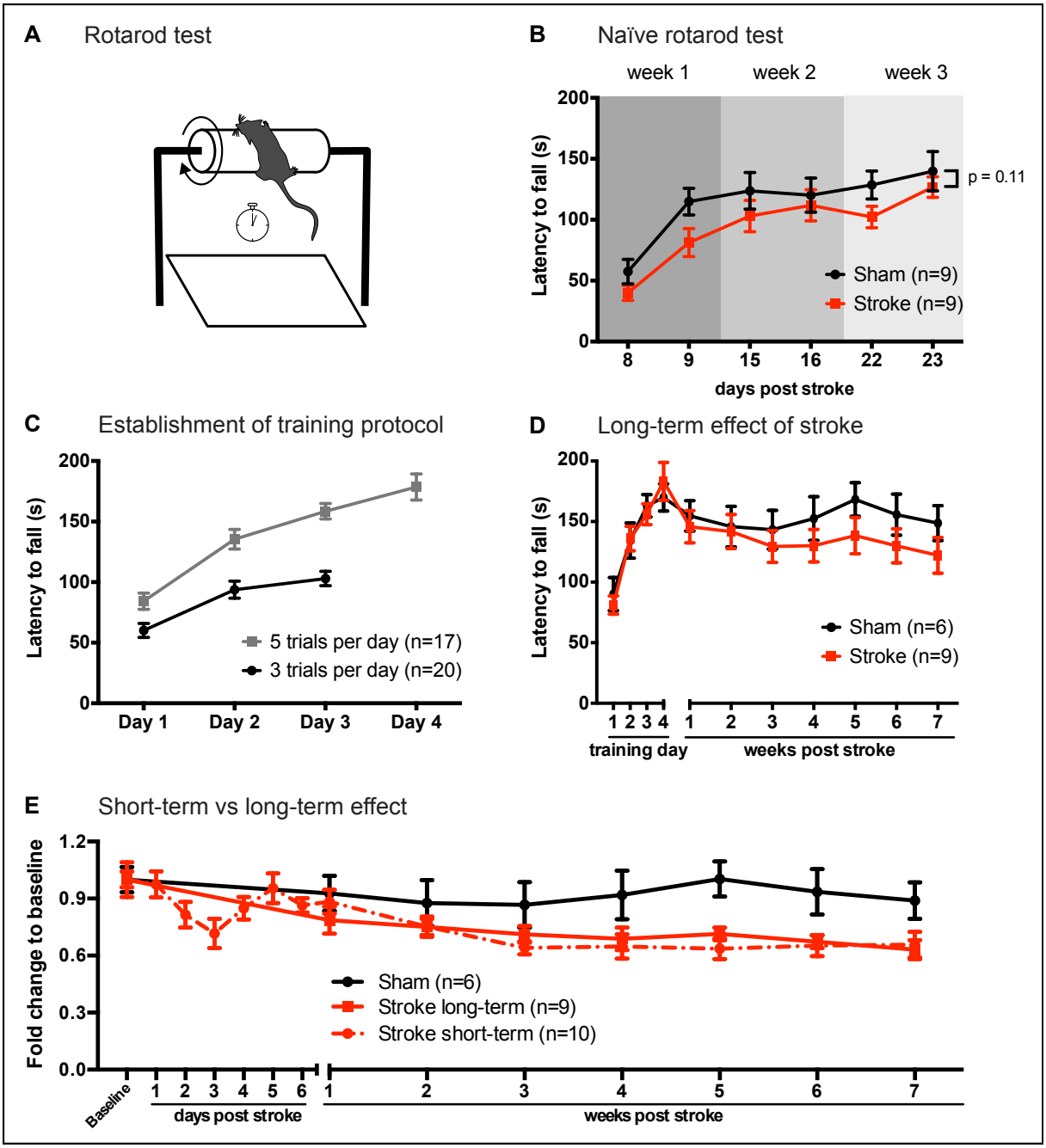

Figure 14: Rotarod test of ET-1 striatum stroke model

(A) Schematic of the rotarod test. (B) Latency to fall (in seconds) from the rotarod of stroke (red) and sham (black) animals is shown as average ± SEM 1, 2 and 3 wps for two consecutive days per week. (C) Latency to fall (in seconds) of animals during training on the rotarod for three (black) or five (grey) trials per day for three or four consecutive days is shown as average ± SEM. (D) Latency to fall (in seconds) of animals (stroke (red) or sham (black)) during training and up to 7 wps as average ± SEM is shown. (E) Same animals from (D) compared to stroke animals tested every day after stroke (red dotted line). Fold change compared to baseline (last day of training) is shown as average ± SEM.

A big issue was the variability especially among sham animals which was addressed by first training the mice before the surgery. In order to establish a training protocol, two different paradigms were tested – three subsequent days of training with three trials per day or four subsequent days with five trials per day (Figure 14C). Mice with the latter protocol outperformed mice with less training in both learning curve and final performance ($p<0.0001$, two-way ANOVA), hence, this was used for further experiments. After training, mice were injected with either ET-1/L-NAME (stroke) or PBS (sham) and subsequently tested on the rotarod once per week (again five trials per day) for a total of seven weeks (Figure 14D). After an initial drop in performance compared to the last day of training for both groups, shams recovered and stayed relatively constant. Stroke animals followed the same pattern but did not plateau at the same level as before. However, this was not statistically significant ($p=0.5714$, two-way ANOVA) and also the magnitude of the supposed effect was small (148.67 ± 35.43 s vs 122.16 ± 44.51 s at 7 wps). In a separate experiment, the short-term effect of stroke was assessed by testing the animals every day on the rotarod in the first week post stroke, followed by the standard weekly testing. When comparing the short-term group to the long-term experiment by expressing the values as fold change compared to baseline, the short-term stroke group seemed to follow the same trend as the long-term stroke group (Figure 14E). Interestingly, there was a big drop in rotarod performance at day 3 post stroke but mice recovered within the remaining days of the first week. Once switched to the weekly rotarod testing, they showed the same initial downwards trend as the long-term tested stroke mice that both groups never recovered from.

Further tests aimed at increasing the potential difference between stroke and sham on the rotarod by various means. A more difficult training protocol (two days of training as before followed by three days of faster acceleration which was maintained for testing after stroke) did not show any difference between sham and stroke (data not shown). Furthermore, both bilateral striatal strokes (instead of unilateral as before) or double injections unilaterally did not even show the previously observed trend of a difference (data not shown). It was therefore concluded that the first long-term experiment (Figure 14D) was not reproducible and thus not biologically relevant.

To summarize, the here used behavioural tests did not reveal a reproducible phenotype after ET-1 striatum stroke although further experiments such as a complex running wheel might allow the detection of subtle differences cause by the small ischemic damage. Subsequently, a combination of both major parts in this thesis – rAAV-4D injection and ET-1 striatum stroke – was only done for histological, but not for behavioural analysis.

3.5 4D increases the number of migrating neuroblasts and survival after stroke

Initially, the aim of this project was combining a clinically applicable 4D-mediated expansion of the NSC pool with a neurodegenerative disease model on both histological and behavioural level to demonstrate the therapeutical potential of 4D. Due to the lack of a suitable behavioural test for the established ET-1 striatum stroke, the focus was set on histology only.

To this end, mice received in a single surgery an ET-1/L-NAME injection into the striatum in one hemisphere and rAAV-4D or -GFP into the contralateral ventricle (Figure 15A).

As previously seen in the ET-1 stroke experiments (Figure 12D-G), the striatal ischemic damage triggered an endogenous response of migrating neuroblasts towards the striatum. Thus, DCX^+ migrating neuroblasts were quantified after stroke and rAAV-4D or -GFP injection 3 wps and 6 wps (Figure 15C). The number of neuroblasts was increased in 4D animals compared to GFP at 3 wps from 3141 ± 2151 cells to 9224 ± 5248 cells (no t-test possible because of n=2 for GFP animals) and at 6 wps from 1236 ± 603 cells to 3536 ± 2259 cells ($p=0.1637$, multiple t-test with Holm-Sidak correction). Normalisation of those numbers to the respective stroke volume did not influence this result (data not shown). Interestingly, the number of DCX^+ cells after 3 weeks in GFP injected animals was very similar to those of only stroke injected animals (3141 ± 2151 cells vs 4348 ± 3171 cells, see also Figure 12F).

In order to assess neuronal survival, newborn cells were birthdated with BrdU in the third week after injection (Figure 15B) because of the previously characterised 4D effect under physiological conditions in this time frame (Figure 8F & Figure 9C). Quantification of newborn neurons in the striatum ($BrdU^+NeuN^+$) normalised to all birthdated cells ($BrdU^+$) did not show any difference in GFP vs 4D animals at 6 wps (19.22 ± 3.65 % vs 19.43 ± 3.79 %, Figure 15D) but the absolute number of $BrdU^+NeuN^+$ cells in the striatum normalised per volume was slightly increased in 4D injected animals (231 ± 122 cells per mm^3 vs 372 ± 143 cells per mm^3, $p=0.2684$, unpaired t-test). A similar experiment was conducted in the 4D mouse line (Bragado Alonso et al., 2019) in collaboration with Dr. Sara Bragado Alonso in our lab (data not shown). Here, BrdU was given in parallel to the 4D induction one day post stroke for four days. Six weeks later, there was a significant increase in $BrdU^+NeuN^+$ cells per volume and similar to the rAAV results, the percentage of newborn neurons among all birthdated cells was unchanged compared to control animals. This data further corroborated the findings presented here.

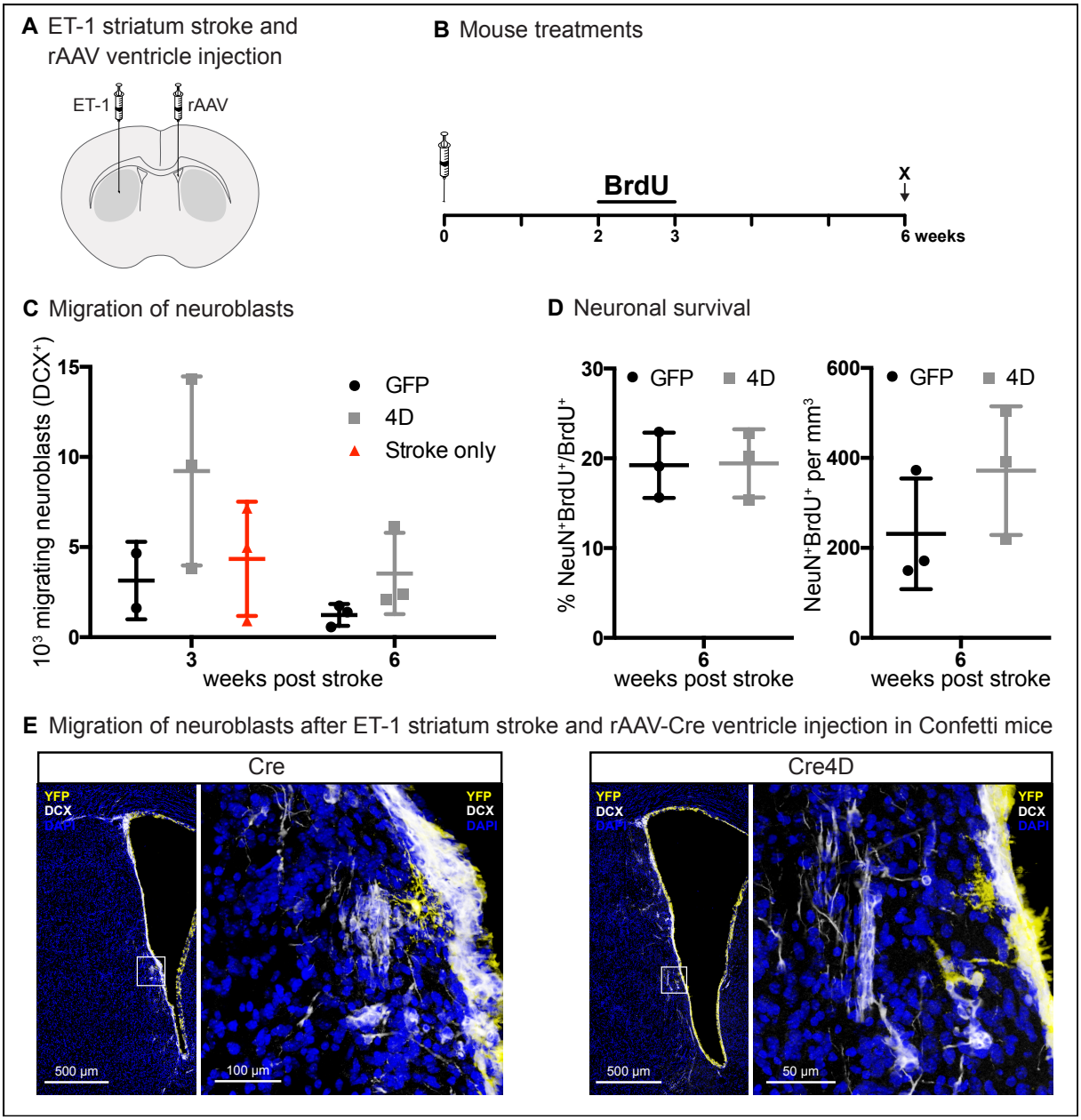

Figure 15: Assessment of rAAV-4D increased neurogenesis after ET-1 striatum stroke

(A) Schematic coronal view of rAAV ventricle and contralateral ET-1 striatum injection. (B) Timeline of mouse treatments in this experiment. 'X' indicates time points of sacrifices, BrdU i.p. injections were given twice per day. (C) DCX^+ cells in the striatum were quantified 3 and 6 wps for GFP and 4D injected animals and compared to stroke only animals at 3 wps. (D) Neuronal survival ($NeuN^+BrdU^+$) was quantified 6 wps either normalised to all $BrdU^+$ cells or per striatal volume for GFP and 4D injected animals. Average ± SD is shown in all graphs. (E) DCX^+ (white) and YFP^+ (yellow) cells of Confetti mice are shown 6 wps for both Cre or Cre4D injected animals.

In line with the previous rAAV injections without stroke (Figure 9), no GFP^+ cell was observed outside of the SVZ also in stroke conditions. In order to better investigate the progeny of rAAV-transduced cells that had migrated to the striatum, the same lineage-tracing approach as before was applied using Confetti mice and rAAV-Cre4D or -Cre. In this experiment, only few YFP^+ cells outside the SVZ were observed 6 weeks post stroke (Figure 15E), some of which were displaying more neuronal or astrocytic morphology. Moreover, there was no DCX^+/YFP^+ cell outside the SVZ identified, although there were still many migrating DCX^+ neuroblasts detected.

In summary, it is still unclear as to how many of the transduced cells actually contributed towards migrating neuroblasts and further functional characterisations are still pending. Nevertheless, this work provides evidence for a rAAV-4D increased number of migrating neuroblasts and a trend of increased neuronal survival after striatal ischemic stroke. Thus, rAAV-mediated 4D overexpression in SVZ NSCs is promising for the therapeutic use of stroke and potentially other neurodegenerative diseases.

4. DISCUSSION

The aims of this thesis were (I) establishing a rAAV-4D overexpression system in NSCs, (II) characterising an ischemic stroke model on histological and behavioural level and (III) testing the rAAV-4D overexpression of NSCs in the stroke model thus providing evidence for the regenerative potential of NSC pool expansion in neurodegenerative diseases. The successful rAAV-4D-mediated increase in SVZ neurogenesis and establishment of a histologically reproducible stroke model enabled the characterisation of the 4D effect after stroke. An increased number of migrating neuroblasts and neuronal survival demonstrated the therapeutic potential of 4D which will be corroborated by future electrophysiological and behavioural investigations.

4.1 rAAVr3.45 transduces NSCs *in vivo*

Recombinant adeno-associated viruses have been used for gene delivery and clinical applications for many years and along with it, different purification methods had been developed (Flotte et al., 1996). Previously, a protocol including long ultracentrifugations and the cytotoxic $CsCl_3$ had been used for *in vivo* applications (Flotte et al., 1992). Later on, researchers had established a shorter protocol involving the biologically inert iodixanol (Zolotukhin et al., 1999). Affinity-based chromatography purification protocols had also been used in the past and are now being designed for multiple serotypes. Yet, these are still more cumbersome than the iodixanol protocol and have to be evaluated and adapted for each serotype (Nass et al., 2018). Importantly, there are reports that the transduction efficiency of the same rAAV serotype *in vivo*, purified with one or the other method, can lead to different apparent tropisms of the virus (Klein et al., 2008). Thus, when testing a certain serotype for its transduction efficiency for a specific cell type, not only the promoter and the serotype itself have to be taken into consideration but also the purification method. For this work, the iodixanol method was chosen since it allows a serotype-independent purification of high titer and high purity rAAVs.

In the last decade, more and more strategies have been developed to increase the amount of different available serotypes. These involved usually starting off with one of the naturally occurring serotypes and introducing mutations in the Cap gene coding for the capsid protein by various means. Combined with different screening methods, this led to a growing amount of so-called engineered serotypes targeting specific cell types *in vivo* (reviewed in (Kotterman and Schaffer, 2014).

Here, an iodixanol purification protocol was adapted from Strobel et al. and established for several naturally occurring serotypes and also for the NSC-engineered serotype r3.45 resulting in high purity rAAVs (Kotterman et al., 2015b; Strobel et al., 2015). The qPCR titration only measured the amount of packaged rAAV particles (vs an unknown amount of non-packaged

particles) but is predominantly used in the field since rAAVs are reportedly very inefficient in *in vitro* transduction of various cell lines (Ellis et al., 2013) and due to the ability to compare titers of different serotypes. Electron microscopy would enable the quantification of unpackaged rAAV particles and the iodixanol method has been shown to result in 20 % of empty purified rAAV particles (Strobel et al., 2015).

As mentioned above, not only the serotype, but also the promoter can influence the apparent transduction efficiency of a cell type. This effect was seen when injecting serotype 9 in the hippocampus with either a CMV-GFP or UbGFP construct (Figure 11). Furthermore, the efficiency of engineered serotypes vs natural serotypes was clearly demonstrated as r3.45 was able to transduce more granule cells than serotype 9 and it was the only one to transduce SVZ NSCs. As r3.45 was a promising candidate for both neurogenic zones but the SVZ NSCs and their progeny have more potential applications for a bigger variety of neurodegenerative diseases including stroke, the characterization of the 4D-mediated effect was continued only in the SVZ NSCs for rAAVr3.45.

4.2 rAAV-4D increases SVZ NSC proliferation and OB neurogenesis

Injection of rAAVr3.45 into the lateral ventricle resulted in widespread transduction of cells in the SVZ, interestingly in both hemispheres although injection was only done in one (Figure 8). Comparing the NSC transduction efficiency of the used rAAVs here (~2 %) to other attempts in the literature is difficult based on the different criteria that had been applied. Using another engineered rAAV serotype, the Schaffer lab claimed to transduce 60 % of SVZ NSCs (Ojala et al., 2018). In this study, cells were labelled with BrdU three days before rAAV injection into the ventricle and NSCs were subsequently regarded as $GFAP^+/BrdU^+/DCX^-$. GFAP is also expressed in astrocytes and known as an important marker for proliferating neuronal progenitors but not necessarily NSCs (Garcia et al., 2004). Thus, the reported number of 60 % transduced NSCs is most likely an overestimation as compared to $Nestin^+/S100\beta^-$ markers in this work. Lentiviruses and retroviruses have also been used in the past but typically by injection into the SVZ directly (as opposed to the ventricle) thereby leading to only a local transduction of cells without proper quantification of transduced NSCs (Carleton et al., 2003; Consiglio et al., 2004).

When investigating the effect of 4D on NSC proliferation, all EdU-labelled cycling cells of the last two days before sacrifice were used as an approximation. Of note, also newborn and cycling progenitors that have not yet migrated from the SVZ towards the RMS were included in this quantification. As expected from previous results in the SVZ using the 4D transgenic mouse line in our lab (Bragado Alonso et al., 2019) or in the SGZ using lentiviruses (Artegiani et al., 2011), an increase in proliferation of 4D vs GFP injected animals was observed after

3 weeks (Figure 8) although there was no concomitant increase in differentiating neuroblasts (DCX^+, Figure 9).

One possible explanation to this apparent discrepancy between increased cell proliferation and unchanged number of neuroblasts is that the produced excess of DCX^+ cells had migrated and thus was not measured in the SVZ. Moreover, rAAVs do not integrate into the genome and are thereby diluted out over cell divisions. It is therefore expected that cells lose both the rAAV genome and the expressed GFP (and 4D) proteins over several cell divisions. This has been reported also in another study transducing SVZ NSCs (Ojala et al., 2018). Since 4D is even promoting cell divisions, this effect is expected to be stronger in 4D expressing cells. Following this logic, observing equal values of DCX^+GFP^+ cells in both 4D and GFP injected animals is still in line with the expected 4D effect.

Similarly, the absence of GFP^+ cells outside the SVZ can be explained. Migrating neuroblasts in the RMS have already undergone several cell divisions and keep on dividing until they finally reach the OB (Ponti et al., 2013). It is therefore not surprising to observe no GFP^+ cell in the RMS or the OB. Importantly, the number of four-week-old BrdU-birthdated newborn neurons was increased a total of seven weeks after rAAV injection (Figure 9C). Interestingly, the magnitude of the effect (~40 % increase in 4D vs GFP) is comparable to the 4D transgenic mouse line (Bragado Alonso et al., 2019) although rAAVs only transduced a small fraction of SVZ NSCs (Figure 8E) as compared to ~50 % of NSCs in the mouse line. This counterintuitive observation could be explained by the different expression time of 4D.

In the transgenic mouse, 4D was only induced for four days whereas rAAV-mediated 4D overexpression was never actively stopped besides the dilution of the viral genome over cell divisions. Thus, it could be assumed that a short time of 4D overexpression in the majority of NSCs resulted in the same neurogenic output as did a longer period of 4D activity in less NSCs. Previous studies in our lab have shown that 4D does not influence the balance of quiescent vs active cycling NSCs (Bragado Alonso et al., 2019) and that cyclinD1 is degraded in non-G_1 cells (Lange et al., 2009). If 4D is overexpressed in many (or all) NSCs, this will not change the fact that only a subpopulation of them is susceptible to its effect over the time course of four days. Whereas in case of the rAAVs, a smaller proportion of NSCs is overexpressing 4D, but this should not be diluted in a non-dividing quiescent NSC. Consequently, there is the potential of a sustained increased level of proliferation over a longer time period because 4D will eventually trigger its effect in any transduced NSC once it switches from quiescence to active, ultimately leading to the same accumulated magnitude of increased neurogenesis after several weeks.

Addressing the issue of absent GFP^+ cells outside the SVZ, it can be excluded that the transduced proliferating cells died because of the increased number of $BrdU^+$ cells observed in the OB of rAAV-4D animals and based on the Cre-lineage tracing with the Confetti mouse.

This experiment also proved migration of the transduced cells via the RMS to the OB further corroborating the dilution-over-cell-divisions hypothesis. A previous study had obtained similar results for a different rAAV serotype using another reporter mouse line (Ojala et al., 2018). Yet, when this mouse line was tested in our lab, it was deemed not ideal, since there were a lot of RFP^+ cells present especially in the OB already before Cre recombination (data not shown). In contrast, in the Confetti mouse line, there was no fluorescent protein detected without Cre expression as expected (data not shown). Thus, the YFP^+ cells observed in the SVZ, RMS and OB can be considered as actual recombination events due to the rAAV-delivered Cre (Figure 10C-E).

In conclusion, the establishment of the rAAV-4D system in mice was successful in the key points of (I) identification of a serotype that transduces NSCs *in vivo*, (II) increasing proliferation of SVZ NSCs, ultimately leading to (III) a higher number of newborn neurons in the olfactory bulb. All this was achieved under circumstances that could be applied to larger animal models and eventually humans since rAAVs are already being used in clinical trials (Bailey et al., 2018; Taghian et al., 2019).

The only concern for clinical applications could be the so far uncontrollable time of 4D expression after transduction since here, a constitutive promoter has been used. However, it has been shown that over cell divisions, the rAAV-driven overexpression is lost and combined with the fact that our lab has demonstrated before that 4D does not have any observable effect on post-mitotic (Artegiani et al., 2011) or quiescent (Bragado Alonso et al., 2019) cells and that cyclinD1 is degraded in non-G_1 cells (Lange et al., 2009), this is not necessarily a major issue. Nevertheless, a Tet-inducible 4D expression system could be used instead of a constitutive promoter. In this case, rtTA expression would be driven by a constitutive promoter and 4D under the control of a TetOn promoter which is only active when doxycyclin-activated rtTA binds to it. Thus, doxycyclin would have to be administered to the animal or patient. Yet, there are reports of an immune response in larger animal models to the TetOn system (Le Guiner et al., 2007), questioning its applicability for clinical trials.

4.3 Establishment of an inducible striatum stroke model

The aim of this thesis was to assess whether 4D overexpression in NSCs could be used as a treatment for stroke. Regarding the stroke model alternatives, MCAo/CCAo were not considered because of the large damage this model typically induces and due to the low controllability of the stroke location. The other two primarily used models in the field – photothrombotic and ET-1 stroke – were both initially assessed regarding their ability to induce a reproducible stroke in the striatum.

Targeting the striatum for the stroke had several reasons. On the one hand, the SVZ NSCs are located next to the striatum. Thus, any damage-induced migration would be much more

likely to happen in an area that is close to the origin of these migrating cells. On the other hand, the aim was to induce a stroke in a brain area that would enable the detection of this damage on a behavioural level since this is at least as clinically relevant as histological analyses. The striatum is known for its importance in motor and cognitive functions (Wise, 2004) such as working memory (Dalley et al., 2004) and motivational and goal-oriented learning (Graybiel, 2008). Consequently, this would enable the investigation of several behavioural aspects and ideally a detailed description and readout of the effects caused by the damage.

4.3.1 ET-1 stroke causes reproducible ischemic striatal damage

Histologically, both tested stroke models generated injuries that were visible three days post stroke in a brightfield view but migrating neuroblasts from the SVZ towards the injury site were only observed in the case of ET-1. This migration was stroke size dependent as reported also in a ET-1 striatum rat model (Lima et al., 2016). Interestingly, the stroke volume assessed at three days and three weeks post stroke with different markers was differing by one order of magnitude indicating that even though a major area of the striatum seemed to show an initial response to the ET-1 injection, not nearly as many neurons were affected by it long-term.

Stainings for astrocytes and microglia at these time points allowed to draw the following model of the timeline for the physiological ET-1 stroke response reaction which had also been observed in other stroke models in rats (Abeysinghe et al., 2014; Rewell et al., 2017):

Within the first few days, microglia invade the ischemic area, possibly to phagocytose dying cells or cell debris. Concomitantly, astrocytes are activated and start surrounding the stroke area. However, maybe for signalling reasons of other cell types, they do not invade yet. This happens some time afterwards, possibly once microglia have finished clearing out dead cells and the astrocytes occupy the area of absent neurons which is called glial scarring. The roles of both microglia and astrocytes in ischemic stroke are still not fully understood but both negative impacts such as glial scarring or inflammatory signals and positive functions like neuroprotection, synaptogenesis or angiogenesis for the recovery have been reported (Becerra-Calixto and Cardona-Gomez, 2017; Qin et al., 2019; Sun et al., 2019).

4.3.2 Behavioural assessment of ET-1 and photothrombotic striatum stroke

On the behavioural level, several tasks were used to assess the functional damage caused by ET-1 striatum stroke. Neither motor functional tests (easy tasks like the Catwalk or more difficult like the rotarod), nor sensorimotor function (corner test) or a striatum-dependent memory test (NOR) showed any reproducible effect on stroke vs sham animals.

The Catwalk data (Figure 13A) never revealed any major parameter changes for both stroke models and more subtle changes of less than 10 % were not reproducibly observable due to the high variability of this test. Efforts to improve the training protocol previously or post-hoc

data analysis such as normalisation to weight or speed of the animal and even to the swing speed of each individual paw did not alleviate this problem. The Catwalk gait analysis has been used in other models of spinal cord injuries (Hamers et al., 2006) and neurodegenerative diseases such as MS (Herold et al., 2016), HD or PD (Timotius et al., 2019). However, these models all impacted the entire animal more severely, supporting the hypothesis that the mild stroke induced here was not enough to show an impairment on the Catwalk.

The corner test (Figure 13B) was conducted once without recording pre-treatment values. Thus, major conclusions cannot be drawn from this single time experiment. The relatively low resolution of 10 % increments could be decreased by recording more turns per animal. Yet, this would still not change the high variability among animals. Moreover, since a rAAV-4D treatment would be probably very difficult to detect with this behaviour test after stroke, the corner test was not considered for the future, especially taking into account another study that demonstrated no difference after ET-1 cortical stroke in this test (Tennant and Jones, 2009).

The NOR task did not show the expected and reported behaviour of the sham mice (Lueptow, 2017) as in spending more time at new objects (Figure 13C). Therefore, the results of the stroke animals cannot be interpreted properly. It cannot be excluded that the new objects were either not different enough from the old one or that they were repelling to the animals for some reason. Both cases could explain the lack of interest or aversion of sham animals regarding the new objects. Thus, a new set of objects first would have to be tested and established for control animals before any treated mice could be analysed with this behavioural task.

Lastly, mice were assessed on the rotarod for motor coordination (Figure 14). While an initial test without pre-training showed a promising trend, it could ultimately not be reproduced despite many efforts of improving both the training protocol as well as analysing the behaviour after stroke. Remarkably, both the massive glial response observed after three days and the detected neuronal loss after three weeks seemed to be concomitant with a respective drop in rotarod performance of stroke animals. Yet, the lack of intermediate histological time points does not allow to draw major conclusions as to why mice seemed to recover from this reduced performance on the rotarod three days and three weeks after stroke, respectively. This could possibly be related to the cellular processes happening in the brain which is still to be revealed.

Considering the histologically detected damage and cellular responses, the question is being raised as to why no behavioural effect could be detected in any of the used tests. Of note, when mice were waking up from the surgery, seizures combined with ipsilateral circling was observed in many stroke animals within the first hour but in none of the shams, indicating an immediate response to the ET-1 injection. Thus, it is very unlikely that the caused damage had no effect on the brain at all.

Admittedly, it is possible that either the damage was not big enough or that the used tests were not appropriate for the striatal damage caused. Concerning the former, injections of double

volume of ET-1 or two single injections in different locations of the striatum (but the same hemisphere) did also not result in behavioural deficits in the rotarod (data not shown). Regarding the latter, it cannot be excluded that other tests could have revealed an effect after striatal stroke. Especially when regarding the olfactometry test for 4D-increased SVZ neurogenesis (Bragado Alonso et al., 2019), a behavioural difference could only be seen when the test was very challenging for the animals. Thus, finding a motor behavioural test that challenges the mice more could reveal subtle differences in animals with small striatal damage. For example, the complex running wheel could be used in order to detect whether striatal stroke could cause a deficit in motor coordination.

4.4 4D increases the number of migrating neuroblasts and neuronal survival after stroke

In stroke and other neurodegenerative diseases, neurons are lost either region- or subtype-specifically or without any obvious preference. Either way, the ultimate goal of regenerative therapies is replacing those lost neurons. Here, I focused on harnessing the endogenous NSC pool and on using rAAV-4D overexpression to increase their proliferative capacity for this purpose in the context of striatal stroke.

Three important criteria had to be fulfilled in order to show therapeutic potential: (I) (increased number of) migrating neuroblasts towards the site of injury, (II) neuronal survival and (III) functional integration into the existing network of remaining neurons.

It had already been reported previously that SVZ NSC progeny migrates towards the site of injury after stroke (Ohab et al., 2006; Marques et al., 2019) which was confirmed also in this work. Furthermore, a trend of higher numbers of migrating neuroblasts and of increased neuronal survival in 4D animals indicated the potential regenerative use of rAAV-4D. Expectedly, the proportion of newborn neurons among all birthdated cells was not changed in 4D- or GFP-injected animals since there is no evidence that 4D influences the fate of NSCs (Lange et al., 2009; Artegiani et al., 2011; Nonaka-Kinoshita et al., 2013; Bragado Alonso et al., 2019; Berdugo-Vega et al., 2020). A similar histological analysis after stroke had also been conducted in our lab using the 4D transgenic mouse line resulting in bigger effects as compared to rAAV-4D further corroborating these findings.

For better analysis of integration of surviving neurons in the striatum originating from SVZ NSCs, a Cre-lineage tracing approach was used and only very few YFP^+ cells were found in the striatum and none of them were DCX^+ (Figure 15). This is in contrast to the discussed data using the BrdU-birthdating approach and one explanation could be the heterogeneity of SVZ NSCs (Young et al., 2007; Obernier and Alvarez-Buylla, 2019). rAAVs possibly transduce only a certain subpopulation of NSCs that can contribute to migrating neuroblasts towards the OB (as shown in the previous lineage tracing experiment, Figure 10) but maybe not to migrating

neuroblasts towards the injury site. In that case, the increased number of migrating neuroblasts and neuronal survival in 4D animals could be explained by a regulatory compensation mechanism. If rAAV-4D transduced NSCs managed to maintain the normal levels of OB neurogenesis, other subpopulations of SVZ NSC could have contributed more to the regenerative purposes.

The fate of the observed migrating neuroblasts and newborn neurons has not yet been further investigated in this work. Previously, several studies have demonstrated that after ischemic striatal damage, neuroblasts from the SVZ migrate towards the site of injury (Zhang et al., 2007) and differentiate to subtypes that naturally are present in the striatum such as DARP-32^{+} (Arvidsson et al., 2002; Parent et al., 2002), GABAergic and cholinergic neurons (Hou et al., 2008) or parvalbumin and neuropeptide Y expressing interneurons (Collin et al., 2005). Of note, these studies were done in rats with the more commonly used MCAo stroke model. Yet, in a recent review, it has been pointed out that it is still not clear whether there is local neurogenesis in the striatum after injury, that results might be species-dependent and that conflicting reports might be due to the different techniques used in those studies both for investigating the origin of newborn neurons and the caused striatal damage (Nemirovich-Danchenko and Khodanovich, 2019). Regarding translational applicability of findings in this and the work of other groups on animal models of stroke, there are a few studies providing evidence for increased neurogenesis in human brains after stroke (Jin et al., 2006; Minger et al., 2007).

Concluding, I presented first data that rAAV-4D overexpression after ET-1 stroke potentially increases both the number of migrating neuroblasts and their survival. Their functional characterization is still pending and future efforts should be made towards identifying a suitable behavioural test to also demonstrate an improvement of the animal beyond cellular regeneration.

4.5 Future perspectives

The work presented in this thesis provided first evidence that a 4D-mediated increase of SVZ NSCs can be a potential treatment for neurodegenerative diseases and for stroke in particular. Moreover, rAAVs (and the 4D overexpression) do not have to be restricted to NSCs. In fact, collaborative research with other groups and other projects in our lab have suggested that 4D is exerting its effect on any stem cell type, from human hematopoietic stem cells in a mouse model (Mende et al., 2015) to oligodendrocyte progenitors in adult mice (unpublished work by Dr. Max Schulze-Steikow). Consequently, identification of a suitable rAAV serotype for the stem cell of choice could quickly lead to a ready-to-use system to expand this stem cell pool and to test it for regenerative purposes. Ongoing research on engineering rAAV serotypes towards specific cell types will expand this tool box and facilitate specific transduction of cell types for gene therapy (Kotterman and Schaffer, 2014).

Proof of an integration of the 4D-produced newborn neurons and investigation of their electrophysiological properties additional to a behavioural readout in the future would further corroborate the findings of this thesis. The research on this stroke disease model could then be expanded to other neurodegenerative disease models increasing the therapeutic potential of rAAV-4D treatments.

.

Summary

Adult neurogenesis in mammals is restricted to two areas of the brain, the hippocampal subgranular zone (SGZ) and the subventricular zone (SVZ) lining the ventricle walls. Previous work in our lab has shown that overexpression of the cell cycle regulators *Cdk4*/*Ccnd1* (4D) in SGZ or SVZ neural stem cells (NSCs) shortens their G_1 thereby resulting in an increased rate of proliferation. This led to a higher number of newborn neurons improving the performances of mice in hippocampus-dependent memory or odour discrimination tasks, respectively. However, the 4D overexpression was so far achieved using integrating lentiviruses (SGZ) or transgenic mice (SVZ) limiting this approach from potential clinical applications such as stroke and other neurodegenerative diseases. In my thesis, I set out to develop a 4D overexpression system that is clinically applicable and to test this in a mouse model of stroke. To this end, a recombinant adeno-associated virus (rAAV) serotype was for the first time identified that enabled the transduction of both SGZ and SVZ NSCs. In the SVZ, 4D overexpression resulted in increased NSC proliferation and neurogenesis providing a proof of principle for the rAAV-4D system. Additionally, a photothrombotic and an endothelin-1 (ET-1) striatum stroke model were established for both histological and behavioural analysis. In the ET-1 model, SVZ-derived neuroblast migration towards the site of injury was observed. Histological analysis of rAAV-mediated 4D overexpression after ET-1 stroke demonstrated an increased number of migrating neuroblasts and neuronal survival in the striatum. Together with future cellular characterizations and behavioural tests, this work provides the basis for potential 4D applications not only for stroke but also for other neurodegenerative diseases. In a bigger picture, identification of rAAV serotypes that transduce other stem and progenitor cells could even further expand the toolbox of rAAV-4D treatments for clinical applications of different areas of regenerative medicine.

Zusammenfassung

Adulte Neurogenese in Säugetieren ist eingeschränkt auf zwei Gehirnbereiche, der subgranulären Zone (SGZ) des Hippocampus und der subventrikulären Zone (SVZ) um die Ventrikelwände herum. Vorhergehende Arbeiten in unserem Labor haben gezeigt, dass Überexpression der Zellzyklusregulatoren *Cdk4*/*Ccnd1* (4D) in neuralen Stammzellen (NSZ) der SGZ oder SVZ ihre G_1 Phase verkürzt und dadurch zu einer erhöhten Proliferationsrate führt. Dies hatte eine höhere Anzahl an neugeborenen Neuronen zur Folge, welche die Performance von Mäusen in Hippocampus-abhängigen Gedächtnis- bzw. in Geruch-unterscheidungstests verbessert hat. Allerdings wurde die 4D Überexpression bislang durch das Benutzen von entweder integrierenden Lentiviren (SGZ) oder transgenen Mäusen (SVZ) durchgeführt, was diese Vorgehensweise einschränkt hinsichtlich potenzieller klinischer Anwendungen wie Schlaganfall oder neurodegenerativen Erkrankungen. In meiner Thesis habe ich ein 4D Überexpressionssystem entwickelt, was klinisch anwendbar ist und dies in einem Mausmodell von Schlaganfall getestet. Zu diesem Zweck wurde zum ersten Mal ein rekombinanter Adeno-assoziierter Virus (rAAV) Serotyp identifiziert, der die Transduktion von sowohl SGZ als auch SVZ NSZs ermöglichte. In der SVZ resultierte die 4D Überexpression in einer erhöhten NSZ Proliferation und Neurogenese, was einen grundlegenden Beweis für das rAAV-4D System lieferte. Zusätzlich wurden ein photothrombotisches und ein Endothelin-1 (ET-1) Striatum Schlaganfallmodell sowohl für histologische als auch Verhaltens-untersuchungen etabliert. Im ET-1 Modell wurde Migration von Neuroblasten zum Bereich der Schädigung hin beobachtet, die von der SVZ stammten. Histologische Analysen der rAAV-4D Überexpression nach ET-1 Schlaganfall wiesen eine erhöhte Anzahl an migrierenden Neuroblasten und Überleben der Neuronen auf. Zusammen mit zukünftigen zellulären Charakterisierungen und Verhaltenstests liefert diese Arbeit die Basis für potenzielle 4D Anwendungen nicht nur für Schlaganfall, sondern auch für andere neurodegenerative Erkrankungen. Perspektivisch könnte die Identifizierung von rAAV Serotypen, die andere Stamm- oder Vorläuferzellen transduzieren, weiter die Toolbox von rAAV-4D Behandlungs-möglichkeiten für klinische Anwendungen anderer Bereiche der regenerativen Medizin erweitern.

Acknowledgements

First and foremost, I want to thank Prof. Federico Calegari for giving me the opportunity to pursue this PhD project in his lab. Thank you especially for giving me the independence that I needed but also the guidance and advice when I asked for it.

Thank you to Prof. Marius Ader and Prof. Frank Buchholz for reviewing my thesis. Moreover, thank you, Marius, for helpful feedback in joint group meetings and to Frank for a lot of questions and suggestions during my TAC meetings.

I also want to thank Dr. Jörg Mansfeld, not only as another TAC member for important and helpful feedback but also for being part of my Thesis Committee. Thank you also to Prof. Dirk Lindemann to chair and Dr. Nadine Bernhardt for being part of the Committee as well, respectively. Your expert opinions on viruses and striatum helped shape this project tremendously.

Thank you, Dr. Gabriel Berdugo Vega, for proof-reading my thesis and giving me crucial feedback and support!

During a long project such as the PhD, it is not only important that you like your project and have a good supervisor, but your colleagues in the lab are in the end the ones who generate the biggest joy of going to the lab day in, day out (and also on weekends from time to time)! So, thank you to all the past and present members of the Calegari lab:

Dr. Sara Bragado Alonso, you have helped me with your big knowledge about neurogenesis, 4D and establishing many stroke and behaviour experiments together (especially photothrombotic stroke, Catwalk, novel object recognition and rotarod) made it much easier!

Leila Haj Abdullah Alieh, thank you for many running sessions that helped coping with the writing phase particularly and all the other fun activities in- and outside the lab.

Dr. Gabriel Berdugo Vega and Dr. Daniel Cavalli – I am still not used to put this title in front of your names, since we did a major part of our PhD journey together. I will miss our quiz sessions, kicker, beer hours and I always appreciated your help and feedback for cloning, behaviour and other more philosophical questions.

Special thanks also to Dr. Florian Noack to show me the little tricks of cloning (thank you, Master!) and to make me run a half marathon several times. I will miss also the evenings discussing about and listening to our favourite music (Tool!) while enjoying craft beer.

A collective thank you to all the other members of the lab including Frank Darmis, Dr. Ivan Mestres, Dr. Julieta Aprea, Beatriz Toledo, Chi-Chieh Lee, “the Boss” Dr. Simone Massalini, Sonali Salvi, Dr. Max Schulze-Steikow, Adrian Lopez, Lorena Bragg Gonzalo, my Master student Ridzky Yuda, June Möller, Maximilian Einsiedel, Maria Mulles, Selina Stahl and Melina Patsoni. A final thank you to our group’s secretary, Jeannette Hoppe, who was always willing to help with bureaucratic and other lab-related issues.

I also want to thank the facilities of CRTD and BIOTEC who made everyday lab work so much smoother and faster, most importantly the animal facility with all its caretakers and the imaging facility.
I have not only found great colleagues and friends within our lab, but also in the rest of CRTD, within my DIPP selection and the entire Biopolis Dresden. Thank you for the fun kicker sessions and frequent beer hours! I will also miss our weekly organised badminton sessions and beach volleyball in summer. Thank you also to “Captain Australia” Sylvia for organising last year’s Biolympics team and making it not only fun but also a great success!
Last, but definitely not least, I want to thank my family and long-time friends for the continued support. Although we might be hundreds (and maybe soon thousands) of kilometres apart, it is invaluable to have beloved ones to always reach out and come back to when needed!

References

Aberg, M.A., Aberg, N.D., Hedbacker, H., Oscarsson, J., and Eriksson, P.S. (2000). Peripheral infusion of IGF-I selectively induces neurogenesis in the adult rat hippocampus. J Neurosci *20*, 2896-2903.

Abeysinghe, H.C., Bokhari, L., Dusting, G.J., and Roulston, C.L. (2014). Brain remodelling following endothelin-1 induced stroke in conscious rats. PLoS One *9*, e97007.

Alamri, F.F., Shoyaib, A.A., Biggers, A., Jayaraman, S., Guindon, J., and Karamyan, V.T. (2018). Applicability of the grip strength and automated von Frey tactile sensitivity tests in the mouse photothrombotic model of stroke. Behav Brain Res *336*, 250-255.

Alonso, M., Lepousez, G., Sebastien, W., Bardy, C., Gabellec, M.M., Torquet, N., and Lledo, P.M. (2012). Activation of adult-born neurons facilitates learning and memory. Nat Neurosci *15*, 897-904.

Altman, J., and Das, G.D. (1965). Autoradiographic and histological evidence of postnatal hippocampal neurogenesis in rats. J Comp Neurol *124*, 319-335.

Alvarez-Sabin, J., and Roman, G.C. (2013). The role of citicoline in neuroprotection and neurorepair in ischemic stroke. Brain Sci *3*, 1395-1414.

An, M.C., Zhang, N., Scott, G., Montoro, D., Wittkop, T., Mooney, S., Melov, S., and Ellerby, L.M. (2012). Genetic correction of Huntington's disease phenotypes in induced pluripotent stem cells. Cell Stem Cell *11*, 253-263.

Andersen, P.M., and Al-Chalabi, A. (2011). Clinical genetics of amyotrophic lateral sclerosis: what do we really know? Nat Rev Neurol *7*, 603-615.

Andreae, L.C. (2018). Adult neurogenesis in humans: Dogma overturned, again and again? Sci Transl Med *10*, eaat3893.

Armstrong, R.J., Watts, C., Svendsen, C.N., Dunnett, S.B., and Rosser, A.E. (2000). Survival, neuronal differentiation, and fiber outgrowth of propagated human neural precursor grafts in an animal model of Huntington's disease. Cell Transplant *9*, 55-64.

Artegiani, B., Lindemann, D., and Calegari, F. (2011). Overexpression of cdk4 and cyclinD1 triggers greater expansion of neural stem cells in the adult mouse brain. J Exp Med *208*, 937-948.

Arvidsson, A., Collin, T., Kirik, D., Kokaia, Z., and Lindvall, O. (2002). Neuronal replacement from endogenous precursors in the adult brain after stroke. Nat Med *8*, 963-970.

Atchison, R.W., Casto, B.C., and Hammon, W.M. (1965). Adenovirus-Associated Defective Virus Particles. Science *149*, 754-756.

Athauda, D., and Foltynie, T. (2016). Challenges in detecting disease modification in Parkinson's disease clinical trials. Parkinsonism Relat Disord *32*, 1-11.

Atkins, H.L., and Freedman, M.S. (2013). Hematopoietic stem cell therapy for multiple sclerosis: top 10 lessons learned. Neurotherapeutics *10*, 68-76.

Bachoud-Levi, A.C., Remy, P., Nguyen, J.P., Brugieres, P., Lefaucheur, J.P., Bourdet, C., Baudic, S., Gaura, V., Maison, P., Haddad, B., Boisse, M.F., Grandmougin, T., Jeny, R., Bartolomeo, P., Dalla Barba, G., Degos, J.D., Lisovoski, F., Ergis, A.M., Pailhous, E., Cesaro,

P., Hantraye, P., and Peschanski, M. (2000). Motor and cognitive improvements in patients with Huntington's disease after neural transplantation. Lancet *356*, 1975-1979.

Bailey, R.M., Armao, D., Nagabhushan Kalburgi, S., and Gray, S.J. (2018). Development of Intrathecal AAV9 Gene Therapy for Giant Axonal Neuropathy. Mol Ther Methods Clin Dev *9*, 160-171.

Balkaya, M., Krober, J.M., Rex, A., and Endres, M. (2013). Assessing post-stroke behavior in mouse models of focal ischemia. J Cereb Blood Flow Metab *33*, 330-338.

Bamford, J., Sandercock, P., Dennis, M., Burn, J., and Warlow, C. (1991). Classification and natural history of clinically identifiable subtypes of cerebral infarction. Lancet *337*, 1521-1526.

Bao, A.M., and Swaab, D.F. (2018). The art of matching brain tissue from patients and controls for postmortem research. Handb Clin Neurol *150*, 197-217.

Becerra-Calixto, A., and Cardona-Gomez, G.P. (2017). The Role of Astrocytes in Neuroprotection after Brain Stroke: Potential in Cell Therapy. Front Mol Neurosci *10*, 88.

Beech, J.S., Williams, S.C., Campbell, C.A., Bath, P.M., Parsons, A.A., Hunter, A.J., and Menon, D.K. (2001). Further characterisation of a thromboembolic model of stroke in the rat. Brain Res *895*, 18-24.

Berdugo-Vega, G., Arias-Gil, G., López-Fernández, A., Artegiani, B., Wasielewska, J.M., Lee, C.-C., Lippert, M.T., Kempermann, G., Takagaki, K., and Calegari, F. (2020). Increasing neurogenesis refines hippocampal activity rejuvenating navigational learning strategies and contextual memory throughout life. Nat Commun *11*, 135.

Bergmann, O., Liebl, J., Bernard, S., Alkass, K., Yeung, M.S., Steier, P., Kutschera, W., Johnson, L., Landen, M., Druid, H., Spalding, K.L., and Frisen, J. (2012). The age of olfactory bulb neurons in humans. Neuron *74*, 634-639.

Bernstock, J.D., Peruzzotti-Jametti, L., Ye, D., Gessler, F.A., Maric, D., Vicario, N., Lee, Y.J., Pluchino, S., and Hallenbeck, J.M. (2017). Neural stem cell transplantation in ischemic stroke: A role for preconditioning and cellular engineering. J Cereb Blood Flow Metab *37*, 2314-2319.

Bertilsson, G., Patrone, C., Zachrisson, O., Andersson, A., Dannaeus, K., Heidrich, J., Kortesmaa, J., Mercer, A., Nielsen, E., Ronnholm, H., and Wikstrom, L. (2008). Peptide hormone exendin-4 stimulates subventricular zone neurogenesis in the adult rodent brain and induces recovery in an animal model of Parkinson's disease. J Neurosci Res *86*, 326-338.

Bhatt, P., Khatri, N., Kumar, M., Baradia, D., and Misra, A. (2015). Microbeads mediated oral plasmid DNA delivery using polymethacrylate vectors: an effectual groundwork for colorectal cancer. Drug Deliv *22*, 849-861.

Birch, A.M., and Kelly, A.M. (2013). Chronic intracerebroventricular infusion of nerve growth factor improves recognition memory in the rat. Neuropharmacology *75*, 255-261.

Blaese, R.M., Culver, K.W., Miller, A.D., Carter, C.S., Fleisher, T., Clerici, M., Shearer, G., Chang, L., Chiang, Y., Tolstoshev, P., Greenblatt, J.J., Rosenberg, S.A., Klein, H., Berger, M., Mullen, C.A., Ramsey, W.J., Muul, L., Morgan, R.A., and Anderson, W.F. (1995). T lymphocyte-directed gene therapy for ADA- SCID: initial trial results after 4 years. Science *270*, 475-480.

Boldrini, M., Fulmore, C.A., Tartt, A.N., Simeon, L.R., Pavlova, I., Poposka, V., Rosoklija, G.B., Stankov, A., Arango, V., Dwork, A.J., Hen, R., and Mann, J.J. (2018). Human Hippocampal Neurogenesis Persists throughout Aging. Cell Stem Cell *22*, 589-599 e585.

Bonaguidi, M.A., Wheeler, M.A., Shapiro, J.S., Stadel, R.P., Sun, G.J., Ming, G.L., and Song, H. (2011). In vivo clonal analysis reveals self-renewing and multipotent adult neural stem cell characteristics. Cell *145*, 1142-1155.

Bond, A.M., Ming, G.L., and Song, H. (2015). Adult Mammalian Neural Stem Cells and Neurogenesis: Five Decades Later. Cell Stem Cell *17*, 385-395.

Bordiuk, O.L., Smith, K., Morin, P.J., and Semenov, M.V. (2014). Cell proliferation and neurogenesis in adult mouse brain. PLoS One *9*, e111453.

Borta, A., and Hoglinger, G.U. (2007). Dopamine and adult neurogenesis. J Neurochem *100*, 587-595.

Bouet, V., Freret, T., Toutain, J., Divoux, D., Boulouard, M., and Schumann-Bard, P. (2007). Sensorimotor and cognitive deficits after transient middle cerebral artery occlusion in the mouse. Exp Neurol *203*, 555-567.

Boussif, O., Lezoualc'h, F., Zanta, M.A., Mergny, M.D., Scherman, D., Demeneix, B., and Behr, J.P. (1995). A versatile vector for gene and oligonucleotide transfer into cells in culture and in vivo: polyethylenimine. Proc Natl Acad Sci U S A *92*, 7297-7301.

Bragado Alonso, S., Reinert, J.K., Marichal, N., Massalini, S., Berninger, B., Kuner, T., and Calegari, F. (2019). An increase in neural stem cells and olfactory bulb adult neurogenesis improves discrimination of highly similar odorants. EMBO J *38*, e98791.

Breton-Provencher, V., Lemasson, M., Peralta, M.R., 3rd, and Saghatelyan, A. (2009). Interneurons produced in adulthood are required for the normal functioning of the olfactory bulb network and for the execution of selected olfactory behaviors. J Neurosci *29*, 15245-15257.

Butler, J.S., Chan, A., Costelha, S., Fishman, S., Willoughby, J.L., Borland, T.D., Milstein, S., Foster, D.J., Goncalves, P., Chen, Q., Qin, J., Bettencourt, B.R., Sah, D.W., Alvarez, R., Rajeev, K.G., Manoharan, M., Fitzgerald, K., Meyers, R.E., Nochur, S.V., Saraiva, M.J., and Zimmermann, T.S. (2016). Preclinical evaluation of RNAi as a treatment for transthyretin-mediated amyloidosis. Amyloid *23*, 109-118.

Calzolari, F., Michel, J., Baumgart, E.V., Theis, F., Gotz, M., and Ninkovic, J. (2015). Fast clonal expansion and limited neural stem cell self-renewal in the adult subependymal zone. Nat Neurosci *18*, 490-492.

Carleton, A., Petreanu, L.T., Lansford, R., Alvarez-Buylla, A., and Lledo, P.M. (2003). Becoming a new neuron in the adult olfactory bulb. Nat Neurosci *6*, 507-518.

Carmona, S., Hardy, J., and Guerreiro, R. (2018). The genetic landscape of Alzheimer disease. Handb Clin Neurol *148*, 395-408.

Chen, J., Zhang, C., Jiang, H., Li, Y., Zhang, L., Robin, A., Katakowski, M., Lu, M., and Chopp, M. (2005). Atorvastatin induction of VEGF and BDNF promotes brain plasticity after stroke in mice. J Cereb Blood Flow Metab *25*, 281-290.

Chevallet, M., Luche, S., and Rabilloud, T. (2006). Silver staining of proteins in polyacrylamide gels. Nat Protoc *1*, 1852-1858.

Chohan, M.O., Li, B., Blanchard, J., Tung, Y.C., Heaney, A.T., Rabe, A., Iqbal, K., and Grundke-Iqbal, I. (2011). Enhancement of dentate gyrus neurogenesis, dendritic and synaptic plasticity and memory by a neurotrophic peptide. Neurobiol Aging *32*, 1420-1434.

Choudhury, S.R., Hudry, E., Maguire, C.A., Sena-Esteves, M., Breakefield, X.O., and Grandi, P. (2017). Viral vectors for therapy of neurologic diseases. Neuropharmacology *120*, 63-80.

Cisbani, G., and Cicchetti, F. (2012). An in vitro perspective on the molecular mechanisms underlying mutant huntingtin protein toxicity. Cell Death Dis *3*, e382.

Clement, A.M., Nguyen, M.D., Roberts, E.A., Garcia, M.L., Boillee, S., Rule, M., McMahon, A.P., Doucette, W., Siwek, D., Ferrante, R.J., Brown, R.H., Jr., Julien, J.P., Goldstein, L.S., and Cleveland, D.W. (2003). Wild-type nonneuronal cells extend survival of SOD1 mutant motor neurons in ALS mice. Science *302*, 113-117.

Codega, P., Silva-Vargas, V., Paul, A., Maldonado-Soto, A.R., Deleo, A.M., Pastrana, E., and Doetsch, F. (2014). Prospective identification and purification of quiescent adult neural stem cells from their in vivo niche. Neuron *82*, 545-559.

Collin, T., Arvidsson, A., Kokaia, Z., and Lindvall, O. (2005). Quantitative analysis of the generation of different striatal neuronal subtypes in the adult brain following excitotoxic injury. Exp Neurol *195*, 71-80.

Consiglio, A., Gritti, A., Dolcetta, D., Follenzi, A., Bordignon, C., Gage, F.H., Vescovi, A.L., and Naldini, L. (2004). Robust in vivo gene transfer into adult mammalian neural stem cells by lentiviral vectors. Proc Natl Acad Sci U S A *101*, 14835-14840.

Cooper, O., and Isacson, O. (2004). Intrastriatal transforming growth factor alpha delivery to a model of Parkinson's disease induces proliferation and migration of endogenous adult neural progenitor cells without differentiation into dopaminergic neurons. J Neurosci *24*, 8924-8931.

Curtis, M.A., Kam, M., Nannmark, U., Anderson, M.F., Axell, M.Z., Wikkelso, C., Holtas, S., van Roon-Mom, W.M., Bjork-Eriksson, T., Nordborg, C., Frisen, J., Dragunow, M., Faull, R.L., and Eriksson, P.S. (2007). Human neuroblasts migrate to the olfactory bulb via a lateral ventricular extension. Science *315*, 1243-1249.

Dalley, J.W., Cardinal, R.N., and Robbins, T.W. (2004). Prefrontal executive and cognitive functions in rodents: neural and neurochemical substrates. Neurosci Biobehav Rev *28*, 771-784.

Davenport, A.P., Hyndman, K.A., Dhaun, N., Southan, C., Kohan, D.E., Pollock, J.S., Pollock, D.M., Webb, D.J., and Maguire, J.J. (2016). Endothelin. Pharmacol Rev *68*, 357-418.

Davis, H.L., Demeneix, B.A., Quantin, B., Coulombe, J., and Whalen, R.G. (1993). Plasmid DNA is superior to viral vectors for direct gene transfer into adult mouse skeletal muscle. Hum Gene Ther *4*, 733-740.

DeCarolis, N.A., Mechanic, M., Petrik, D., Carlton, A., Ables, J.L., Malhotra, S., Bachoo, R., Gotz, M., Lagace, D.C., and Eisch, A.J. (2013). In vivo contribution of nestin- and GLAST-lineage cells to adult hippocampal neurogenesis. Hippocampus *23*, 708-719.

DeJesus-Hernandez, M., Mackenzie, I.R., Boeve, B.F., Boxer, A.L., Baker, M., Rutherford, N.J., Nicholson, A.M., Finch, N.A., Flynn, H., Adamson, J., Kouri, N., Wojtas, A., Sengdy, P., Hsiung, G.Y., Karydas, A., Seeley, W.W., Josephs, K.A., Coppola, G., Geschwind, D.H., Wszolek, Z.K., Feldman, H., Knopman, D.S., Petersen, R.C., Miller, B.L., Dickson, D.W., Boylan, K.B., Graff-Radford, N.R., and Rademakers, R. (2011). Expanded GGGGCC hexanucleotide repeat in noncoding region of C9ORF72 causes chromosome 9p-linked FTD and ALS. Neuron *72*, 245-256.

Deng, W., Saxe, M.D., Gallina, I.S., and Gage, F.H. (2009). Adult-born hippocampal dentate granule cells undergoing maturation modulate learning and memory in the brain. J Neurosci *29*, 13532-13542.

Dennis, C.V., Suh, L.S., Rodriguez, M.L., Kril, J.J., and Sutherland, G.T. (2016). Human adult neurogenesis across the ages: An immunohistochemical study. Neuropathol Appl Neurobiol *42*, 621-638.

Diederich, K., Quennet, V., Bauer, H., Muller, H.D., Wersching, H., Schabitz, W.R., Minnerup, J., and Sommer, C. (2012). Successful regeneration after experimental stroke by granulocyte-colony stimulating factor is not further enhanced by constraint-induced movement therapy either in concurrent or in sequential combination therapy. Stroke *43*, 185-192.

Draghia-Akli, R., Li, X., and Schwartz, R.J. (1997). Enhanced growth by ectopic expression of growth hormone releasing hormone using an injectable myogenic vector. Nat Biotechnol *15*, 1285-1289.

Dupret, D., Revest, J.M., Koehl, M., Ichas, F., De Giorgi, F., Costet, P., Abrous, D.N., and Piazza, P.V. (2008). Spatial relational memory requires hippocampal adult neurogenesis. PLoS One *3*, e1959.

Ellis, B.L., Hirsch, M.L., Barker, J.C., Connelly, J.P., Steininger, R.J., 3rd, and Porteus, M.H. (2013). A survey of ex vivo/in vitro transduction efficiency of mammalian primary cells and cell lines with Nine natural adeno-associated virus (AAV1-9) and one engineered adeno-associated virus serotype. Virol J *10*, 74.

Encinas, J.M., Michurina, T.V., Peunova, N., Park, J.H., Tordo, J., Peterson, D.A., Fishell, G., Koulakov, A., and Enikolopov, G. (2011). Division-coupled astrocytic differentiation and age-related depletion of neural stem cells in the adult hippocampus. Cell Stem Cell *8*, 566-579.

England, T.J., Sprigg, N., Alasheev, A.M., Belkin, A.A., Kumar, A., Prasad, K., and Bath, P.M. (2016). Granulocyte-Colony Stimulating Factor (G-CSF) for stroke: an individual patient data meta-analysis. Sci Rep *6*, 36567.

Eriksson, P.S., Perfilieva, E., Bjork-Eriksson, T., Alborn, A.M., Nordborg, C., Peterson, D.A., and Gage, F.H. (1998). Neurogenesis in the adult human hippocampus. Nat Med *4*, 1313-1317.

Ernst, A., Alkass, K., Bernard, S., Salehpour, M., Perl, S., Tisdale, J., Possnert, G., Druid, H., and Frisen, J. (2014). Neurogenesis in the striatum of the adult human brain. Cell *156*, 1072-1083.

Espinera, A.R., Ogle, M.E., Gu, X., and Wei, L. (2013). Citalopram enhances neurovascular regeneration and sensorimotor functional recovery after ischemic stroke in mice. Neuroscience *247*, 1-11.

Farshim, P.P., and Bates, G.P. (2018). Mouse Models of Huntington's Disease. Methods Mol Biol *1780*, 97-120.

Flotte, T., Carter, B., Conrad, C., Guggino, W., Reynolds, T., Rosenstein, B., Taylor, G., Walden, S., and Wetzel, R. (1996). A phase I study of an adeno-associated virus-CFTR gene vector in adult CF patients with mild lung disease. Hum Gene Ther *7*, 1145-1159.

Flotte, T.R., Solow, R., Owens, R.A., Afione, S., Zeitlin, P.L., and Carter, B.J. (1992). Gene expression from adeno-associated virus vectors in airway epithelial cells. Am J Respir Cell Mol Biol *7*, 349-356.

Frielingsdorf, H., Simpson, D.R., Thal, L.J., and Pizzo, D.P. (2007). Nerve growth factor promotes survival of new neurons in the adult hippocampus. Neurobiol Dis *26*, 47-55.

Gage, F.H., and Temple, S. (2013). Neural stem cells: generating and regenerating the brain. Neuron *80*, 588-601.

Gao, X., Wang, X., Xiong, W., and Chen, J. (2016). In vivo reprogramming reactive glia into iPSCs to produce new neurons in the cortex following traumatic brain injury. Sci Rep *6*, 22490.

Garcia, A.D., Doan, N.B., Imura, T., Bush, T.G., and Sofroniew, M.V. (2004). GFAP-expressing progenitors are the principal source of constitutive neurogenesis in adult mouse forebrain. Nat Neurosci *7*, 1233-1241.

Garza, J.C., Guo, M., Zhang, W., and Lu, X.Y. (2008). Leptin increases adult hippocampal neurogenesis in vivo and in vitro. J Biol Chem *283*, 18238-18247.

Ge, S., Yang, C.H., Hsu, K.S., Ming, G.L., and Song, H. (2007). A critical period for enhanced synaptic plasticity in newly generated neurons of the adult brain. Neuron *54*, 559-566.

Gerriets, T., Stolz, E., Walberer, M., Muller, C., Rottger, C., Kluge, A., Kaps, M., Fisher, M., and Bachmann, G. (2004). Complications and pitfalls in rat stroke models for middle cerebral artery occlusion: a comparison between the suture and the macrosphere model using magnetic resonance angiography. Stroke *35*, 2372-2377.

Gheusi, G., Cremer, H., McLean, H., Chazal, G., Vincent, J.D., and Lledo, P.M. (2000). Importance of newly generated neurons in the adult olfactory bulb for odor discrimination. Proc Natl Acad Sci U S A *97*, 1823-1828.

Glorioso, J.C., Cohen, J.B., Carlisle, D.L., Munoz-Sanjuan, I., and Friedlander, R.M. (2015). Moving toward a gene therapy for Huntington's disease. Gene Ther *22*, 931-933.

Goncalves, J.T., Schafer, S.T., and Gage, F.H. (2016). Adult Neurogenesis in the Hippocampus: From Stem Cells to Behavior. Cell *167*, 897-914.

Grande, A., Sumiyoshi, K., Lopez-Juarez, A., Howard, J., Sakthivel, B., Aronow, B., Campbell, K., and Nakafuku, M. (2013). Environmental impact on direct neuronal reprogramming in vivo in the adult brain. Nat Commun *4*, 2373.

Graybiel, A.M. (2008). Habits, rituals, and the evaluative brain. Annu Rev Neurosci *31*, 359-387.

Grimm, D., and Zolotukhin, S. (2015). E Pluribus Unum: 50 Years of Research, Millions of Viruses, and One Goal--Tailored Acceleration of AAV Evolution. Mol Ther *23*, 1819-1831.

Gudasheva, T.A., Povarnina, P., Logvinov, I.O., Antipova, T.A., and Seredenin, S.B. (2016). Mimetics of brain-derived neurotrophic factor loops 1 and 4 are active in a model of ischemic stroke in rats. Drug Des Devel Ther *10*, 3545-3553.

Guo, Z., Zhang, L., Wu, Z., Chen, Y., Wang, F., and Chen, G. (2014). In vivo direct reprogramming of reactive glial cells into functional neurons after brain injury and in an Alzheimer's disease model. Cell Stem Cell *14*, 188-202.

Hamers, F.P., Koopmans, G.C., and Joosten, E.A. (2006). CatWalk-assisted gait analysis in the assessment of spinal cord injury. J Neurotrauma *23*, 537-548.

Hao, J., Mdzinarishvili, A., Abbruscato, T.J., Klein, J., Geldenhuys, W.J., Van der Schyf, C.J., and Bickel, U. (2008). Neuroprotection in mice by NGP1-01 after transient focal brain ischemia. Brain Res *1196*, 113-120.

Happ, D., Tasker, R.A., and Wegener, G. (2018). P.2.038 - Endothelin-1 injection into the left medial prefrontal cortex induces anxiety-like symptoms – a possible model for post-stroke anxiety? Eur Neuropsychopharmacol *28*, S48-S49.

Heinzerling, L., Burg, G., Dummer, R., Maier, T., Oberholzer, P.A., Schultz, J., Elzaouk, L., Pavlovic, J., and Moelling, K. (2005). Intratumoral injection of DNA encoding human interleukin 12 into patients with metastatic melanoma: clinical efficacy. Hum Gene Ther *16*, 35-48.

Henry, R.A., Hughes, S.M., and Connor, B. (2007). AAV-mediated delivery of BDNF augments neurogenesis in the normal and quinolinic acid-lesioned adult rat brain. Eur J Neurosci *25*, 3513-3525.

Herold, S., Kumar, P., Jung, K., Graf, I., Menkhoff, H., Schulz, X., Bahr, M., and Hein, K. (2016). CatWalk gait analysis in a rat model of multiple sclerosis. BMC Neurosci *17*, 78.

Horie, N., Maag, A.L., Hamilton, S.A., Shichinohe, H., Bliss, T.M., and Steinberg, G.K. (2008). Mouse model of focal cerebral ischemia using endothelin-1. J Neurosci Methods *173*, 286-290.

Horton, H.M., Anderson, D., Hernandez, P., Barnhart, K.M., Norman, J.A., and Parker, S.E. (1999). A gene therapy for cancer using intramuscular injection of plasmid DNA encoding interferon alpha. Proc Natl Acad Sci U S A *96*, 1553-1558.

Hou, S.W., Wang, Y.Q., Xu, M., Shen, D.H., Wang, J.J., Huang, F., Yu, Z., and Sun, F.Y. (2008). Functional integration of newly generated neurons into striatum after cerebral ischemia in the adult rat brain. Stroke *39*, 2837-2844.

Hunter, A.J., Hatcher, J., Virley, D., Nelson, P., Irving, E., Hadingham, S.J., and Parsons, A.A. (2000). Functional assessments in mice and rats after focal stroke. Neuropharmacology *39*, 806-816.

Imayoshi, I., Sakamoto, M., Ohtsuka, T., Takao, K., Miyakawa, T., Yamaguchi, M., Mori, K., Ikeda, T., Itohara, S., and Kageyama, R. (2008). Roles of continuous neurogenesis in the structural and functional integrity of the adult forebrain. Nat Neurosci *11*, 1153-1161.

Ishizaka, S., Horie, N., Satoh, K., Fukuda, Y., Nishida, N., and Nagata, I. (2013). Intra-arterial cell transplantation provides timing-dependent cell distribution and functional recovery after stroke. Stroke *44*, 720-726.

Jankowsky, J.L., and Zheng, H. (2017). Practical considerations for choosing a mouse model of Alzheimer's disease. Mol Neurodegener *12*, 89.

Jin, K., Wang, X., Xie, L., Mao, X.O., and Greenberg, D.A. (2010). Transgenic ablation of doublecortin-expressing cells suppresses adult neurogenesis and worsens stroke outcome in mice. Proc Natl Acad Sci U S A *107*, 7993-7998.

Jin, K., Wang, X., Xie, L., Mao, X.O., Zhu, W., Wang, Y., Shen, J., Mao, Y., Banwait, S., and Greenberg, D.A. (2006). Evidence for stroke-induced neurogenesis in the human brain. Proc Natl Acad Sci U S A *103*, 13198-13202.

Joglekar, A.V., and Sandoval, S. (2017). Pseudotyped Lentiviral Vectors: One Vector, Many Guises. Hum Gene Ther Methods *28*, 291-301.

Kalamakis, G., Brune, D., Ravichandran, S., Bolz, J., Fan, W., Ziebell, F., Stiehl, T., Catala-Martinez, F., Kupke, J., Zhao, S., Llorens-Bobadilla, E., Bauer, K., Limpert, S., Berger, B., Christen, U., Schmezer, P., Mallm, J.P., Berninger, B., Anders, S., Del Sol, A., Marciniak-Czochra, A., and Martin-Villalba, A. (2019). Quiescence Modulates Stem Cell Maintenance and Regenerative Capacity in the Aging Brain. Cell *176*, 1407-1419 e1414.

Kempermann, G., Gage, F.H., Aigner, L., Song, H., Curtis, M.A., Thuret, S., Kuhn, H.G., Jessberger, S., Frankland, P.W., Cameron, H.A., Gould, E., Hen, R., Abrous, D.N., Toni, N., Schinder, A.F., Zhao, X., Lucassen, P.J., and Frisen, J. (2018). Human Adult Neurogenesis: Evidence and Remaining Questions. Cell Stem Cell *23*, 25-30.

Kempermann, G., Kuhn, H.G., and Gage, F.H. (1997). More hippocampal neurons in adult mice living in an enriched environment. Nature *386*, 493-495.

Kim, J.H., Auerbach, J.M., Rodriguez-Gomez, J.A., Velasco, I., Gavin, D., Lumelsky, N., Lee, S.H., Nguyen, J., Sanchez-Pernaute, R., Bankiewicz, K., and McKay, R. (2002). Dopamine neurons derived from embryonic stem cells function in an animal model of Parkinson's disease. Nature *418*, 50-56.

Kim, W.R., Kim, Y., Eun, B., Park, O.H., Kim, H., Kim, K., Park, C.H., Vinsant, S., Oppenheim, R.W., and Sun, W. (2007). Impaired migration in the rostral migratory stream but spared olfactory function after the elimination of programmed cell death in Bax knock-out mice. J Neurosci *27*, 14392-14403.

Klein, C., and Westenberger, A. (2012). Genetics of Parkinson's disease. Cold Spring Harb Perspect Med *2*, a008888.

Klein, R.L., Dayton, R.D., Tatom, J.B., Henderson, K.M., and Henning, P.P. (2008). AAV8, 9, Rh10, Rh43 vector gene transfer in the rat brain: effects of serotype, promoter and purification method. Mol Ther *16*, 89-96.

Knoth, R., Singec, I., Ditter, M., Pantazis, G., Capetian, P., Meyer, R.P., Horvat, V., Volk, B., and Kempermann, G. (2010). Murine features of neurogenesis in the human hippocampus across the lifespan from 0 to 100 years. PLoS One *5*, e8809.

Koizumi, J.-i., Yoshida, Y., Nakazawa, T., and Ooneda, G. (1986). Experimental studies of ischemic brain edema 1. A new experimental model of cerebral embolism in rats in which recirculation can be introduced in the ischemic area. Nosotchu *8*, 1-8.

Kotterman, M.A., Chalberg, T.W., and Schaffer, D.V. (2015a). Viral Vectors for Gene Therapy: Translational and Clinical Outlook. Annu Rev Biomed Eng *17*, 63-89.

Kotterman, M.A., and Schaffer, D.V. (2014). Engineering adeno-associated viruses for clinical gene therapy. Nat Rev Genet *15*, 445-451.

Kotterman, M.A., Vazin, T., and Schaffer, D.V. (2015b). Enhanced selective gene delivery to neural stem cells in vivo by an adeno-associated viral variant. Development *142*, 1885-1892.

Kriks, S., Shim, J.W., Piao, J., Ganat, Y.M., Wakeman, D.R., Xie, Z., Carrillo-Reid, L., Auyeung, G., Antonacci, C., Buch, A., Yang, L., Beal, M.F., Surmeier, D.J., Kordower, J.H., Tabar, V., and Studer, L. (2011). Dopamine neurons derived from human ES cells efficiently engraft in animal models of Parkinson's disease. Nature *480*, 547-551.

Kuhn, H.G., Biebl, M., Wilhelm, D., Li, M., Friedlander, R.M., and Winkler, J. (2005). Increased generation of granule cells in adult Bcl-2-overexpressing mice: a role for cell death during continued hippocampal neurogenesis. Eur J Neurosci *22*, 1907-1915.

Kuroiwa, T., Xi, G., Hua, Y., Nagaraja, T.N., Fenstermacher, J.D., and Keep, R.F. (2009). Development of a rat model of photothrombotic ischemia and infarction within the caudoputamen. Stroke *40*, 248-253.

Lange, C., Huttner, W.B., and Calegari, F. (2009). Cdk4/cyclinD1 overexpression in neural stem cells shortens G1, delays neurogenesis, and promotes the generation and expansion of basal progenitors. Cell Stem Cell *5*, 320-331.

Lazarini, F., Mouthon, M.A., Gheusi, G., de Chaumont, F., Olivo-Marin, J.C., Lamarque, S., Abrous, D.N., Boussin, F.D., and Lledo, P.M. (2009). Cellular and behavioral effects of cranial irradiation of the subventricular zone in adult mice. PLoS One *4*, e7017.

Le Guiner, C., Stieger, K., Snyder, R.O., Rolling, F., and Moullier, P. (2007). Immune responses to gene product of inducible promoters. Curr Gene Ther *7*, 334-346.

Lee, J., Duan, W., Long, J.M., Ingram, D.K., and Mattson, M.P. (2000). Dietary restriction increases the number of newly generated neural cells, and induces BDNF expression, in the dentate gyrus of rats. J Mol Neurosci *15*, 99-108.

Lee, Y., Stevens, D.A., Kang, S.U., Jiang, H., Lee, Y.I., Ko, H.S., Scarffe, L.A., Umanah, G.E., Kang, H., Ham, S., Kam, T.I., Allen, K., Brahmachari, S., Kim, J.W., Neifert, S., Yun, S.P., Fiesel, F.C., Springer, W., Dawson, V.L., Shin, J.H., and Dawson, T.M. (2017). PINK1 Primes Parkin-Mediated Ubiquitination of PARIS in Dopaminergic Neuronal Survival. Cell Rep *18*, 918-932.

Li, H., and Chen, G. (2016). In Vivo Reprogramming for CNS Repair: Regenerating Neurons from Endogenous Glial Cells. Neuron *91*, 728-738.

Li, H., Zhang, N., Lin, H.Y., Yu, Y., Cai, Q.Y., Ma, L., and Ding, S. (2014). Histological, cellular and behavioral assessments of stroke outcomes after photothrombosis-induced ischemia in adult mice. BMC Neurosci *15*, 58.

Li, Y.F., Cheng, Y.F., Huang, Y., Conti, M., Wilson, S.P., O'Donnell, J.M., and Zhang, H.T. (2011). Phosphodiesterase-4D knock-out and RNA interference-mediated knock-down enhance memory and increase hippocampal neurogenesis via increased cAMP signaling. J Neurosci *31*, 172-183.

Licht, T., and Keshet, E. (2015). The vascular niche in adult neurogenesis. Mech Dev *138 Pt 1*, 56-62.

Liebetanz, D., and Merkler, D. (2006). Effects of commissural de- and remyelination on motor skill behaviour in the cuprizone mouse model of multiple sclerosis. Exp Neurol *202*, 217-224.

Lim, D.A., and Alvarez-Buylla, A. (2016). The Adult Ventricular-Subventricular Zone (V-SVZ) and Olfactory Bulb (OB) Neurogenesis. Cold Spring Harb Perspect Biol *8*, a018820.

Lima, R.R., Santana, L.N., Fernandes, R.M., Nascimento, E.M., Oliveira, A.C., Fernandes, L.M., Dos Santos, E.M., Tavares, P.A., Dos Santos, I.R., Gimaraes-Santos, A., and Gomes-Leal, W. (2016). Neurodegeneration and Glial Response after Acute Striatal Stroke: Histological Basis for Neuroprotective Studies. Oxid Med Cell Longev *2016*, 3173564.

Lin, R., and Iacovitti, L. (2015). Classic and novel stem cell niches in brain homeostasis and repair. Brain Res *1628*, 327-342.

Lin, X., Parisiadou, L., Sgobio, C., Liu, G., Yu, J., Sun, L., Shim, H., Gu, X.L., Luo, J., Long, C.X., Ding, J., Mateo, Y., Sullivan, P.H., Wu, L.G., Goldstein, D.S., Lovinger, D., and Cai, H. (2012). Conditional expression of Parkinson's disease-related mutant alpha-synuclein in the

midbrain dopaminergic neurons causes progressive neurodegeneration and degradation of transcription factor nuclear receptor related 1. J Neurosci *32*, 9248-9264.

Liu, F., Song, Y., and Liu, D. (1999). Hydrodynamics-based transfection in animals by systemic administration of plasmid DNA. Gene Ther *6*, 1258-1266.

Liu, Y., Pattamatta, A., Zu, T., Reid, T., Bardhi, O., Borchelt, D.R., Yachnis, A.T., and Ranum, L.P. (2016). C9orf72 BAC Mouse Model with Motor Deficits and Neurodegenerative Features of ALS/FTD. Neuron *90*, 521-534.

Liu, Y.W., Curtis, M.A., Gibbons, H.M., Mee, E.W., Bergin, P.S., Teoh, H.H., Connor, B., Dragunow, M., and Faull, R.L. (2008). Doublecortin expression in the normal and epileptic adult human brain. Eur J Neurosci *28*, 2254-2265.

Lo Furno, D., Mannino, G., and Giuffrida, R. (2018). Functional role of mesenchymal stem cells in the treatment of chronic neurodegenerative diseases. J Cell Physiol *233*, 3982-3999.

Logroscino, G., and Tortelli, R. (2015). Epidemiology of neurodegenerative diseases. In: Saba, L. (ed.) Imaging in Neurodegenerative Disorders. Oxford University Press, Oxford, UK, pp. 3-19.

Lueptow, L.M. (2017). Novel Object Recognition Test for the Investigation of Learning and Memory in Mice. J Vis Exp *126*, e55718.

Lujan, E., Chanda, S., Ahlenius, H., Sudhof, T.C., and Wernig, M. (2012). Direct conversion of mouse fibroblasts to self-renewing, tripotent neural precursor cells. Proc Natl Acad Sci U S A *109*, 2527-2532.

Lynch, J.L., Gallus, N.J., Ericson, M.E., and Beitz, A.J. (2008). Analysis of nociception, sex and peripheral nerve innervation in the TMEV animal model of multiple sclerosis. Pain *136*, 293-304.

Ma, M., Ma, Y., Yi, X., Guo, R., Zhu, W., Fan, X., Xu, G., Frey, W.H., 2nd, and Liu, X. (2008). Intranasal delivery of transforming growth factor-beta1 in mice after stroke reduces infarct volume and increases neurogenesis in the subventricular zone. BMC Neurosci *9*, 117.

Magnusson, J.P., and Frisen, J. (2016). Stars from the darkest night: unlocking the neurogenic potential of astrocytes in different brain regions. Development *143*, 1075-1086.

Manthorpe, M., Cornefert-Jensen, F., Hartikka, J., Felgner, J., Rundell, A., Margalith, M., and Dwarki, V. (1993). Gene therapy by intramuscular injection of plasmid DNA: studies on firefly luciferase gene expression in mice. Hum Gene Ther *4*, 419-431.

Marques, B.L., Carvalho, G.A., Freitas, E.M.M., Chiareli, R.A., Barbosa, T.G., Di Araujo, A.G.P., Nogueira, Y.L., Ribeiro, R.I., Parreira, R.C., Vieira, M.S., Resende, R.R., Gomez, R.S., Oliveira-Lima, O.C., and Pinto, M.C.X. (2019). The role of neurogenesis in neurorepair after ischemic stroke. Semin Cell Dev Biol *95*, 98-110.

Mathews, K.J., Allen, K.M., Boerrigter, D., Ball, H., Shannon Weickert, C., and Double, K.L. (2017). Evidence for reduced neurogenesis in the aging human hippocampus despite stable stem cell markers. Aging Cell *16*, 1195-1199.

Mende, N., Kuchen, E.E., Lesche, M., Grinenko, T., Kokkaliaris, K.D., Hanenberg, H., Lindemann, D., Dahl, A., Platz, A., Hofer, T., Calegari, F., and Waskow, C. (2015). CCND1-CDK4-mediated cell cycle progression provides a competitive advantage for human hematopoietic stem cells in vivo. J Exp Med *212*, 1171-1183.

Mendez, I., Sanchez-Pernaute, R., Cooper, O., Vinuela, A., Ferrari, D., Bjorklund, L., Dagher, A., and Isacson, O. (2005). Cell type analysis of functional fetal dopamine cell suspension transplants in the striatum and substantia nigra of patients with Parkinson's disease. Brain *128*, 1498-1510.

Mendez, I., Vinuela, A., Astradsson, A., Mukhida, K., Hallett, P., Robertson, H., Tierney, T., Holness, R., Dagher, A., Trojanowski, J.Q., and Isacson, O. (2008). Dopamine neurons implanted into people with Parkinson's disease survive without pathology for 14 years. Nat Med *14*, 507-509.

Menn, B., Garcia-Verdugo, J.M., Yaschine, C., Gonzalez-Perez, O., Rowitch, D., and Alvarez-Buylla, A. (2006). Origin of oligodendrocytes in the subventricular zone of the adult brain. J Neurosci *26*, 7907-7918.

Miller, S.D., and Karpus, W.J. (2007). Experimental autoimmune encephalomyelitis in the mouse. Curr Protoc Immunol *77*, 15.01.01-15.01.18.

Minger, S.L., Ekonomou, A., Carta, E.M., Chinoy, A., Perry, R.H., and Ballard, C.G. (2007). Endogenous neurogenesis in the human brain following cerebral infarction. Regen Med *2*, 69-74.

Mirzadeh, Z., Merkle, F.T., Soriano-Navarro, M., Garcia-Verdugo, J.M., and Alvarez-Buylla, A. (2008). Neural stem cells confer unique pinwheel architecture to the ventricular surface in neurogenic regions of the adult brain. Cell Stem Cell *3*, 265-278.

Mohapel, P., Frielingsdorf, H., Haggblad, J., Zachrisson, O., and Brundin, P. (2005). Platelet-derived growth factor (PDGF-BB) and brain-derived neurotrophic factor (BDNF) induce striatal neurogenesis in adult rats with 6-hydroxydopamine lesions. Neuroscience *132*, 767-776.

Moreno-Jimenez, E.P., Flor-Garcia, M., Terreros-Roncal, J., Rabano, A., Cafini, F., Pallas-Bazarra, N., Avila, J., and Llorens-Martin, M. (2019). Adult hippocampal neurogenesis is abundant in neurologically healthy subjects and drops sharply in patients with Alzheimer's disease. Nat Med *25*, 554-560.

Mouret, A., Lepousez, G., Gras, J., Gabellec, M.M., and Lledo, P.M. (2009). Turnover of newborn olfactory bulb neurons optimizes olfaction. J Neurosci *29*, 12302-12314.

Nabel, G.J., Nabel, E.G., Yang, Z.Y., Fox, B.A., Plautz, G.E., Gao, X., Huang, L., Shu, S., Gordon, D., and Chang, A.E. (1993). Direct gene transfer with DNA-liposome complexes in melanoma: expression, biologic activity, and lack of toxicity in humans. Proc Natl Acad Sci U S A *90*, 11307-11311.

Nair, J.K., Willoughby, J.L., Chan, A., Charisse, K., Alam, M.R., Wang, Q., Hoekstra, M., Kandasamy, P., Kel'in, A.V., Milstein, S., Taneja, N., O'Shea, J., Shaikh, S., Zhang, L., van der Sluis, R.J., Jung, M.E., Akinc, A., Hutabarat, R., Kuchimanchi, S., Fitzgerald, K., Zimmermann, T., van Berkel, T.J., Maier, M.A., Rajeev, K.G., and Manoharan, M. (2014). Multivalent N-acetylgalactosamine-conjugated siRNA localizes in hepatocytes and elicits robust RNAi-mediated gene silencing. J Am Chem Soc *136*, 16958-16961.

Naldini, L. (2015). Gene therapy returns to centre stage. Nature *526*, 351-360.

Naldini, L., Blomer, U., Gallay, P., Ory, D., Mulligan, R., Gage, F.H., Verma, I.M., and Trono, D. (1996). In vivo gene delivery and stable transduction of nondividing cells by a lentiviral vector. Science *272*, 263-267.

Nass, S.A., Mattingly, M.A., Woodcock, D.A., Burnham, B.L., Ardinger, J.A., Osmond, S.E., Frederick, A.M., Scaria, A., Cheng, S.H., and O'Riordan, C.R. (2018). Universal Method for

the Purification of Recombinant AAV Vectors of Differing Serotypes. Mol Ther Methods Clin Dev *9*, 33-46.

Nemirovich-Danchenko, N.M., and Khodanovich, M.Y. (2019). New Neurons in the Post-ischemic and Injured Brain: Migrating or Resident? Front Neurosci *13*, 588.

Neumann, M., Sampathu, D.M., Kwong, L.K., Truax, A.C., Micsenyi, M.C., Chou, T.T., Bruce, J., Schuck, T., Grossman, M., Clark, C.M., McCluskey, L.F., Miller, B.L., Masliah, E., Mackenzie, I.R., Feldman, H., Feiden, W., Kretzschmar, H.A., Trojanowski, J.Q., and Lee, V.M. (2006). Ubiquitinated TDP-43 in frontotemporal lobar degeneration and amyotrophic lateral sclerosis. Science *314*, 130-133.

Nonaka-Kinoshita, M., Reillo, I., Artegiani, B., Martinez-Martinez, M.A., Nelson, M., Borrell, V., and Calegari, F. (2013). Regulation of cerebral cortex size and folding by expansion of basal progenitors. EMBO J *32*, 1817-1828.

Obernier, K., and Alvarez-Buylla, A. (2019). Neural stem cells: origin, heterogeneity and regulation in the adult mammalian brain. Development *146*, dev156059.

Obernier, K., Cebrian-Silla, A., Thomson, M., Parraguez, J.I., Anderson, R., Guinto, C., Rodas Rodriguez, J., Garcia-Verdugo, J.M., and Alvarez-Buylla, A. (2018). Adult Neurogenesis Is Sustained by Symmetric Self-Renewal and Differentiation. Cell Stem Cell *22*, 221-234 e228.

Ohab, J.J., Fleming, S., Blesch, A., and Carmichael, S.T. (2006). A neurovascular niche for neurogenesis after stroke. J Neurosci *26*, 13007-13016.

Ojala, D.S., Sun, S., Santiago-Ortiz, J.L., Shapiro, M.G., Romero, P.A., and Schaffer, D.V. (2018). In Vivo Selection of a Computationally Designed SCHEMA AAV Library Yields a Novel Variant for Infection of Adult Neural Stem Cells in the SVZ. Mol Ther *26*, 304-319.

Okabe, N., Himi, N., Maruyama-Nakamura, E., Hayashi, N., Narita, K., and Miyamoto, O. (2017). Rehabilitative skilled forelimb training enhances axonal remodeling in the corticospinal pathway but not the brainstem-spinal pathways after photothrombotic stroke in the primary motor cortex. PLoS One *12*, e0187413.

Olanow, C.W., Goetz, C.G., Kordower, J.H., Stoessl, A.J., Sossi, V., Brin, M.F., Shannon, K.M., Nauert, G.M., Perl, D.P., Godbold, J., and Freeman, T.B. (2003). A double-blind controlled trial of bilateral fetal nigral transplantation in Parkinson's disease. Ann Neurol *54*, 403-414.

Ottone, C., Krusche, B., Whitby, A., Clements, M., Quadrato, G., Pitulescu, M.E., Adams, R.H., and Parrinello, S. (2014). Direct cell-cell contact with the vascular niche maintains quiescent neural stem cells. Nat Cell Biol *16*, 1045-1056.

Pahle, J., and Walther, W. (2016). Vectors and strategies for nonviral cancer gene therapy. Expert Opin Biol Ther *16*, 443-461.

Palmer, T.D., Schwartz, P.H., Taupin, P., Kaspar, B., Stein, S.A., and Gage, F.H. (2001). Cell culture. Progenitor cells from human brain after death. Nature *411*, 42-43.

Parent, J.M., Vexler, Z.S., Gong, C., Derugin, N., and Ferriero, D.M. (2002). Rat forebrain neurogenesis and striatal neuron replacement after focal stroke. Ann Neurol *52*, 802-813.

Paul, G., and Anisimov, S.V. (2013). The secretome of mesenchymal stem cells: potential implications for neuroregeneration. Biochimie *95*, 2246-2256.

Peng, J., Xie, L., Jin, K., Greenberg, D.A., and Andersen, J.K. (2008). Fibroblast growth factor 2 enhances striatal and nigral neurogenesis in the acute 1-methyl-4-phenyl-1,2,3,6-tetrahydropyridine model of Parkinson's disease. Neuroscience *153*, 664-670.

Peruga, I., Hartwig, S., Thone, J., Hovemann, B., Gold, R., Juckel, G., and Linker, R.A. (2011). Inflammation modulates anxiety in an animal model of multiple sclerosis. Behav Brain Res *220*, 20-29.

Philips, T., and Rothstein, J.D. (2015). Rodent Models of Amyotrophic Lateral Sclerosis. Curr Protoc Pharmacol *69*, 05.67.01-05.67.21.

Pilz, G.A., Bottes, S., Betizeau, M., Jorg, D.J., Carta, S., Simons, B.D., Helmchen, F., and Jessberger, S. (2018). Live imaging of neurogenesis in the adult mouse hippocampus. Science *359*, 658-662.

Pinnock, S.B., and Herbert, J. (2008). Brain-derived neurotropic factor and neurogenesis in the adult rat dentate gyrus: interactions with corticosterone. Eur J Neurosci *27*, 2493-2500.

Pluchino, S., Zanotti, L., Rossi, B., Brambilla, E., Ottoboni, L., Salani, G., Martinello, M., Cattalini, A., Bergami, A., Furlan, R., Comi, G., Constantin, G., and Martino, G. (2005). Neurosphere-derived multipotent precursors promote neuroprotection by an immunomodulatory mechanism. Nature *436*, 266-271.

Ponti, G., Obernier, K., Guinto, C., Jose, L., Bonfanti, L., and Alvarez-Buylla, A. (2013). Cell cycle and lineage progression of neural progenitors in the ventricular-subventricular zones of adult mice. Proc Natl Acad Sci U S A *110*, E1045-1054.

Procaccini, C., De Rosa, V., Pucino, V., Formisano, L., and Matarese, G. (2015). Animal models of Multiple Sclerosis. Eur J Pharmacol *759*, 182-191.

Qin, C., Zhou, L.Q., Ma, X.T., Hu, Z.W., Yang, S., Chen, M., Bosco, D.B., Wu, L.J., and Tian, D.S. (2019). Dual Functions of Microglia in Ischemic Stroke. Neurosci Bull *35*, 921-933.

Renton, A.E., Majounie, E., Waite, A., Simon-Sanchez, J., Rollinson, S., Gibbs, J.R., Schymick, J.C., Laaksovirta, H., van Swieten, J.C., Myllykangas, L., Kalimo, H., Paetau, A., Abramzon, Y., Remes, A.M., Kaganovich, A., Scholz, S.W., Duckworth, J., Ding, J., Harmer, D.W., Hernandez, D.G., Johnson, J.O., Mok, K., Ryten, M., Trabzuni, D., Guerreiro, R.J., Orrell, R.W., Neal, J., Murray, A., Pearson, J., Jansen, I.E., Sondervan, D., Seelaar, H., Blake, D., Young, K., Halliwell, N., Callister, J.B., Toulson, G., Richardson, A., Gerhard, A., Snowden, J., Mann, D., Neary, D., Nalls, M.A., Peuralinna, T., Jansson, L., Isoviita, V.M., Kaivorinne, A.L., Holtta-Vuori, M., Ikonen, E., Sulkava, R., Benatar, M., Wuu, J., Chio, A., Restagno, G., Borghero, G., Sabatelli, M., Consortium, I., Heckerman, D., Rogaeva, E., Zinman, L., Rothstein, J.D., Sendtner, M., Drepper, C., Eichler, E.E., Alkan, C., Abdullaev, Z., Pack, S.D., Dutra, A., Pak, E., Hardy, J., Singleton, A., Williams, N.M., Heutink, P., Pickering-Brown, S., Morris, H.R., Tienari, P.J., and Traynor, B.J. (2011). A hexanucleotide repeat expansion in C9ORF72 is the cause of chromosome 9p21-linked ALS-FTD. Neuron *72*, 257-268.

Rewell, S.S., Churilov, L., Sidon, T.K., Aleksoska, E., Cox, S.F., Macleod, M.R., and Howells, D.W. (2017). Evolution of ischemic damage and behavioural deficit over 6 months after MCAo in the rat: Selecting the optimal outcomes and statistical power for multi-centre preclinical trials. PLoS One *12*, e0171688.

Reynolds, B.A., and Weiss, S. (1992). Generation of neurons and astrocytes from isolated cells of the adult mammalian central nervous system. Science *255*, 1707-1710.

Rogers, S., and Pfuderer, P. (1968). Use of viruses as carriers of added genetic information. Nature *219*, 749-751.

Roome, R.B., Bartlett, R.F., Jeffers, M., Xiong, J., Corbett, D., and Vanderluit, J.L. (2014). A reproducible Endothelin-1 model of forelimb motor cortex stroke in the mouse. J Neurosci Methods *233*, 34-44.

Sakata, H., Narasimhan, P., Niizuma, K., Maier, C.M., Wakai, T., and Chan, P.H. (2012a). Interleukin 6-preconditioned neural stem cells reduce ischaemic injury in stroke mice. Brain *135*, 3298-3310.

Sakata, H., Niizuma, K., Yoshioka, H., Kim, G.S., Jung, J.E., Katsu, M., Narasimhan, P., Maier, C.M., Nishiyama, Y., and Chan, P.H. (2012b). Minocycline-preconditioned neural stem cells enhance neuroprotection after ischemic stroke in rats. J Neurosci *32*, 3462-3473.

Salganik, M., Hirsch, M.L., and Samulski, R.J. (2015). Adeno-associated Virus as a Mammalian DNA Vector. Microbiol Spectr *3*, MDNA3-0052-2014.

Savitt, J.M., Dawson, V.L., and Dawson, T.M. (2006). Diagnosis and treatment of Parkinson disease: molecules to medicine. J Clin Invest *116*, 1744-1754.

Saxe, M.D., Battaglia, F., Wang, J.W., Malleret, G., David, D.J., Monckton, J.E., Garcia, A.D., Sofroniew, M.V., Kandel, E.R., Santarelli, L., Hen, R., and Drew, M.R. (2006). Ablation of hippocampal neurogenesis impairs contextual fear conditioning and synaptic plasticity in the dentate gyrus. Proc Natl Acad Sci U S A *103*, 17501-17506.

Sehgal, A., Vaishnaw, A., and Fitzgerald, K. (2013). Liver as a target for oligonucleotide therapeutics. J Hepatol *59*, 1354-1359.

Shaw, A., and Cornetta, K. (2014). Design and Potential of Non-Integrating Lentiviral Vectors. Biomedicines *2*, 14-35.

Shaw, A.M., Joseph, G.L., Jasti, A.C., Sastry-Dent, L., Witting, S., and Cornetta, K. (2017). Differences in vector-genome processing and illegitimate integration of non-integrating lentiviral vectors. Gene Ther *24*, 12-20.

Shim, G., Kim, D., Le, Q.V., Park, G.T., Kwon, T., and Oh, Y.K. (2018). Nonviral Delivery Systems for Cancer Gene Therapy: Strategies and Challenges. Curr Gene Ther *18*, 3-20.

Shin, J.H., Ko, H.S., Kang, H., Lee, Y., Lee, Y.I., Pletinkova, O., Troconso, J.C., Dawson, V.L., and Dawson, T.M. (2011). PARIS (ZNF746) repression of PGC-1alpha contributes to neurodegeneration in Parkinson's disease. Cell *144*, 689-702.

Shook, B.A., Manz, D.H., Peters, J.J., Kang, S., and Conover, J.C. (2012). Spatiotemporal changes to the subventricular zone stem cell pool through aging. J Neurosci *32*, 6947-6956.

Snippert, H.J., van der Flier, L.G., Sato, T., van Es, J.H., van den Born, M., Kroon-Veenboer, C., Barker, N., Klein, A.M., van Rheenen, J., Simons, B.D., and Clevers, H. (2010). Intestinal crypt homeostasis results from neutral competition between symmetrically dividing Lgr5 stem cells. Cell *143*, 134-144.

Sorrells, S.F., Paredes, M.F., Cebrian-Silla, A., Sandoval, K., Qi, D., Kelley, K.W., James, D., Mayer, S., Chang, J., Auguste, K.I., Chang, E.F., Gutierrez, A.J., Kriegstein, A.R., Mathern, G.W., Oldham, M.C., Huang, E.J., Garcia-Verdugo, J.M., Yang, Z., and Alvarez-Buylla, A. (2018). Human hippocampal neurogenesis drops sharply in children to undetectable levels in adults. Nature *555*, 377-381.

Spalding, K.L., Bergmann, O., Alkass, K., Bernard, S., Salehpour, M., Huttner, H.B., Bostrom, E., Westerlund, I., Vial, C., Buchholz, B.A., Possnert, G., Mash, D.C., Druid, H., and Frisen, J. (2013). Dynamics of hippocampal neurogenesis in adult humans. Cell *153*, 1219-1227.

Strobel, B., Miller, F.D., Rist, W., and Lamla, T. (2015). Comparative Analysis of Cesium Chloride- and Iodixanol-Based Purification of Recombinant Adeno-Associated Viral Vectors for Preclinical Applications. Hum Gene Ther Methods *26*, 147-157.

Sun, L., Zhang, Y., Liu, E., Ma, Q., Anatol, M., Han, H., and Yan, J. (2019). The roles of astrocyte in the brain pathologies following ischemic stroke. Brain Inj *33*, 712-716.

Swarup, V., Phaneuf, D., Bareil, C., Robertson, J., Rouleau, G.A., Kriz, J., and Julien, J.P. (2011). Pathological hallmarks of amyotrophic lateral sclerosis/frontotemporal lobar degeneration in transgenic mice produced with TDP-43 genomic fragments. Brain *134*, 2610-2626.

Taghian, T., Marosfoi, M.G., Puri, A.S., Cataltepe, O.I., King, R.M., Diffie, E.B., Maguire, A.S., Martin, D.R., Fernau, D., Batista, A.R., Kuchel, T., Christou, C., Perumal, R., Chandra, S., Gamlin, P.D., Bertrand, S.G., Flotte, T.R., McKenna-Yasek, D., Tai, P.W.L., Aronin, N., Gounis, M.J., Sena-Esteves, M., and Gray-Edwards, H.L. (2019). A Safe and Reliable Technique for CNS Delivery of AAV Vectors in the Cisterna Magna. Mol Ther *28*, 411-421.

Takahashi, K., Tanabe, K., Ohnuki, M., Narita, M., Ichisaka, T., Tomoda, K., and Yamanaka, S. (2007). Induction of pluripotent stem cells from adult human fibroblasts by defined factors. Cell *131*, 861-872.

Takahashi, K., and Yamanaka, S. (2006). Induction of pluripotent stem cells from mouse embryonic and adult fibroblast cultures by defined factors. Cell *126*, 663-676.

Tande, D., Hoglinger, G., Debeir, T., Freundlieb, N., Hirsch, E.C., and Francois, C. (2006). New striatal dopamine neurons in MPTP-treated macaques result from a phenotypic shift and not neurogenesis. Brain *129*, 1194-1200.

Taylor, J.P., Brown, R.H., Jr., and Cleveland, D.W. (2016). Decoding ALS: from genes to mechanism. Nature *539*, 197-206.

Tennant, K.A., and Jones, T.A. (2009). Sensorimotor behavioral effects of endothelin-1 induced small cortical infarcts in C57BL/6 mice. J Neurosci Methods *181*, 18-26.

Theus, M.H., Wei, L., Cui, L., Francis, K., Hu, X., Keogh, C., and Yu, S.P. (2008). In vitro hypoxic preconditioning of embryonic stem cells as a strategy of promoting cell survival and functional benefits after transplantation into the ischemic rat brain. Exp Neurol *210*, 656-670.

Thier, M., Worsdorfer, P., Lakes, Y.B., Gorris, R., Herms, S., Opitz, T., Seiferling, D., Quandel, T., Hoffmann, P., Nothen, M.M., Brustle, O., and Edenhofer, F. (2012). Direct conversion of fibroblasts into stably expandable neural stem cells. Cell Stem Cell *10*, 473-479.

Thomson, J.A., Itskovitz-Eldor, J., Shapiro, S.S., Waknitz, M.A., Swiergiel, J.J., Marshall, V.S., and Jones, J.M. (1998). Embryonic stem cell lines derived from human blastocysts. Science *282*, 1145-1147.

Timotius, I.K., Canneva, F., Minakaki, G., Moceri, S., Plank, A.C., Casadei, N., Riess, O., Winkler, J., Klucken, J., Eskofier, B., and von Horsten, S. (2019). Systematic data analysis and data mining in CatWalk gait analysis by heat mapping exemplified in rodent models for neurodegenerative diseases. J Neurosci Methods *326*, 108367.

Tobin, M.K., Musaraca, K., Disouky, A., Shetti, A., Bheri, A., Honer, W.G., Kim, N., Dawe, R.J., Bennett, D.A., Arfanakis, K., and Lazarov, O. (2019). Human Hippocampal Neurogenesis Persists in Aged Adults and Alzheimer's Disease Patients. Cell Stem Cell *24*, 974-982 e973.

Toda, T., and Gage, F.H. (2018). Review: adult neurogenesis contributes to hippocampal plasticity. Cell Tissue Res *373*, 693-709.

Toni, N., and Schinder, A.F. (2015). Maturation and Functional Integration of New Granule Cells into the Adult Hippocampus. Cold Spring Harb Perspect Biol *8*, a018903.

Toni, N., Teng, E.M., Bushong, E.A., Aimone, J.B., Zhao, C., Consiglio, A., van Praag, H., Martone, M.E., Ellisman, M.H., and Gage, F.H. (2007). Synapse formation on neurons born in the adult hippocampus. Nat Neurosci *10*, 727-734.

Toyoshima, A., Yasuhara, T., and Date, I. (2017). Mesenchymal Stem Cell Therapy for Ischemic Stroke. Acta Med Okayama *71*, 263-268.

Toyoshima, A., Yasuhara, T., Kameda, M., Morimoto, J., Takeuchi, H., Wang, F., Sasaki, T., Sasada, S., Shinko, A., Wakamori, T., Okazaki, M., Kondo, A., Agari, T., Borlongan, C.V., and Date, I. (2015). Intra-Arterial Transplantation of Allogeneic Mesenchymal Stem Cells Mounts Neuroprotective Effects in a Transient Ischemic Stroke Model in Rats: Analyses of Therapeutic Time Window and Its Mechanisms. PLoS One *10*, e0127302.

Udo, H., Yoshida, Y., Kino, T., Ohnuki, K., Mizunoya, W., Mukuda, T., and Sugiyama, H. (2008). Enhanced adult neurogenesis and angiogenesis and altered affective behaviors in mice overexpressing vascular endothelial growth factor 120. J Neurosci *28*, 14522-14536.

van den Berg, R., Laman, J.D., van Meurs, M., Hintzen, R.Q., and Hoogenraad, C.C. (2016). Rotarod motor performance and advanced spinal cord lesion image analysis refine assessment of neurodegeneration in experimental autoimmune encephalomyelitis. J Neurosci Methods *262*, 66-76.

van den Berge, S.A., van Strien, M.E., and Hol, E.M. (2013). Resident adult neural stem cells in Parkinson's disease--the brain's own repair system? Eur J Pharmacol *719*, 117-127.

van Praag, H., Kempermann, G., and Gage, F.H. (1999). Running increases cell proliferation and neurogenesis in the adult mouse dentate gyrus. Nat Neurosci *2*, 266-270.

Vingill, S., Connor-Robson, N., and Wade-Martins, R. (2018). Are rodent models of Parkinson's disease behaving as they should? Behav Brain Res *352*, 133-141.

Wang, W., Lu, S., Li, T., Pan, Y.W., Zou, J., Abel, G.M., Xu, L., Storm, D.R., and Xia, Z. (2015a). Inducible activation of ERK5 MAP kinase enhances adult neurogenesis in the olfactory bulb and improves olfactory function. J Neurosci *35*, 7833-7849.

Wang, Z., Peng, W., Zhang, C., Sheng, C., Huang, W., Wang, Y., and Fan, R. (2015b). Effects of stem cell transplantation on cognitive decline in animal models of Alzheimer's disease: A systematic review and meta-analysis. Sci Rep *5*, 12134.

Watson, B.D., Dietrich, W.D., Busto, R., Wachtel, M.S., and Ginsberg, M.D. (1985). Induction of reproducible brain infarction by photochemically initiated thrombosis. Ann Neurol *17*, 497-504.

Wen, Z., Xu, X., Xu, L., Yang, L., Xu, X., Zhu, J., Wu, L., Jiang, Y., and Liu, X. (2017). Optimization of behavioural tests for the prediction of outcomes in mouse models of focal middle cerebral artery occlusion. Brain Res *1665*, 88-94.

Wilson, J.M. (2009). Lessons learned from the gene therapy trial for ornithine transcarbamylase deficiency. Mol Genet Metab *96*, 151-157.

Windle, V., Szymanska, A., Granter-Button, S., White, C., Buist, R., Peeling, J., and Corbett, D. (2006). An analysis of four different methods of producing focal cerebral ischemia with endothelin-1 in the rat. Exp Neurol *201*, 324-334.

Wise, R.A. (2004). Dopamine, learning and motivation. Nat Rev Neurosci *5*, 483-494.

Xiong, Y., Neifert, S., Karuppagounder, S.S., Liu, Q., Stankowski, J.N., Lee, B.D., Ko, H.S., Lee, Y., Grima, J.C., Mao, X., Jiang, H., Kang, S.U., Swing, D.A., Iacovitti, L., Tessarollo, L., Dawson, T.M., and Dawson, V.L. (2018). Robust kinase- and age-dependent dopaminergic and norepinephrine neurodegeneration in LRRK2 G2019S transgenic mice. Proc Natl Acad Sci U S A *115*, 1635-1640.

Xu, W., Mu, X., Wang, H., Song, C., Ma, W., Jolkkonen, J., and Zhao, C. (2017). Chloride Co-transporter NKCC1 Inhibitor Bumetanide Enhances Neurogenesis and Behavioral Recovery in Rats After Experimental Stroke. Mol Neurobiol *54*, 2406-2414.

Yamashita, T., Shang, J., Nakano, Y., Morihara, R., Sato, K., Takemoto, M., Hishikawa, N., Ohta, Y., and Abe, K. (2019). In vivo direct reprogramming of glial linage to mature neurons after cerebral ischemia. Sci Rep *9*, 10956.

Yin, H., Xue, W., Chen, S., Bogorad, R.L., Benedetti, E., Grompe, M., Koteliansky, V., Sharp, P.A., Jacks, T., and Anderson, D.G. (2014). Genome editing with Cas9 in adult mice corrects a disease mutation and phenotype. Nat Biotechnol *32*, 551-553.

Young, K.M., Fogarty, M., Kessaris, N., and Richardson, W.D. (2007). Subventricular zone stem cells are heterogeneous with respect to their embryonic origins and neurogenic fates in the adult olfactory bulb. J Neurosci *27*, 8286-8296.

Yu, S.J., Tseng, K.Y., Shen, H., Harvey, B.K., Airavaara, M., and Wang, Y. (2013). Local administration of AAV-BDNF to subventricular zone induces functional recovery in stroke rats. PLoS One *8*, e81750.

Zeng, L., He, X., Wang, Y., Tang, Y., Zheng, C., Cai, H., Liu, J., Wang, Y., Fu, Y., and Yang, G.Y. (2014). MicroRNA-210 overexpression induces angiogenesis and neurogenesis in the normal adult mouse brain. Gene Ther *21*, 37-43.

Zhang, J., Mu, X., Breker, D.A., Li, Y., Gao, Z., and Huang, Y. (2017). Atorvastatin treatment is associated with increased BDNF level and improved functional recovery after atherothrombotic stroke. Int J Neurosci *127*, 92-97.

Zhang, L., Schallert, T., Zhang, Z.G., Jiang, Q., Arniego, P., Li, Q., Lu, M., and Chopp, M. (2002). A test for detecting long-term sensorimotor dysfunction in the mouse after focal cerebral ischemia. J Neurosci Methods *117*, 207-214.

Zhang, R.L., LeTourneau, Y., Gregg, S.R., Wang, Y., Toh, Y., Robin, A.M., Zhang, Z.G., and Chopp, M. (2007). Neuroblast division during migration toward the ischemic striatum: a study of dynamic migratory and proliferative characteristics of neuroblasts from the subventricular zone. J Neurosci *27*, 3157-3162.

Zhong, J., Chan, A., Morad, L., Kornblum, H.I., Fan, G., and Carmichael, S.T. (2010). Hydrogel matrix to support stem cell survival after brain transplantation in stroke. Neurorehabil Neural Repair *24*, 636-644.

Zigova, T., Pencea, V., Wiegand, S.J., and Luskin, M.B. (1998). Intraventricular administration of BDNF increases the number of newly generated neurons in the adult olfactory bulb. Mol Cell Neurosci *11*, 234-245.

Zolotukhin, S., Byrne, B.J., Mason, E., Zolotukhin, I., Potter, M., Chesnut, K., Summerford, C., Samulski, R.J., and Muzyczka, N. (1999). Recombinant adeno-associated virus purification using novel methods improves infectious titer and yield. Gene Ther *6*, 973-985.

Anlage 1

Technische Universität Dresden
Medizinische Fakultät Carl Gustav Carus
Promotionsordnung vom 24. Juli 2011

Erklärungen zur Eröffnung des Promotionsverfahrens

1. Hiermit versichere ich, dass ich die vorliegende Arbeit ohne unzulässige Hilfe Dritter und ohne Benutzung anderer als der angegebenen Hilfsmittel angefertigt habe; die aus fremden Quellen direkt oder indirekt übernommenen Gedanken sind als solche kenntlich gemacht.

2. Bei der Auswahl und Auswertung des Materials sowie bei der Herstellung des Manuskripts habe ich Unterstützungsleistungen von folgenden Personen erhalten:
nicht zutreffend

3. Weitere Personen waren an der geistigen Herstellung der vorliegenden Arbeit nicht beteiligt. Insbesondere habe ich nicht die Hilfe eines kommerziellen Promotionsberaters in Anspruch genommen. Dritte haben von mir weder unmittelbar noch mittelbar geldwerte Leistungen für Arbeiten erhalten, die im Zusammenhang mit dem Inhalt der vorgelegten Dissertation stehen.

4. Die Arbeit wurde bisher weder im Inland noch im Ausland in gleicher oder ähnlicher Form einer anderen Prüfungsbehörde vorgelegt.

5. Die Inhalte dieser Dissertation wurden in folgender Form veröffentlicht:
nicht zutreffend

6. Ich bestätige, dass es keine zurückliegenden erfolglosen Promotionsverfahren gab.

7. Ich bestätige, dass ich die Promotionsordnung der Medizinischen Fakultät der Technischen Universität Dresden anerkenne.

8. Ich habe die Zitierrichtlinien für Dissertationen an der Medizinischen Fakultät der Technischen Universität Dresden zur Kenntnis genommen und befolgt.

Dresden, den

Simon Hertlein

Anlage 2

Hiermit bestätige ich die Einhaltung der folgenden aktuellen gesetzlichen Vorgaben im Rahmen meiner Dissertation

- das zustimmende Votum der Ethikkommission bei Klinischen Studien, epidemiologischen Untersuchungen mit Personenbezug oder Sachverhalten, die das Medizinproduktegesetz betreffen
  Aktenzeichen der zuständigen Ethikkommission: entfällt

- die Einhaltung der Bestimmungen des Tierschutzgesetzes
  Aktenzeichen der Genehmigungsbehörde zum Vorhaben/zur Mitwirkung
  TVV13/2016 und TVV39/2018

- die Einhaltung des Gentechnikgesetzes
  Projektnummer DD 24-9168.11-1/2011-11

- die Einhaltung von Datenschutzbestimmungen der Medizinischen Fakultät und des Universitätsklinikums Carl Gustav Carus.

Dresden, den

Simon Hertlein